IN-37033

P187

DOE/NASA/0311-1
NASA CR-175042
MTI 85SESD24

Ceramic Automotive Stirling Engine Program

(NASA-CR-175042) CERAMIC AUTOMOTIVE STIRLING ENGINE PROGRAM (Mechanical Technology, Inc.) 187 p CSCL 10B

N87-12047

Unclas
G3/44 44662

Mechanical Technology Incorporated

August 1986

Prepared for
NATIONAL AERONAUTICS AND SPACE ADMINISTRATION
Lewis Research Center
Under Contract DEN 3-311

for
U.S. DEPARTMENT OF ENERGY
Conservation and Renewable Energy
Office of Vehicle and Engine R&D

DISCLAIMER

This report was prepared as an account of work sponsored by an agency of the United States Government. Neither the United States Government nor any agency thereof, nor any of their employees, makes any warranty, express or implied, or assumes any legal liability or responsibility for the accuracy, completeness, or usefulness of any information, apparatus, product, or process disclosed, or represents that its use would not infringe privately owned rights. Reference herein to any specific commercial product, process, or service by trade name, trademark, manufacturer, or otherwise, does not necessarily constitute or imply its endorsement, recommendation, or favoring by the United States Government or any agency thereof. The views and opinions of authors expressed herein do not necessarily state or reflect those of the United States Government or any agency thereof.

Printed in the United States of America

Available from
National Technical Information Service
U.S. Department of Commerce
5285 Port Royal Road
Springfield, VA 22161

NTIS price codes[1]
Printed copy: A09
Microfiche copy: A01

[1]Codes are used for pricing all publications. The code is determined by the number of pages in the publication. Information pertaining to the pricing codes can be found in the current issues of the following publications, which are generally available in most libraries: *Energy Research Abstracts (ERA); Government Reports Announcements* and Index (*GRA* and I); *Scientific and Technical Abstract Reports (STAR);* and publication, NTIS-PR-360 available from NTIS at the above address.

DOE/NASA/0311-1
NASA CR-175042
MTI 85SESD24

Ceramic Automotive Stirling Engine Program

Mechanical Technology Incorporated
Latham, New York 12110

August 1986

Prepared for
National Aeronautics and Space Administration
Lewis Research Center
Cleveland, Ohio 44135
Under Contract DEN 3-311

for
U.S. DEPARTMENT OF ENERGY
Conservation and Renewable Energy
Office of Vehicle and Engine R&D
Washington, D.C. 20545
Under Interagency Agreement DE-AI01-85CE50112

TABLE OF CONTENTS

Section		Page
1.0	PROGRAM SUMMARY	1-1
	1.1 Program Objectives	1-1
	1.2 Task Descriptions	1-3
	1.2.1 Task I - Concept Design	1-3
	1.2.2 Task II - Performance Evaluations	1-3
	1.2.3 Task III - Production and Cost Evaluation	1-3
	1.3 Program Summary and Conclusions	1-3
2.0	TASK I - CONCEPTUAL DESIGN OF A STIRLING ENGINE WITH CERAMIC COMPONENTS	2-1
	2.1 Design Approach	2-1
	2.1.1 Stirling Engine Background	2-1
	2.1.2 1981 RESD	2-5
	2.1.3 Objectives of Design Study	2-9
	2.1.4 Approach to Design Study	2-9
	2.2 Material Evaluations and Properties Summaries	2-12
	2.2.1 Group 1 Material	2-13
	2.2.2 Group 2 Material	2-15
	2.2.3 Group 3 Material	2-15
	2.3 Ceramics Guidelines Design and Processes	2-27
	2.3.1 Design of Ceramic Components	2-27
	2.3.2 Ceramic, as Opposed to Metallic, Design	2-27
	2.3.3 The Design Process	2-29
	2.4 Preliminary Design Concepts	2-36
	2.4.1 Design Considerations	2-36
	2.4.2 Existing Ceramic Heater Head Conceptual Designs	2-36
	2.5 Final Design Concept Description	2-43
	2.5.1 Heater Head	2-43
	2.5.2 Other Hot System Components	2-48
	2.5.3 EHS	2-48
	2.6 Heater Head Stress Analysis	2-50
	2.6.1 Introduction	2-50
	2.6.2 Stress Analysis Procedure of Ceramic Components	2-54
	2.6.3 Material Data	2-58
	2.6.4 Simplified Anlaysis Approach	2-58
	2.6.5 Stress Analysis of the Heater Housing	2-60
	2.6.6 Material Characterization from Thermal Transient Point of View	2-68
	2.6.7 Stress Analysis Based on Transient Loading Conditions	2-68
	2.6.8 The Manifolds from the Stress Point of View	2-78
	2.6.9 The Heater Tubes from the Stress Point of View	2-78
	2.6.10 Conclusions	2-78
3.0	TASK II - PERFORMANCE EVALUATIONS	3-1
	3.1 Preliminary Design Evaluations	3-1
	3.2 Final Design Optimization	3-4
	3.3 CASE Emission Considerations	3-11

PRECEDING PAGE BLANK NOT FILMED

Section		Page
4.0	MANUFACTURING COST STUDY	4-1
	4.1 Objective	4-1
	4.2 Cost Analysis Data	4-1
	4.3 Basis of Cost Analysis	4-2
	4.4 Manufacturing Cost Estimate	4-2
	4.4.1 Ceramic Material Costs	4-2
	4.4.2 Cost Summary for CASE Components	4-3
	4.4.3 Comparison of CASE and 1981 RESD Manufacturing Costs	4-3
	4.5 Manufacturing Technology	4-9
	4.6 CASE Costing Methodology	4-12
	4.6.2 Detailed Costing Methodology	4-12
	4.7 Engine Cost Comparison; CASE, 1981 RESD, and I.C	4-16
5.0	ADVANCED CASE DESIGN	5-1
	5.1 Opposed Piston	5-2
	5.2 Turbo-Compound Engine Concept	5-7
	5.3 Single Acting In-Line Concept	5-10
6.0	CONCLUSIONS AND RECOMMENDATIONS	6-1
	6.1 Recommendations	6-1
7.0	REFERENCES	7-1
8.0	APPENDIX A - DRAWINGS	8-1

1.0 PROGRAM SUMMARY

1.1 Program Objectives

The objective of the Ceramic Automotive Stirling Engine (CASE) Program has been to perform the conceptual design, performance analysis, and cost estimate of an automotive Stirling engine (ASE) which incorporates selected ceramic components into the 1981 Reference Engine System Design (RESD) developed under the ASE Program.

The use of ceramic components in Stirling engines has long been considered an attractive concept for several reasons, primarily associated with potential efficiency and cost benefits. The efficiency of a Stirling engine, as is true of all heat engines, is sensitive to the peak cycle temperature and the higher the cycle temperature, the higher the efficiency. Conventional Stirling engines utilize a metallic "heater head" to transfer heat from an external source (usually combustion gas) to the engine's internal working fluid. The metal temperature of the heater head therefore sets the resulting peak temperature and heat transfer into the working gas cycle. The maximum temperature that can be tolerated by metallic heater heads is in the range of 700-800°C. This limit is due to the reduction in strength and corrosion resistance which occurs at high temperatures in all metals. Those metals which exhibit good high temperature properties tend to contain large quantities of nickel, chromium, cobalt, and other strategic materials. However many ceramic materials retain significant strength and oxidation resistance up to 1100-1200°C. Most ceramic materials do not contain strategic materials and are made up of inexpensive minerals or raw materials (silicon, carbon, nitrogen, etc.). In addition, ceramic materials offer physical properties such as thermal conductivity which are outside the range of metallics. Obviously, the application of ceramic materials to the high temperature components of a Stirling engine appears to offer significant advantages. However, the use of ceramics in structural/high temperature applications introduces new concerns and design requirements which are specific to these types of materials. Unlike metals, ceramics are brittle materials and are sensitive to any cracks or flaws which occur in processing or use. The state of specification and property development of ceramic materials as engineered materials significantly lags similar applications using metallic materials. Thus the application of ceramics to the Stirling engine while offering many potential benefits, also entails a high degree of risk and technical uncertainty.

Based on the preceeding brief discussion of the application of ceramics to Stirling engines, the overall objective of the CASE program can be subdivided as follows:

1. Identification of ceramic materials having physical properties suited to the Stirling application.

2. Development of ceramic component designs which address the problem areas of ceramic properties, and are adaptable to mass production techniques. The major component to be evaluated will be the heater head, although other high temperature components, such as combustor parts, displacer domes and preheaters will also be included.

3. Evaluation of overall engine performance in a vehicle system to identify the impact on combined Federal driving cycle mileage.

4. Determination of materials and processes required for mass production and an estimate of the production costs. The estimated ceramic component costs should be compared to conventional metallic component costs.

5. Projection of material properties and identification of areas requiring development.

The basis for comparison and evaluation of the CASE design was the 1981 Reference Engine System Design (RESD) developed under the ASE Program. The CASE design is based on the 1981 RESD and utilizes the same basic engine configuration and frictional/auxiliary losses. In addition to the CASE design based on the 1981 RESD, an additional design concept (advanced CASE) was developed and evaluated. The advanced CASE concept was not based on the use of an existing design, such as the 1981 RESD. The design was specifically developed to make maximum advantage of the potential offered by advanced ceramic materials.

1.2 Task Descriptions

1.2.1 Task I - Concept Design

The objective of this task was to identify the ceramic materials suitable for the CASE design and develop an engine design based on the incorporation of these materials in a ceramic heater head. This task also includes the development of a preliminary stress analysis for the ceramic heater head, as well as a design guide for the use of ceramic materials, and identification of material standards. The development of an advanced CASE design was also performed as part of this task.

1.2.2 Task II - Performance Evaluations

The performance evaluation task included the assessment of the performance of the CASE design. It includes the development of engine maps and mileage projections.

1.2.3 Task III - Production and Cost Evaluation

The objective of the production and cost evaluation task was to perform a manufacturing study of each of the ceramic components in the CASE design. This task will evaluate the feasibility of mass production methods for the ceramic design based on 300,000 units per year. This evaluation will include a detailed cost estimate comparing the cost of the CASE design to conventional all-metal Stirling engine and conventional internal combustion (IC) engines.

1.3 Program Summary and Conclusions

As a result of the preliminary screening study, an annular heater head utilizing a tube and manifold design was chosen. The manifold material is a matrix composite comprised of mullite and silicon carbide whiskers. The tubes and fins are silicon carbide. The design was chosen based on several factors including: minimum hot mass, symmetric and highly effective heat transfer characteristics, low thermal conductivity to the cold end of the engine, and geometric characteristics amenable to mass production techniques.

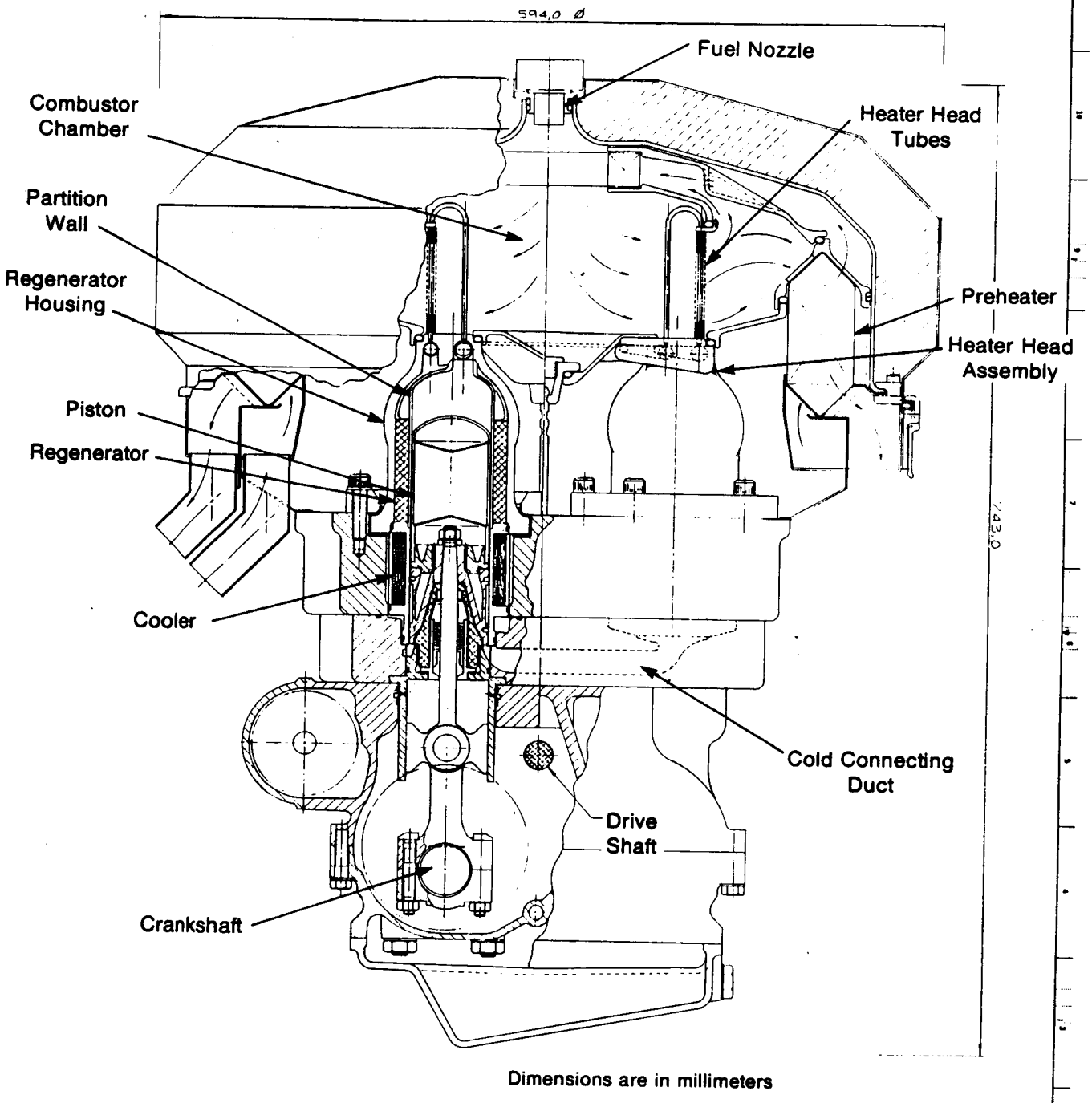


Figure 1-1 CASE Engine Layout

The overall engine layout incorporating the annular ceramic heater head is shown in Figure 1-1. Geometric sizing for this design was prepared for three basic groups of materials:

1. Silicon carbide housing/manifold and tubes
2. Silicon nitride housing/manifold and tubes
3. Mullite matrix housing/manifold and silicon carbide tubes.

Each of the three Groups represents progressive advancement in the state of ceramic development. The use of silicon carbide is considered fairly well developed today, while silicon nitride technology is less well developed. The mullite matrix materials are currently in the laboratory/experimental stage and will not reach the stage of development of silicon carbide for 10-15 years. In addition, each of these materials offers unique material properties. Silicon carbide and silicon nitride have good strength characteristics and relatively high thermal conductivities, while the mullite matrix materials have less strength and much lower thermal conductivity. The performance evaluation of each of the three material Groups is summarized in Table 1-1. This data is based on a heater head temperature of 1020°C (as compared to current metallic heater head temperatures of 820°C). The Group 1 design performance is somewhat worse than the 1981 RESD. This is primarily due to large conduction losses associated with the high thermal conductivity of silicon carbide. The Group 2 material design achieves performance approximately equal to the 1981 RESD, although the conduction losses are still high. The Group 3 material design results in a slight improvement over the 1981 RESD, resulting in a 2% improvement in peak efficiency to 44.4%. Based on the results of this comparison, the Group 3 design was chosen for final optimization. An optimization with regard to heater head temperature was carried out for the Group 3 design. The result of this analysis showed that combined vehicle mileage was essentially insensitive to heater head temperature between 1000 and 1200°C due to increased conduction and cold start penalty (CSP)*. The Group 3 design was optimized at a heater head temperature of 1020°C and an updated layout and a detailed stress analysis was performed on the heater head housing which contains the worst case stress conditions. A combined mileage of 39.9 mpg was predicted

*Cold start penalty (CSP) represents the amount of fuel required to bring the engine from a cold condition to operating temperature.

for the optimized Group 3 design, as compared to 37.6 mpg for the 1981 RESD using the latest United Stirling A.B. (USAB) vehicle performance model. This represents a 4.4% improvement on mileage.

In conjunction with the Carborundum Company, a manufacturing cost study was performed. The study was based on the use of injection molding/sintering (techniques used today for silicon carbide) methods for the fabrication of the mullite matrix/silicon carbide heater heads and other ceramic components used in the Group 3 design. The results of the manufacturing study indicate that significant cost savings could be realized for specific components such as the heater head. A comparison of selected component costs is shown in Table 1-2. However, the costs shown in Table 1-2 are projections based on substantial advancements in material processing and manufacturing techniques.

As an ancillary task, the evaluation of an advanced CASE design was performed. The advanced CASE design concepts were not constrained to a double-acting U-4 (1981 RESD) configuration. Thus, the advanced CASE evaluations included concepts such as single-acting designs, turbo-compounding, ceramic rolling element bearings and "hot" piston rings. The results of this study are discussed in Section 5.0 of this report.

The overall conclusions of this study can be summarized as follows:

- Performance improvements due to the use of ceramic materials in an engine based on the 1981 RESD results in a small (4.3%) mileage improvement over the all-metal 1981 RESD. Peak engine efficiencies are improved by ↶2% over the 1981 RESD, to 44.4% net.

- Cost improvements associated with the use of ceramic materials could be significant. However, this is based on the assumption that injection molding/sintering techniques for silicon carbide/mullite matrix materials become well developed in the next 10-15 years.

- The use of ceramics in conjunction with advanced engine features such as nonlubricated ceramic rolling element bearings, nonlubricated (or solid lubricated) ceramic piston rings and a pressurized crankcase can result in significant performance benefits. However, this advanced type of engine is

TABLE 1-1

PERFORMANCE COMPARISON OF ALTERNATE MATERIALS FOR CASE DESIGN

	1981 RESD	Group 1	Group 2	Group 3
Head Temperature °C	820	1020	1020	1020
Part Load Efficiency% (12 kW at 2000 rpm)	37.6	34.5	37.7	39.2
Full Load Efficiency%	34.2	33.3	35.2	36.9
Part Load Conduction Loss (kW)	1.6	4.9	2.4	1.5
Cold Start Penalty (grams of fuel)	134	126	119	116
Combined Mileage*	37.6	35.2	38.5	39.9

*Mileage projections per latest USAB model. Earlier models techniques predicted 41.1 mpg for 81 RESD, however, mileage modeling have been extensively improved since 1981, these results are all based on the most recent model.

TABLE 1-2

COST COMPARISON OF SELECTED CERAMIC COMPONENTS VERSUS METALLIC COMPONENTS IN 1981 RESD

Component	CASE Mfg Cost 1984 $	1981 RESD Mfg Cost 1984 $
Heater Head Assembly	153.09	575.23
Displacer Dome	24.06	80.83
Regenerator	166	429.56* (35.51**)

* stainless steel
**carbon steel (not technically acceptable)

radically different from the engines currently under development in the ASE Program, although selected features could be incorporated in ASE engines.

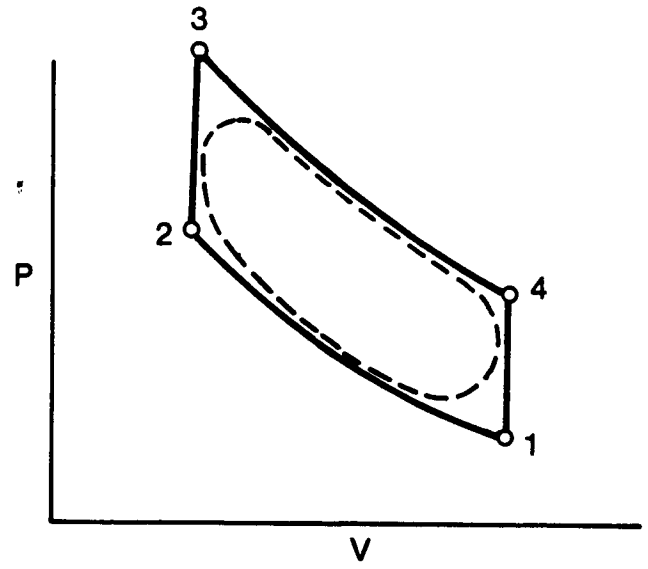
2.0 TASK I - CONCEPTUAL DESIGN OF A STIRLING ENGINE WITH CERAMIC COMPONENTS

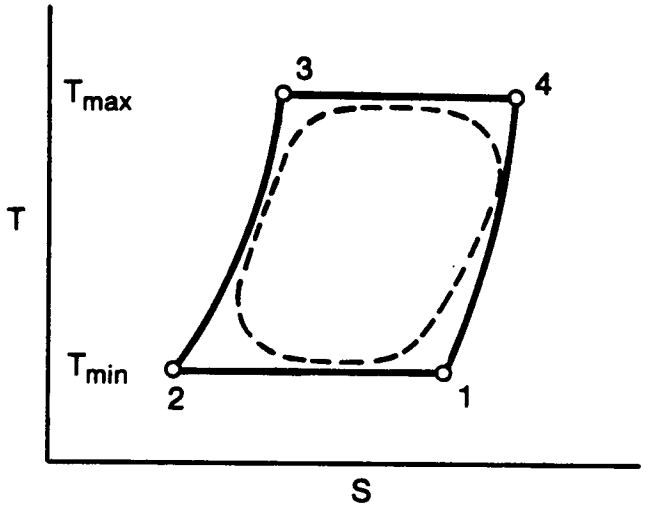
2.1 Design Approach

2.1.1 Stirling Engine Background

Stirling engines are heat engines which utilize a gaseous working fluid to approximate the idealized Stirling thermodynamic cycle. The engine consists of a closed working space containing a "hot space" and a "cold space", each of which can be made to vary in volume. The hot space and cold space are, in turn, connected by constant volume components called the cooler, regenerator, and heater. The volume of the cold space and hot space are made to vary, using pistons, such that the hot space volume is out of phase with the cold space volume. The cycle operates on the following general principle: while the working gas is in the cold space, it is compressed. The heat generated during the compression is rejected to the cooler, thus the compression is isothermal. The gas is then shifted from the cold to the hot space under constant volume conditions. This process forces the gas through the regenerator where stored heat from the previous cycle is absorbed by the gas. The gas is also forced through the heater where the gas temperature is further increased. When the gas is in the hot space, it is expanded. Heat is added during the expansion process so as to make the expansion isothermal. The gas is then shifted to the cold space through the heater and the regenerator, under constant volume conditions. During this process heat from the gas is stored in the regenerator. The gas is then cooled by the cooler before entering the cold space again and repeating the cycle. This ideal process is shown in Figure 2-1 in a P-V diagram and in a temperature-entropy (T-S) diagram. Since more power is generated during the expansion than is required for the compression, net power is generated by the cycle.

In actual practice the processes in a Stirling engine only approximate the ideal Stirling cycle process. For example, purely isothermal expansion and compression processes are impossible to achieve. Similarily, in real Stirling engines the heater, regenerator, cooler, and connecting manifolds all have finite volumes. Thus, some of the gas which remains in these volumes does not participate in the overall cyclic temperature varations. These nonideal effects result in an actual cycle as is also shown in Figure 2-1.





—— Ideal Stirling Cycle

1-2 Isothermal Compression — Heat Transfer from Working Fluid at T_{min} to External Dump

2-3 Constant Volume — Heat Transfer to Working Fluid from Regenerator

3-4 Isothermal Expansion — Heat Transfer to Working Fluid at T_{max} from External Source

4-1 Constant Volume — Heat Transfer from Working Fluid to Regenerator Matrix

— — — Real Stirling Cycle Machine

Figure 2-1 Stirling Thermodynamic Cycle

Although the ideal Stirling cycle operating between two temperatures (T-hot, or the heater temperature, and T-cold, cooler temperature) offers a cycle efficiency equal to an ideal Carnot cycle operating between the same temperatures, the effect of nonidealized processes and other unavoidable losses results in cycle efficiencies less than the ideal Carnot cycle. Despite the effects of nonideal processes in real Stirling engines, the basic efficiency of the engine is directly related to the maximum temperature (T-hot) of the engine, assuming that the heat rejection temperature (T-cold) is fixed. In general, Stirling engine efficiency is some portion of the corresponding Carnot efficiency, and subject to the same temperature influences. However, if the basic ideal Carnot efficiency is examined at high temperatures, as shown in Figure 2-2, it is evident that as higher temperatures are considered, the corresponding increase in Carnot efficiency becomes increasingly small.

If the loss mechanisms of the engine are examined, particularly those mechanisms which are known as conduction losses, it is noted that some losses are directly proportional to the temperature difference between T-hot and T-cold. These conduction losses are due to the direct conduction of heat from the hot engine components (i.e., heater head, and piston dome) to the cold engine components such as the water jacket and cooler. The magnitude of the conduction loss is thus a function of the materials, geometry and temperature difference.

In addition to conduction losses, the other loss mechanism associated with nonideal processes, such as hysteresis losses, mixing losses, and flow losses also vary with peak cycle temperature, thus some practical limits on engine efficiency should exist.

In actual practice, the peak temperature of the cycle is set by the maximum temperature of the heater head, since the heater head transfers heat into the cycle working gas. Because the cycle working gas must be contained at high pressures (up to 19 MPa in ASE designs), the heater head must act as a pressure vessel as well as a heat exchanger. In addition, the external surface of the heater head is exposed to combustion products and the attendant corrosion/oxidation problems. Clearly, from a materials standpoint, the heater head of a Stirling engine represents a difficult engineering problem.

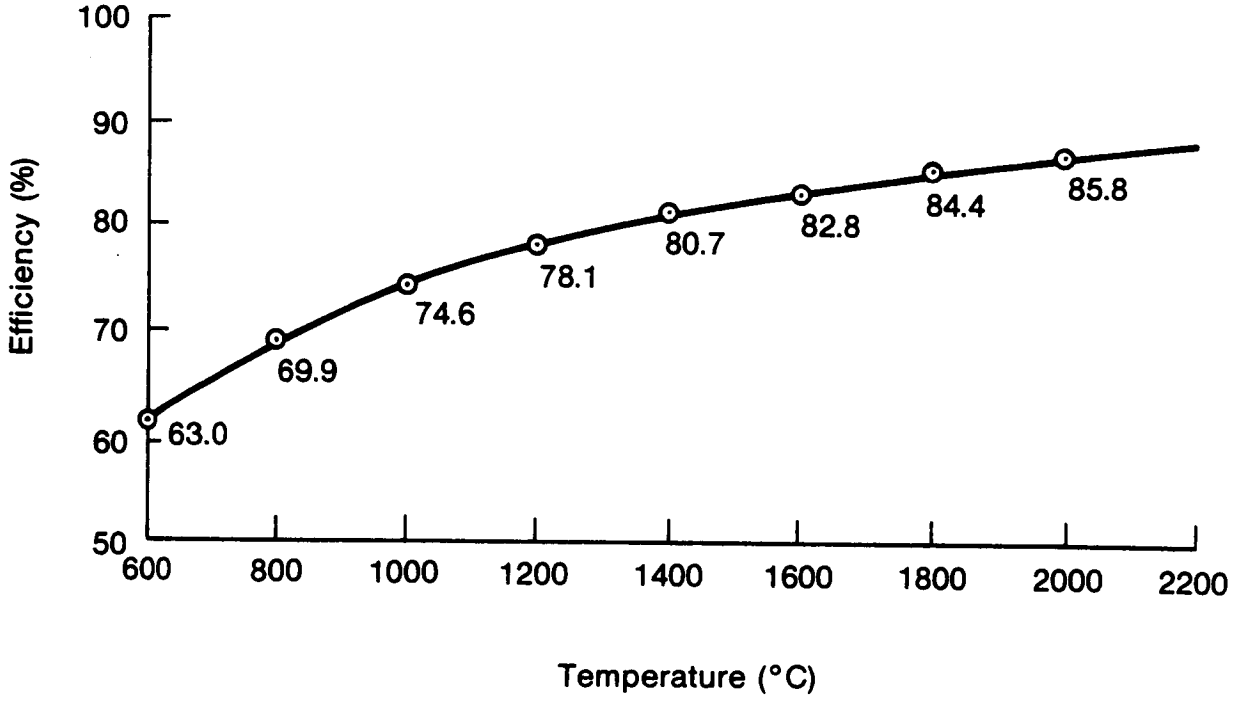


Figure 2-2 Ideal Carnot Cycle Efficiency versus Peak Cycle Temperature (Based on 50°C Rejection Temperature)

Currently high performance Stirling engines utilize tubular heater heads fabricated from nickel/chromium or nickel/cobalt superalloys. These materials tend to be creep limited to average heater head temperatures of 800-900°C. Although these heater head temperatures result in engines with peak net efficiencies in the 40% range, the use of metallic heater heads at these temperatures presents two basic limitations: 1) the use of superalloys for heater heads may be ultimately prohibitive from a cost standpoint for an automotive application; and, 2) the advancement of Stirling engine efficiencies is limited since peak temperatures are limited by material considerations.

2.1.2 1981 RESD

The design of the CASE engine is based on the general configuration of the ASE Program's 1981 RESD. The ASE program is an ongoing program at MTI, sponsored by NASA and DOE, with the objective of developing a Stirling engine for automotive use which will demonstrate a 30% improvement in fuel mileage over conventional internal combustion engines. In addition the program goals include the requirements that the engine developed be cost and performance competitive with conventional engines. Under the ASE program a RESD is periodically developed. The RESD concept represents a "paper design" which incorporates the most current engine concepts and approaches, and is a goal for the actual engine design and development activities. Thus the 1981 RESD represents the most advanced concepts which existed in the ASE program at that time.

The 1981 RESD is a four cylinder, four cycle Stirling engine arranged in what is termed a U-4 configuration. The four cylinders are connected to two crankshafts, which are in turn geared to a separate output shaft. A cross-section of the 1981 RESD is shown in Figure 2-3. The pistons in the design are double acting, with the space above the piston acting as the expansion volume, and the space below the piston acting as the compression space of the adjacent cycle. The regenerator and cooler of each cycle are contained in a separate housing connected to the cylinder housing by an involute tubed heater head. The double acting engine concept has been chosen for the automotive application because it offers high specific power which is important due to the packaging constraints required to fit the engine in a conventional automobile. Similiarly, the heater head of the ASE is designed to operate at high heat flux levels to minimize the size of the heater head, and

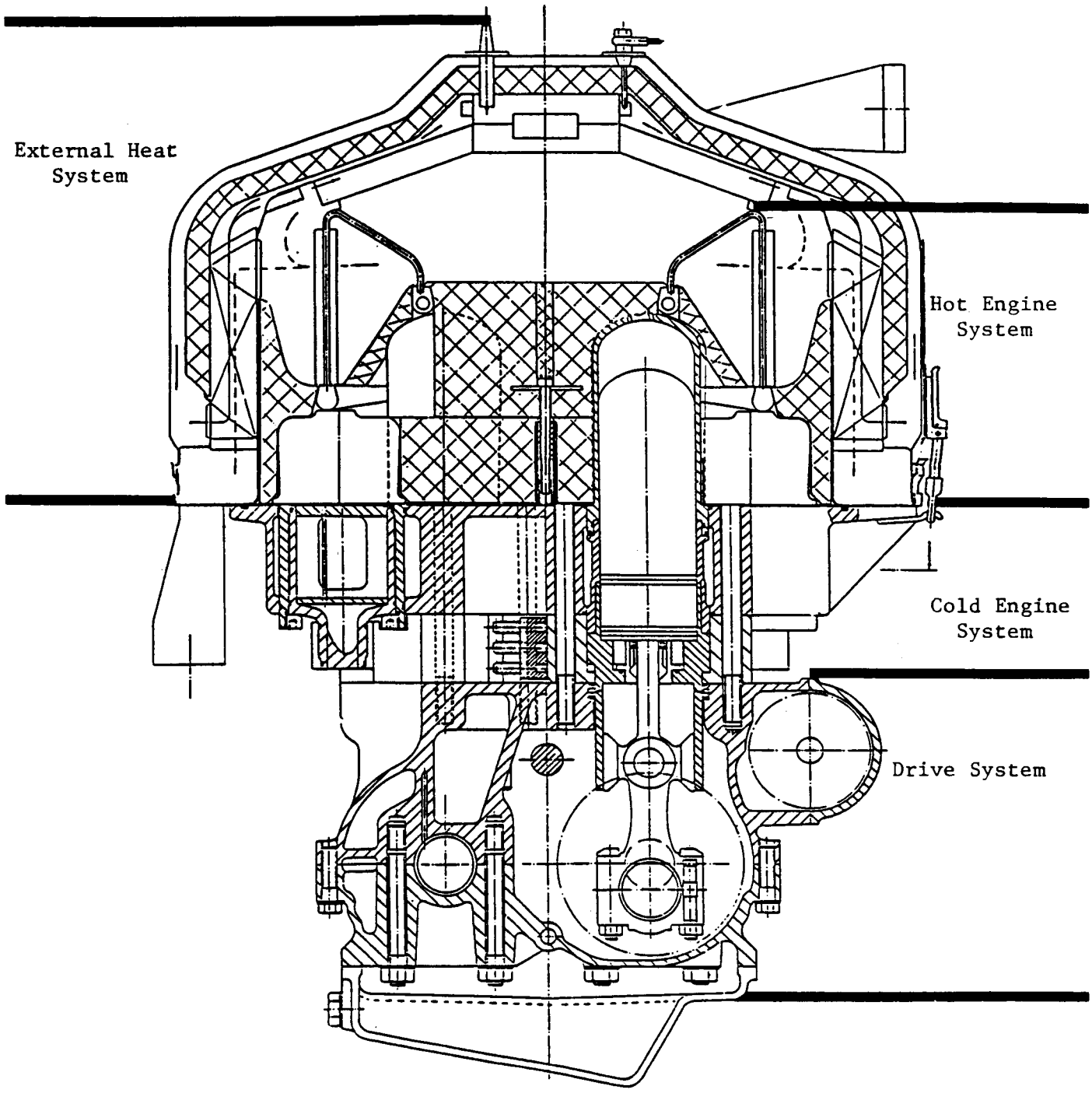


Figure 2-3 1981 Reference Engine System Design (RESD)

therefore the internal volume and mass of the heater tubes for a positive effect on engine performance and overall mileage.

The working volume of the engine is sealed at the piston rod by oil lubricated sliding seals. An external heat system (EHS) including a blower, a preheater, and a combustor provide heat to the heater tubes which operate at 820°C. A detailed description of the 1981 RESD can be found in Reference 1. A summary of the engine parameters for the 1981 RESD are shown in Table 2-1.

It should be recognized that optimizing an engine design (regardless of the type of engine) for an automotive application is not a straightforward task. Because the ultimate objective is to maximize mileage (as measured by specific EPA procedures) many factors and trade-offs must be considered. Although automotive mileage is clearly related to the efficiency of the engine, the relationship between the load characteristics and the engine efficiency characteristics must be matched to maximize the overall mileage. The average 3000 lb automobile duty cycle has an average engine operating point (AOP) at ~12 kW at 2000 rpm, while to provide required acceleration, a maximum power of 60-70 kW is needed. This is a wide range of power requirements. However, due to the low AOP the engine efficiency at the lower power range has a much greater impact on overall mileage. The impact of engine efficiency improvements must be considered not only at the peak efficiency point but over the entire automotive load range.

Another factor in maximizing the mileage of the engine-vehicle system is the CSP. This term refers to the urban cycle portion of the EPA driving cycle in which the engine is started from a "cold" condition. Since a Stirling engine must be brought to operating temperature before it can produce power, the amount of fuel which must be consumed then produces no mileage and may significantly decrease the overall urban mileage. To minimize the CSP the product of the mass and specific heat of the hot components must be minimized. This basically means that great care must be taken to minimize the size and weight of the hot components. It should be noted that the CSP is directly proportional to the peak engine temperature. Therefore, for equal sized engines the CSP will increase linearly with temperature. Another consideration in the evaluation of engine efficiency with increasing heater head temperatures is the effect of EHS efficiency. As heater head temperature is increased, overall EHS efficiency will decrease unless the effectiveness of the preheater is increased. Increasing preheater effectiveness

TABLE 2-1

PERFORMANCE OF THE REFERENCE ENGINE

FULL LOAD POINT	p = 15 MPa n = 4000 rpm	
Indicated Power		73.3 kW
Friction		9.6 kW
Auxiliaries		3.6 kW
Net Power		60.1 kW
External Heating Efficiency		90.5 %
Net Efficiency		34.2 %
PART LOAD POINT	p = 5 MPa n = 2000 rpm	
Indicated power		15.0 kW
Friction		2.0 kW
Auxiliaries		0.8 kW
Net Power		12.2 kW
External Heating Efficiency		91.7 %
Net Efficiency		37.7 %
MAXIMUM EFFICIENCY POINT	p = 15 MPa n = 1100 rpm	
Indicated Power		24.8 kW
Friction		2.2 kW
Auxiliaries		0.5 kW
Net Power		22.1 kW
External Heating Efficiency		92.4 %
Net Efficiency		43.5 %
LOW LOAD POINT	p = 5 MPa n = 1000 rpm	
Indicated Power		7.9 kW
Friction		0.9 kW
Auxiliaries		0.4 kW
Net Power		6.6 kW
External Heating Efficiency		89.8 %
Net Efficiency		36.4 %

above the current ASE levels is very difficult without developing a much larger preheater with the attendant increase in hot mass.

In addition to these mileage related issues the ASE must be physically capable of being packaged in a conventional automobile, meet all required automotive emissions requirements and have a life of over 3500 hours including over 50,000 start/stop cycles. Obviously, the automotive application requires a wide range of considerations in engine design, aside from high thermodynamic efficiency, which impact the vehicle mileage and overall commercial acceptability.

2.1.3 Objectives of Design Study

The objective of this study is to evaluate the feasibility of utilizing ceramic materials in place of metallic components in the high temperature portion of the 1981 RESD ASE. The potential benefits of this material substitution are two-fold: the use of ceramic materials for the engine heater head can produce improved engine efficiency due to higher cycle peak temperatures, and reduced conduction losses through engine hot components. A second, and perhaps more important benefit is the elimination of strategic materials and the possible reduction of manufacturing costs associated with ceramics.

2.1.4 Approach to Design Study

The prime component studied in this program is the engine heater head. This engine component is clearly the most critical component in terms of engine performance and is a major contributor to engine manufacturing cost. The heater head operates at maximum cycle temperature, must withstand internal pressures of up to 19 MPa (in 1981 RESD) and is directly exposed to combustion products. Currently the heater head contains the most strategic materials of any component in the engine. In addition, the heater head represents the most complex component in the engine, requiring complex castings for the regenerator/cylinder housings which must be brazed to the heater tubes/fins to form a leak tight pressure vessel. The design of the heater head must result in even working gas flow distribution among the heater tubes, while minimizing the "dead volume" in the connecting manifolds. The walls of the regenerator/cylinder housings and maniolds must be thick enough to contain the cycle pressure, yet the thickness must be minimized to limit conduction down the walls as well as thermal shock caused by

the rapid start-up transients. The outer surface of the heater head must be resistant to corrosion (and possibly erosion) by the combustion products, and capable of being finned to augment the heat transfer to the tubes.

The approach used in this study was to develop a heater head design that would isolate the effects of the materials change in the heater head. Overall changes to the engine configuration were limited to those required by the increased temperatures (use of ceramics in combustor and piston domes) or those required to make ceramic construction feasible. The auxiliary, drive, and cold systems were all maintained the same as the 191981 RESD except as required by specific aspects of the ceramic design. Several basic heater head configurations were considered to assess the feasibility of manufacture and develop qualitative comparisons regarding combustion gas flow, cycle gas flow distribution, hot mass and manifold volume ("dead volume") effects. Once the basic heater head configuration (annular regenerator with straight "U" heater tubes) was determined, the engine geometry was optimized utilizing the Stirling engine optimization code. This is the same procedure that would be used in the design of a metallic heater head. However, the optimization was performed using the mechanical properties of the ceramic material. These properties include the strength (based on a preliminary Weibull analysis), thermal conductivity and specific heat.

Initially a wide range of ceramic materials were reviewed to determine the appropriate materials properties, fabricability techniques and limitations, and the current state of development. As expected, the materials reviewed were in various stages of development varying from commercially available to experimental. As a result of this review, three basic material groups were identified each representing the potential state-of-the-art at various periods in the future.

Group 1 materials were identified as materials currently commercially available, having demonstrated and repeatable properties. These materials utilize the most recent forming processes which are well developed (injection molding) and appear adequate for the CASE geometry. These materials could be used to demonstrate the feasiblity of fabricating and operating a ceramic heater head. The material identified as meeting the Group 1 requirements is silicon carbide. Although this material represents the most advanced ceramic material in terms of fabricability and commercial maturity, the materials properties of silicon carbide are not well suited to a Stirling heater head. The thermal conductivity of the material is

quite high and significant conduction losses down the cylinder/regenerator housings could be expected. However, silicon carbide is relatively inexpensive and contains no strategic materials. In addition, the forming technology developed for silicon carbide is well developed and capable of producing complex shapes.

The second group of materials identified (Group 2) represents the best available current material properties without regard to the state of forming technology. The fabricability of these materials is assumed to be developed to the level of the Group 1 materials in the 5-10 year time period. These materials could be used to demonstrate the near term fabricability of a ceramic heater head, however, again these materials will not have the ideal properties for a Stirling engine. This group was based on the silicon nitride family of materials.

The third group (Group 3) will represent the best material properties available in noncommercial (i.e., experimental) form, and without regard to forming technologies. These materials represented the best combination of strength, fracture toughness, good thermal shock capability, and low thermal conductivity. This material group will be essentially "optimized" for the Stirling application. The forming and joining technology for these materials are assumed to be 10-15 years of continued development from maturity. The results of the design based on the Group 3 materials intended to show the potential for advanced ceramics in a Stirling application, and should act as a guide to the development of ceramics for high temperature Stirling applications.

Once the design optimization for the three materials groups was completed, design layouts and detail drawings of the ceramic components were generated. These detail drawings formed the basis of the manufacturing cost estimate performed by MTI and Carborundum, and are discussed in Section 4.0. The detail drawing of the CASE components were developed based on manufacturing recommendations from Carborundum regarding the size, shape, and tolerance of parts.

As an extension of the CASE design study, a preliminary design study addressing our advanced CASE study was performed. The objective of the advanced CASE effort was to incorporate the material and fabrication information developed during the CASE study into an advanced ceramic design not limited to the 1981 RESD configuration. The advanced CASE design (discussed in Section 5.0) incorporated a number of design features which are clearly developmental in nature. However, the

performance gains associated with the advanced CASE design may justify the development of those technologies.

2.2 Material Evaluations and Properties Summaries

As previously discussed, the conditions imposed on the ceramic in the heater head and manifold components are the most demanding of any of the components in a Stirling engine.

The material chosen for these parts must be resistant to thermal shock, impermeable to pressurized hydrogen at a T_{max} of up to 1100°C and possess strength sufficient to sustain internal pressure of 30 MPa (ASE proof pressure). In addition, the selected ceramic must belong to a material system mature enough to allow for its fabrication to the complex configurations of the heater head and manifold.

Initially a wide variety of ceramic materials were considered for use in the CASE design. These groups included: silicon carbides, silicon nitrides, alumina, zicronia, and mixed oxides (MgO, Si_2O and Al_2O_3). Each of these materials was reviewed with respect to strength, conductivity, thermal shock resistance, Weibull modulus, fracture toughness and maturity of forming and processing technology. On the basis of these considerations, the three material groups were identified as providing a progression of properties from those available today to materials with properties well suited to Stirling engines, but not expected to be available for 10-15 years.

Three materials were chosen for the heater head and manifold components. A reaction-bonded silicon carbide (RB-SiC) was selected for the Group 1 engine, a sintered silicon nitride (SSN) for the Group 2 engine, and a SiC whisker reinforced mullite matrix composite was chosen for the Group 3 engine concept. Each of these materials belongs to a separate "family" of ceramics and as such displays differences in physical and mechanical properties. Additionally, the processing capabilities associated with each have been developed to varying levels of maturity. For purposes of this report it was necessary to project developments in the areas of properties and processing over a specific time period for the materials considered. These projections are based on the direction and stated objectives of numerous developmental activities currently underway which are aimed at advancing

the state-of-the-art of structural ceramics specifically for automotive engine applications.

2.2.1 Group 1 Material

The Group 1 CASE concept is based on ceramic technology which is commercially available today. From considerations of both property maturity and processing maturity, a RB-SiC material appeared to be the most viable ceramic available for implementation into an ASE. Specifically selected for this study was a grade of material developed by Carborundum Company and referred to as KX-03. It is an advanced version of the commercially available KX-01 RB-SiC and consists of ultrafine grain SiC powder with a 10% free silicon intergranular phase. Test bar data for this material shows improved properties over the KX-01 grade, particularly at elevated temperatures. Additional work, however, is required to ensure a good translation of these improved properties to actual engine components. The property data presented for this material in Table 2-2 is based on a combination of both observed and projected values. The excellent high temperature properties of this material are derived mainly from the existence of an intergranular silicon metal phase which softens at elevated temperatures. The softening of this phase allows for the blunting of potentially critical flaws as well as the arrest of propagating cracks.

The effects of the silicon phase are manifest in values of flexure strength, Weibull modulus and K_{IC} which increase with temperature to 1200°C. Beyond this temperature, the load sustaining capability of the material begins to decrease rapidly as softening of the silicon phase predominates.

For the Group 1 CASE, all other structural components in the EHS portion of the engine are to be similarly fabricated of KX-03 RB-SiC. Various plastic forming techniques would be used to manufacture these parts and are described in Section 2.3. The high thermal conductivity behavior of this material makes it especially attractive for the heater tubes and fins, where the transfer of heat from the combustion gases to the working fluid occurs. Though the high conductivity is considered a detriment to the function of the heater head (conduction of heat down the wall of the heater head to the cold section of the engine causes significant thermodynamic losses in the ASE) it provides a distinct advantage to combustor

TABLE 2-2

PROPERTIES OF KX-03 REACTION BONDED SiC

Density - kg/m^3	3100
Flexural Strength - MPa (4PT)	RT - 655; 1200°C - 758
Weibull Modulus	RT - 10; 1200°C - 16
Young's Modulus - MPa	RT - 3.86×10^5; 1200°C - 3.52×10^5
Poisson's Ratio	.127
Ultimate Compressive Strength - MPa	3450
KiC - MPa $m^{1/2}$ (single edge notched beam)	RT - 4.97 1000°C - 5.04; 1200°C - 5.74
Coefficient of Thermal Expansion - $10^{-6}/°C$	RT - 500°C - 3.44 500°C - 1400°C - 5.02
Specific Heat - J/kg-°C	RT - 712 600°C - 1089; 800°C - 1173; 1000°C - 1257; 1200°C - 1341
Thermal Conductivity - W/m-°C	RT - 88 500°C - 54; 800°C - 46; 1100°C - 41

components by minimizing "hot spots" which very often contribute to failure via thermomechanical stress generation.

2.2.2 Group 2 Material

For the mid-term CASE concept (Group 2), SSN was selected as the candidate material for the heater head and EHS components of the engine. Considering the current level of research activity with this material aimed at improving its properties and associated processing technology, it seems reasonable to predict that within a five year time period fabrication of CASE components will be feasible. This material is attractive for engine component manufacturing due to its ability to be formed to near net shape without the application of pressure to cause consolidation.

A commercially available SSN material was chosen to serve as a basis from which projections of enhanced material properties could be made. SNW-1000, a version of SSN, developed and produced by GTE Laboratories served as the base for these property projections which are listed in Table 2-3.

These projected properties, particularly the values of Weibull modulus and strength, are believed to be realizable should the size and frequency of processing related flaws be significantly reduced. In order for this to occur, the complex relationship existing between various sintering aids, processing parameters and resultant microstructures must be thoroughly understood. Recent advances made in understanding this relationship lend a good degree of credibility to the projected values.

As in the Group 1 CASE, all components in the heater head and external heating system of the Group 2 CASE are to be fabricated of the projected SSN. Plastic forming methods similar to those assumed for the fabrication of components of the Group 1 CASE would be utilized to fashion the SSN material to the desired configurations.

2.2.3 Group 3 Material

In selecting a structural ceramic material for the Group 3 CASE, a great deal of latitude existed due to the extended range allowed for projecting material capa-

TABLE 2-3

PROPERTIES OF SINTERED SILICON NITRIDE

Density - kg/m^3	3240
Flexural Strength - MPa (4-PT)	RT - 655; 1200°C - 517
Weibull Modulus	RT - 15; 1200°C - 20
Young's Modulus - MPa	RT - 2.76×10^5
Poisson's Ratio	.23
Ultimate Compressive Strength - MPa	4138
KiC - MPa $m^{1/2}$ (single edge notched beam)	RT - 3.9 1000°C - 4.9
Coefficient of Thermal Expansion - $10^{-6}/°C$	RT - 600°C - 2.9 RT - 1000°C - 34
Specific Heat - J/kg-°C	RT - 810 220°C - 990; 440°C - 1060; 680°C - 1120; 880°C - 1140; 1100°C - 1170
Thermal Conductivity - W/m-°C	RT - 28 500°C - 19; 800°C - 16; 1100°C - 14

bilities. Since the Group 3 CASE is based on materials technology projected to 1995, the most recently emergent class of ceramic materials having the properties desired was targeted for implementation into CASE. A silicon carbide (SiC) whisker-reinforced mullite matrix composite material was specifically chosen for this application from a relatively large field of developmental ceramic matrix composites. Mullite is characterized as a mixed oxide type of ceramic being composed of $3\ Al_2O_3 \cdot 2\ Si_iO_2$. Preliminary laboratory investigation of this specific composite material conducted at Oak Ridge National Laboratory (ORNL) has yielded some basic physical and mechanical property data. This is presented in Table 2-4, as are additional properties projected to be attainable for this material by 1995.

The increase in fracture toughness for whisker reinforced matrices over continuous fiber reinforced matrices makes whisker reinforcement a very attractive option for enhancing ceramic material properties. Additionally, a reinforced ceramic component subject to mechanical loading has the ability to undergo a high degree of strain-to-failure and thus warn of impending catastrophic component failure.

The phenomenon of fracture toughening enhances the reliability of a ceramic component regardless of the nature of the in-service stresses. It should be noted, however, that numbers for fracture toughness in reinforced ceramic composites may be somewhat misleading since the measurement of toughness has little meaning in a material where complete separation of two surfaces cannot be accomplished. For whisker reinforced ceramic composites, the forming of complex geometries is much less restrictive than that for continuous fiber composites. This is due to the fact that continuous fiber composites must be "wound" over a mandrel to maintain a specified orientation. In contrast, with whisker reinforced ceramics the fiber are mixed with the unsintered matrix material and the composite mixture can then be injection molded into complex shapes. Also, if a critical aspect ratio of the whisker is maintained, whisker reinforced composites have been shown to display higher fracture toughness behavior than do continuous fiber ceramic matrix composites (Reference 2).

It is being assumed for this report that the various plastic forming processes proposed for forming components of RB-SiC and SSN could also be used for forming components of this material. Obviously, a great deal of development work remains to be completed before reliable processing of this material would be possible. To allow for exploitation of this whisker reinforced mullite in a CASE application, a

TABLE 2-4

2% VOLUME SiC WHISKER - MULLITE MATRIX COMPOSITE

Density - kg/m^3	2600
Flexural Strength - MPa (4-PT)	RT - 445; 1200°C - 445
Weibull Modulus	RT - 20; 1200°C - 20
Young's Modulus - MPa	RT - 1.40×10^5
Poisson's Ratio	.25
KiC - MPa $m^{1/2}$	RT - 4.6; 1000°C - 4.6
Coefficient of Thermal Expansion - $10^{-6}/°C$	RT - 1000°C - 2.9
Specific Heat - J/kg-°C	RT - 629 200°C - 922; 400°C - 1068; 600°C - 1127; 1500°C - 1349
Thermal Conductivity - W/m-°C	RT - 5.5 300°C - 5.2; 575°C - 4.3; 850°C - 4.0 1100°C - 3.8; 1250°C - 3.8

good understanding of the fiber/matrix interface characteristics and the resulting stress state is essential.

The tubes and fins for the Group 3 CASE are projected to be made of RB-SiC, where the high conductivity of the material would be advantageous. This presents an additional consideration of joining of the RB-SiC tubes to the SiC-mullite matrix manifold.

It should be noted that significant development will be needed to optimize the joining mechanism between the mullite matrix housing and the silicon carbide tubes. However, a mullite-cordierite composition has been developed which precisely matches silicon carbide's coefficient of thermal expansion. The control of the expansion coefficient is essential in the joining of dissimilar ceramics. Clearly, this case will require an extensive amount of development, although is considered ultimately feasible.

The large components comprising the combustor shell in the Group 3 CASE design are envisioned as beng composed of a lightweight SiC composite. This composite would be constructed in such a way as to result in a cellular SiC core with a very thin skin layer of a SiC matrix composite. The porous SiC would provide structural integrity while displaying good strength/weight characteristics, and the SiC matrix composite covering would render the structure impermeable to gas flow and thus prevent leakage. The cellular structure combined with the high strength composite outer layer would minimize the risk of thermal stress damages which might be expected in such large combustor components. Additionally, by containing the porous SiC between two thin layers of a SiC composite an insulative effect would be enhanced, and the potential for conductive heat losses through the structure is reduced.

2.2.3.1 Preheater. The combustion air preheater selected for this study and projected for use in all three of the CASE engine concepts is a compact counterflow heat exchanger made of a low expansion oxide ceramic. The properties of this material, whose composition is proprietary to Coors Porcelain Company, are listed in Table 2-5. This material was designed specifically for heat exchanger applications in that it is plastically formable and displays excellent resistance to corrosion and thermally induced stress damage. The technology for manufacturing preheater modules as depicted in the design layout of the CASE has been demon-

TABLE 2-5

PROPERTIES OF COORS CORDIERITE (266 M)

Modulus of Rupture	(MPa)	RT	158.6
Modulus of Elasticity	(MPa)		144.8×10^3
Specific Heat	(J/kg-°C)	RT	880
		593°C	1048
Thermal Conductivity	(W/m-°C)	RT	3.1
		593°C	2.6
Thermal Expansion		RT-600°C	1.48×10^{-6}/°C

strated in a joint effort between MTI and Coors Porcelain Company. This effort is currently continuing with the objective of incorporating preheater modules into the Mod II ASE. Improvements on the existing technology can therefore be expected during the next five to ten years.

2.2.3.2 Regenerator. Two different regenerator materials are proposed for the CASE study each to exist in an identical geometrical configuration. The configuration of the regenerator assumes a series of screens woven of the candidate material in a tightly controlled orientation so as to maintain pores of equal hydraulic diameter. The screens are then stacked on top of one another. Depending upon the material comprising the weave, additional processing is done to consolidate the points of contact between the screens and impart some structural integrity to the screen layup.

In considering currently available materials (Group 1) for the regenerator weave, Inconel 625 wire was selected. The technology for manufacturing a highly controlled weave with this material exists, though its long term durability at the temperature extremes projected is suspect. Performance testing of a higher temperature material (ceramic SiC reticulate foam) for a regenerator application has been conducted at MTI as part of the ASE Development Program. Results indicated performance penalties associated with both the physical properties of the ceramic and the nonuniform geometry of the pore network within the ceramic reticulate foam. It is proposed for the longer term CASE concepts (Group 2 and Group 3) that a ceramic fiber material be substituted for the Inconel wire and fashioned into a regenerator in a similar manner. Suitable for this application would be a yarn of Nextel Fiber* which consists of many small (11 μm) fibers wound to form a single thicker (55 μm) strand.

Currently, 76 μm Nextel Fiber manufactured in this manner is commercially available. For the purposes of this study, it is reasonable to assume that 55 μm fiber could be wound. A more critical assumption is that the fibers can be woven into a screen configuration having well controlled directional orientation of the fibers. The screens would then be stacked to the required porosity. However no basic technology limitations seem to exist in developing this type of regenerator.

---

*a product of the 3M company

2.2.3.3 Hydrogen Permeability/Interaction on Candidate Ceramics. An important issue in considering materials to be used as heater head components in the CASE design is the compatability of these materials with the Stirling cycle working fluid. Since the working fluid in the RESD engine is commercial grade hydrogen a survey of the literature was conducted to help determine the suitability of the candidate ceramic materials for use in a hydrogen environment. Though research on this topic has not been extensive, the survey did yield some information relevant to this study. Specifically, SiC displays a relatively low permeability to hydrogen in the temperature range of 1200-1450°C at pressure of 2-50 kPa. A second finding was that mullite reacts with H_2 to cause degradation.

A study to evaluate hydrogen transport parameters in nonmetallic materials for fusion reactors generated H_2-permeability data for KT-SiC tubes (Reference 3). KT-SiC is a commercial grade of RB-SiC manufactured by the Carborundum Company, similar to the Group 1 KX-03 RB-SiC except for a coarser grained microstructure and the resultant lower mechanical properties. In this study, hydrogen diffusion through tube sample walls was monitored at various temperatures by the detection of tritium used as a tracer in a H_2 gas mixture. The H_2 diffusion coefficients were obtained by fitting to an analytical expression, the measured kinetic permeation rates through the tube. Following a permeation run, the investigators were able to remove the hydrogen from inside of the sample tube and to apply heat to drive out the tritium and hydrogen absorbed in the walls. The total amount of tritium released from the tube yielded a value of hydrogen solubility.

The hydrogen permeability behavior of the KT-SiC observed in this investigation is shown in Figure 2-4.

Diffusion coefficients were determined by fitting the time dependent permeation rate of hydrogen to the rate predicted by classical diffusion theory. This procedure yielded the diffusion data shown in Figure 2-5.

The results reported in this study allowed the following conclusions to be drawn:

> The hydrogen permeability in KT-SiC is two orders of magnitude less than the least permeable of the refractory metals.

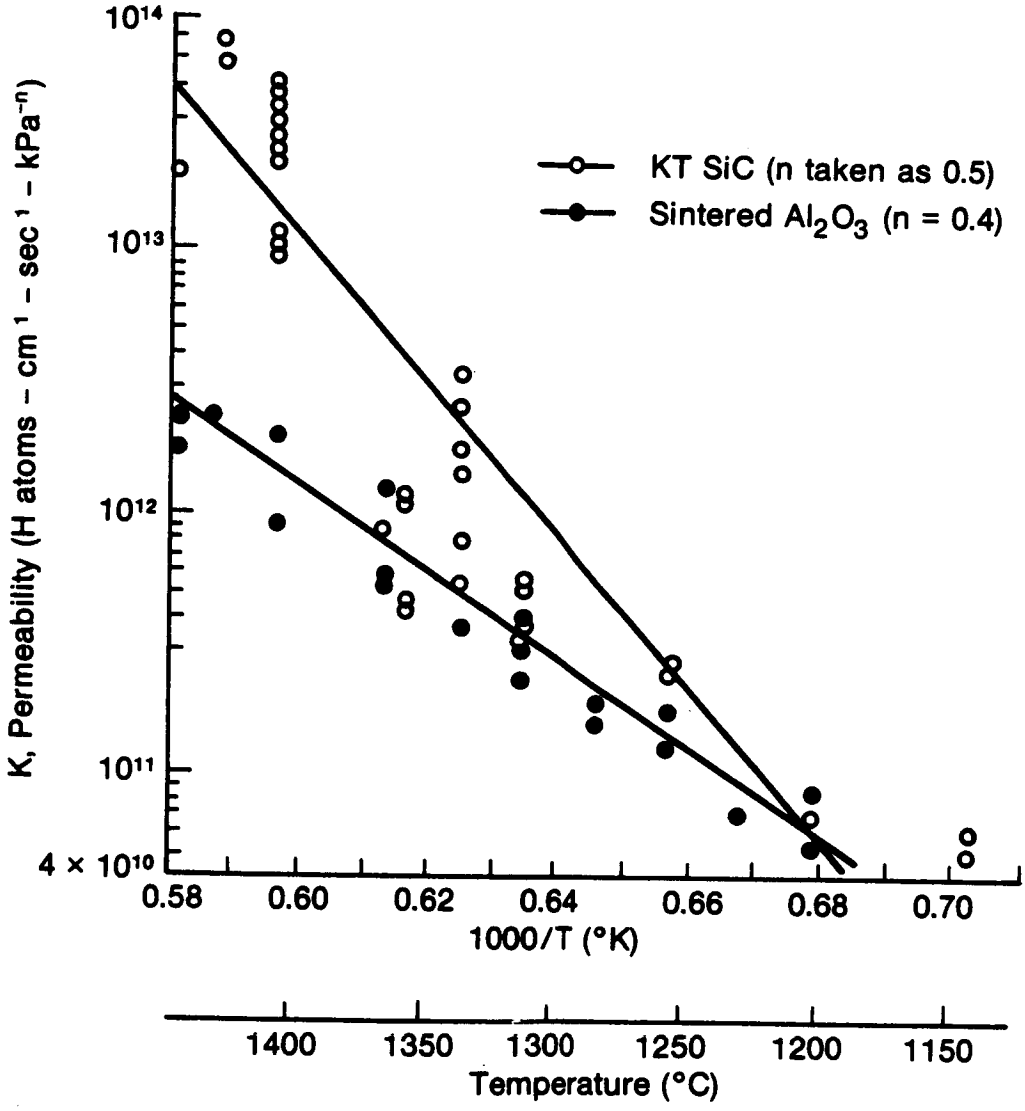


Figure 2-4 Hydrogen Permeability of KT-SiC and Sintered Al_2O_3 at 102.3 KPa

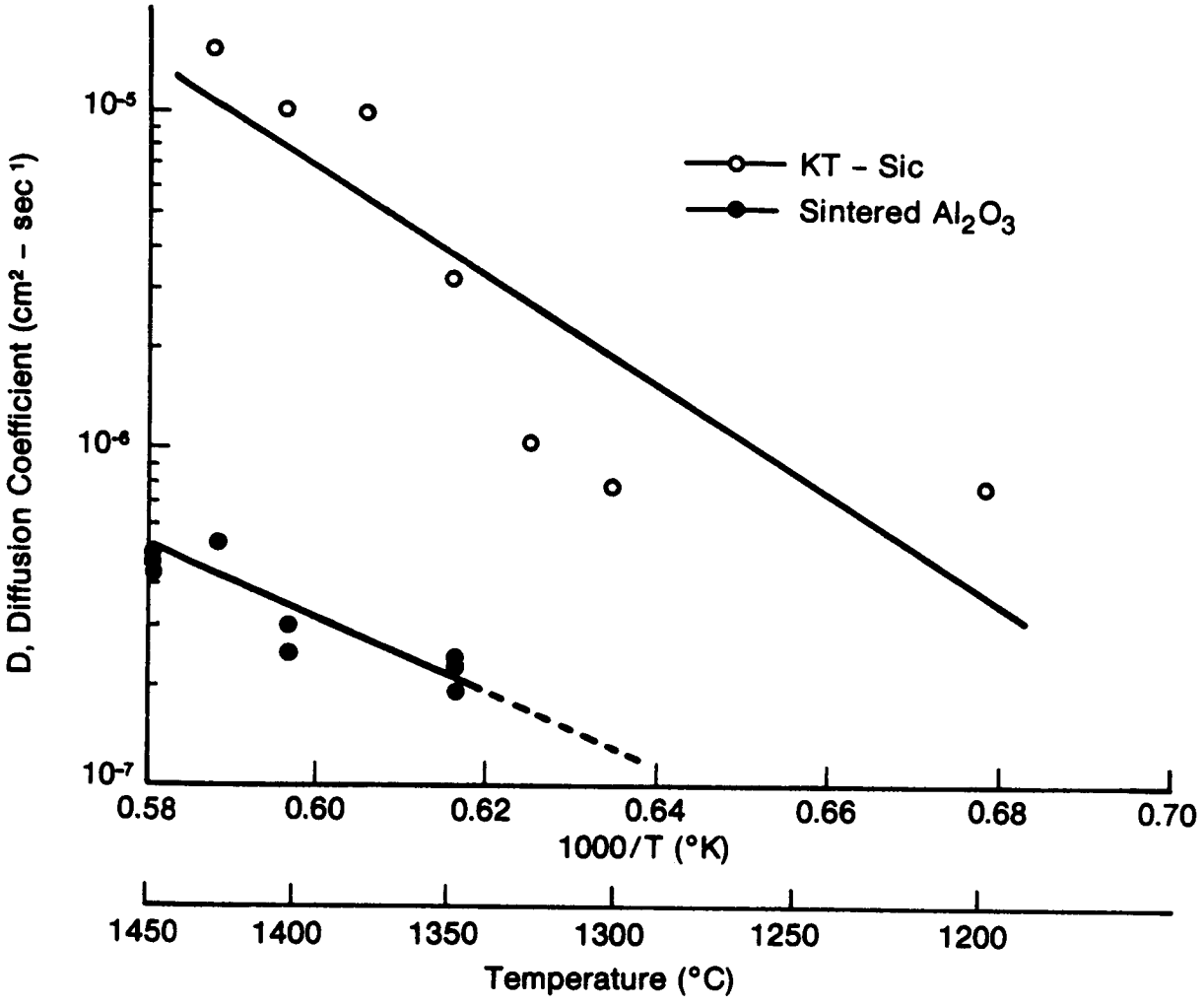


Figure 2-5 Hydrogen Diffusion Coefficients in KT-SiC and Sintered Al_2O_3

- For the KT-SiC, the measured permeability values are approximately an order of magnitude higher than the value predicted on the basis of diffusivity and solubility values in vapor-deposited B-SiC, implying some hydrogen migration along grain boundaries and other microstructural defects.

From these conclusions it may be surmised that the KX-03 material, with its finer grained microstructure and associated increased grain boundary area, would display a slightly higher permeability than the KT-SiC material evaluated in this study. Further investigation of the KX-03 material is necessary to determine hydrogen permeability and interaction at the 15 MPa hydrogen pressures anticipated for the CASE application.

For the Group 2 material, sintered silicon nitride, no literature references could be found which addressed the issue of hydrogen permeability and interaction. An investigation similar to that conducted for the KT-SiC would be quite appropriate for this material.

A limited treatment of the effects of hydrogen on mullite (the matrix material of the ceramic composite projected for the Group 3 CASE) was found (in Reference 4). Clearly identified in this study was the propensity of hydrogen gas (99.999% pure and a dew point of -84.4°C) to react with mullite in the experimental temperature ranges of 1350 to 1500°C. The reaction layer formed by this interaction consisted of α-Al_2O_3 residue but is not the rate limiting step in the reaction. A composition profile through the reactant layer seemed to indicate that the actual reaction of the hydrogen with SiO_2 is rate limiting. A graph of weight loss versus time for mullite from 1350 to 1500°C is shown in Figure 2-6. The investigators attempted to sinter the porous αAl_2O_3 into a dense layer to act as a protective barrier. These efforts, however, did not prove completely successful as cracking of the sintered layer occured upon cooling.

Much work remains to be completed in order to understand the interactive effects of hydrogen and mullite. Of particular interest would be the effect of water vapor on the kinetics of the reaction between hydrogen and mullite. Despite these potential problems, the use of reinforced mullite matrix remains the most attractive option for ceramic heater head material. Additionally, further efforts to develop a durable sintered αAl_2O_3 reactant layer should be conducted, as should an investigation of potential protective coatings for the mullite material. At the

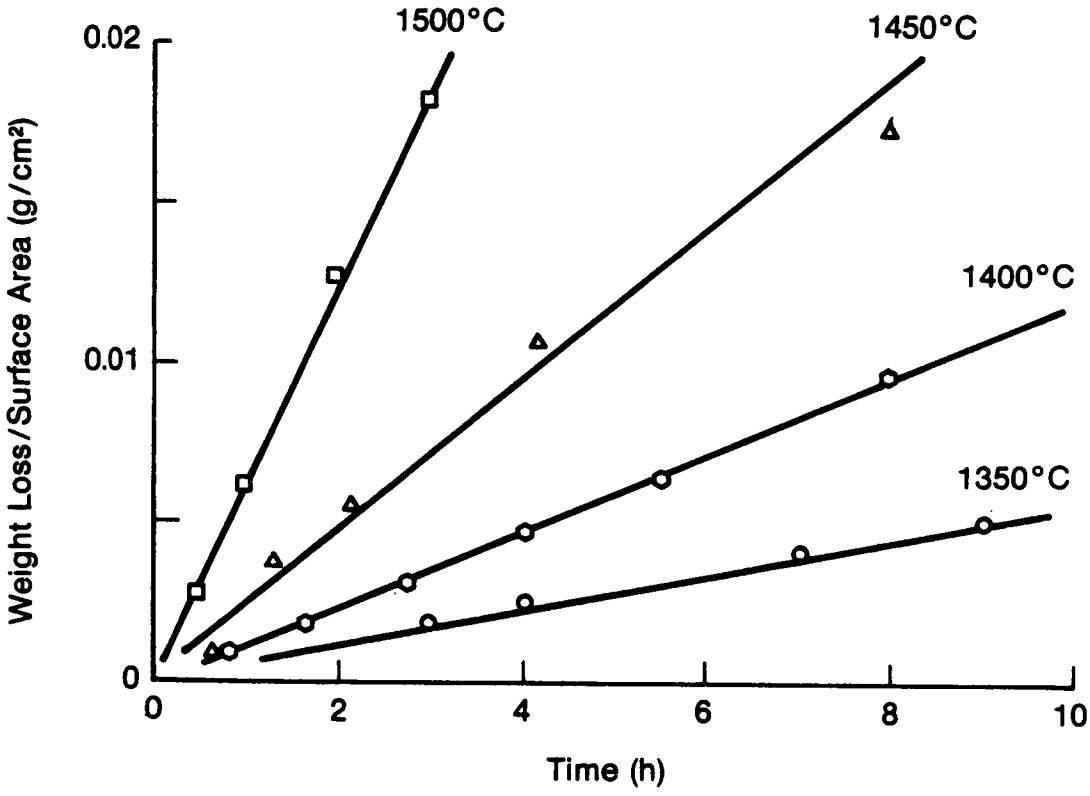


Figure 2-6 Weight Loss versus Time Mullite from 1350 to 1500°C in Flowing H_2 Gas

time of this report, research is underway at NASA/LeRC addressing the effect of H_2O content in hydrogen on the reaction of hydrogen with mullite.

2.3 Ceramics Guidelines Design and Processes

2.3.1 Design of Ceramic Components

To ensure the successful design of a ceramic component, not only must a designer be aware of the demands an application will require of the component; he must also understand the fundamental aspects of brittle material design. This often requires a certain degree of re-education for designers considering their familiarity and experience with the design of metal components. The following section will discuss some basic elements and philosophies appropriate to designing with advanced ceramics for severe mechanical environments. This discussion will be topical in nature and is derived from a treatment on the design aspects of advanced ceramics written by R.N. Katz of Army Materials and Mechanics Research Center (AMMRC).

2.3.2 Ceramic, as Opposed to Metallic, Design

Ceramics materials, even those which claim the distinction of being high performance ceramics, are brittle. Brittle does not imply weak, but rather that failure occurs at a low amount of strain even on the scale of the smallest subelement of the component. Metals, on the other hand, have sufficient capacity for plastic deformation to redistribute loads on a microscopic basis in the presence of stress concentrations. This gives them the ability to accomodate large strains, at least locally, which is not true of ceramics. As a consequence, ceramics are extremely sensitive to any condition which creates a stress concentration where the local peak stress might exceed the strength of the material, even though the average stress would be well below the material's strength. Therefore, ceramic materials are very sensitive to internal and surface flaws, point loads and thermal gradients which cause stress gradients. To assure the integrity of a ceramic component it is essential to maintain very close control over the development of the ceramic microstructure, machining and surface treatments, load transfer between various portions of the structure, and thermal loading of the component.

Since, by their nature, ceramic materials are not ductile, they cannot (in general) be subjected to the secondary thermal-mechanical processing (cold working, hot working, heat treatment, etc.) effective in metals processing at reducing or eliminating flaws. Thus, the microstructure and flaw distributions which result from the primary processing of ceramic components will be present for the life of the part. Each primary ceramic fabrication technique (i.e., slip casting, injection molding, dry pressing, tape forming, etc.) will produce its own unique flaw population. The key to understanding process control and its effect on this flaw population is in recognizing the critical interdependence of the sequential processing steps. The results from any step in a process are strongly influenced by all of the previous steps. For example, any flaw introduced during powder consolidation will be present after sintering. Thus, reproducible and reliable processing (and properties through the microstructure) require an understanding and control of each manufacturing step. Machining processes are an additional source of flaws in ceramic components and the surface flaws imparted by these processes provide the most severe stress concentrators in the form of cracks.

The reduction in strength resulting from the existence of cracks is described generally by the following relationship:

$$\sigma = \text{Constant } K_{IC}\ C^{-1/2}$$

where K_{IC} is the fracture toughness (an intrinsic materials property which defines the resistance to crack propagation), σ is the fracture stress and C is the flaw (crack) size. A distribution of flaws will create a distribution of strengths throughout the component. The distribution is greater in ceramics than in metals due to the inability of the ceramic to yield locally and reduce the severity of the flaws. Thus, a corollary of brittleness is a comparatively wide strength distribution. Since it is imperative to define this distribution accurately, many more strength measurements are required in the case of ceramics as contrasted to metals. Such strength distributions lead to a fundamental difference in the design philosophy between ceramics and metals. Namely, while conventional metallic design is deterministic, ceramic design is probabalistic. The strength of most metals is treated as a fixed value, (in instances where some variability exists, design allowables are set at 1, 2, or 3 standard deviations below the average strength) while the strength of a ceramic is given as a probability function (and the design allowable then transforms into an acceptable probability of

failure). In the limit, both methods converge since setting a design level based on some number of standard deviations of a fixed average value is also setting an implicit probability of failure. What this suggests is that what is implicit in metals design, becomes explicit in ceramic design.

2.3.3 The Design Process

From the previous discussion, it is clear that design with brittle materials requires a precise definition of the state of stress at every point in the component. Successful brittle material design of components in highly stressed applications should begin with the careful application of two- and three-dimensional computerized finite element thermal and stress analysis techniques. These analyses are at the core of the materials/design/engineering trade-off process shown schematically in Figure 2-7. To a first approximation, the additional complexity that designing on a probabalistic basis brings to the design process is that for each element in the finite element grid, a distribution of values rather than a fixed value is inputted for strength. From here, the design is developed until an acceptably low probability of component (or system) failure is attained. Because of the high level of precision required in defining local stresses and stress gradients in a ceramic component, a much finer finite element grid is required with ceramics than with metals.

Though finite element design codes developed specifically for ceramics have been successfully verified, the designer of ceramic components must still rely heavily upon the use of "rules of thumb" to serve as initial design guidelines. The following "rules of thumb" were used in designing components for the CASE layout and proved to be useful in evaluating some of the preliminary designs.

1. Avoid Point Loads - To minimize stress in areas where loads are transferred, it is best to use area loading. Spherical surfaces are particularly good with line loading next best.

2. Maintain Structural Compliance - Due to the inability of a ceramic to yield, the function of compliance should be shifted from the material to the structure itself. The use of compliant layers, springs, and radius mating parts comprise optimal design configurations.

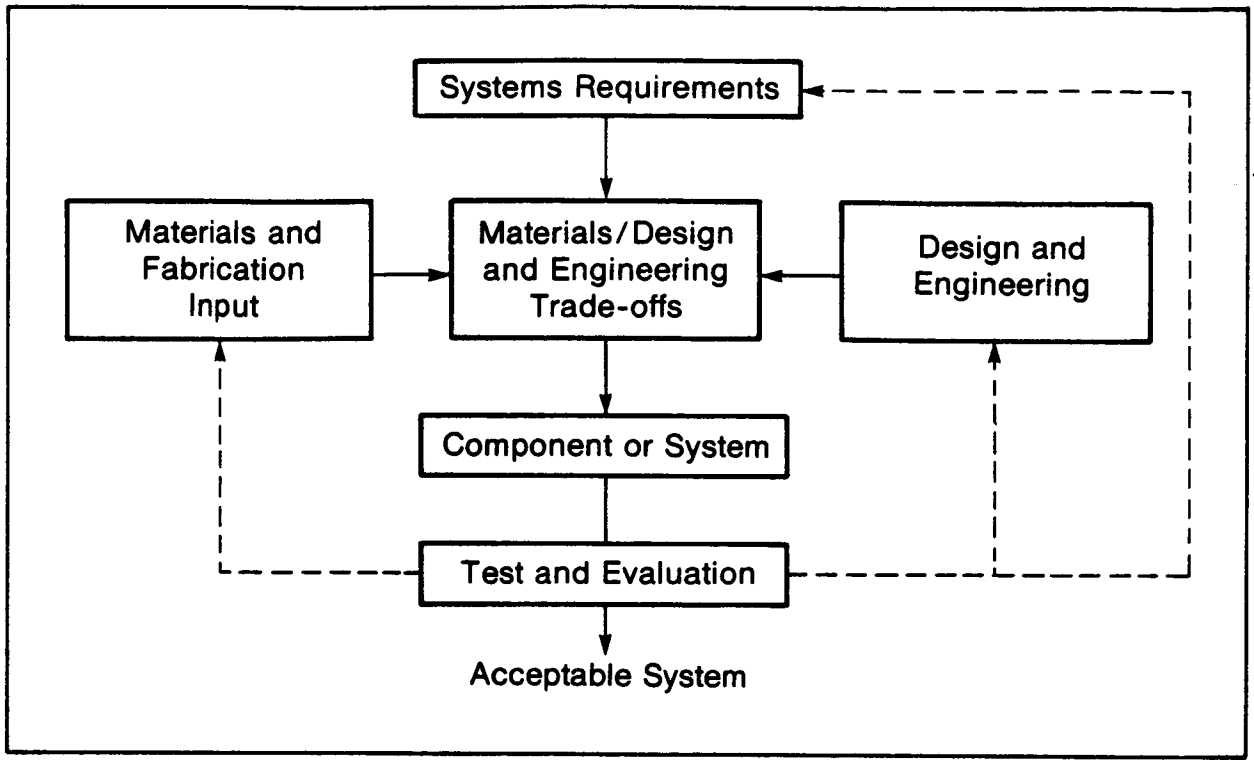


Figure 2-7 "Brittle Materials Design" Systems Trade-Off Logic

3. Avoid Stress Concentrators - Sharp corners, rapid changes in section size, holes, etc. should be minimized and avoided in design where possible.

4. Minimize the Impact of Thermal Stresses - This can be accomplished by using components of the smallest section size possible with the highest degree of symmetry possible. Where appropriate, complex components should be broken down into simpler, more symmetrical subcomponents. Also, for components subjected to thermal extremes, uniform heating and temperature exposure are best.

5. Keep Components as Small as Possible - The flaw distribution of ceramics makes the strength of components size-dependent, thus minimizing the component size increases the reliability.

6. Minimize Severity of Impact - For component applications where impact (particulate erosion) cannot be avoided, a design which allows only low angle impact to occur is preferred.

7. Minimize Machining Required - Cost considerations aside, minimal and careful machining of components will increase their reliability by decreasing the strength-reducing surface or near-surface cracks introduced during machining processes.

Using these preliminary component design guidelines and a systems-oriented, brittle material design methodology, reliable design with structural ceramics can be achieved.

In performing the initial CASE component design layout, fundamental considerations of component survival probability and the statistical nature of the material strength were applied.

Figure 2-8 shows survival probabilities of a simple component which may be representative of the mechanical stresses in the heater head housing assembly of a Stirling engine. The housing is modeled as a tube, 4 in. long with a 3.54 in. internal diameter with wall thicknesses ranging from 0.1575-.3150 in. The tube

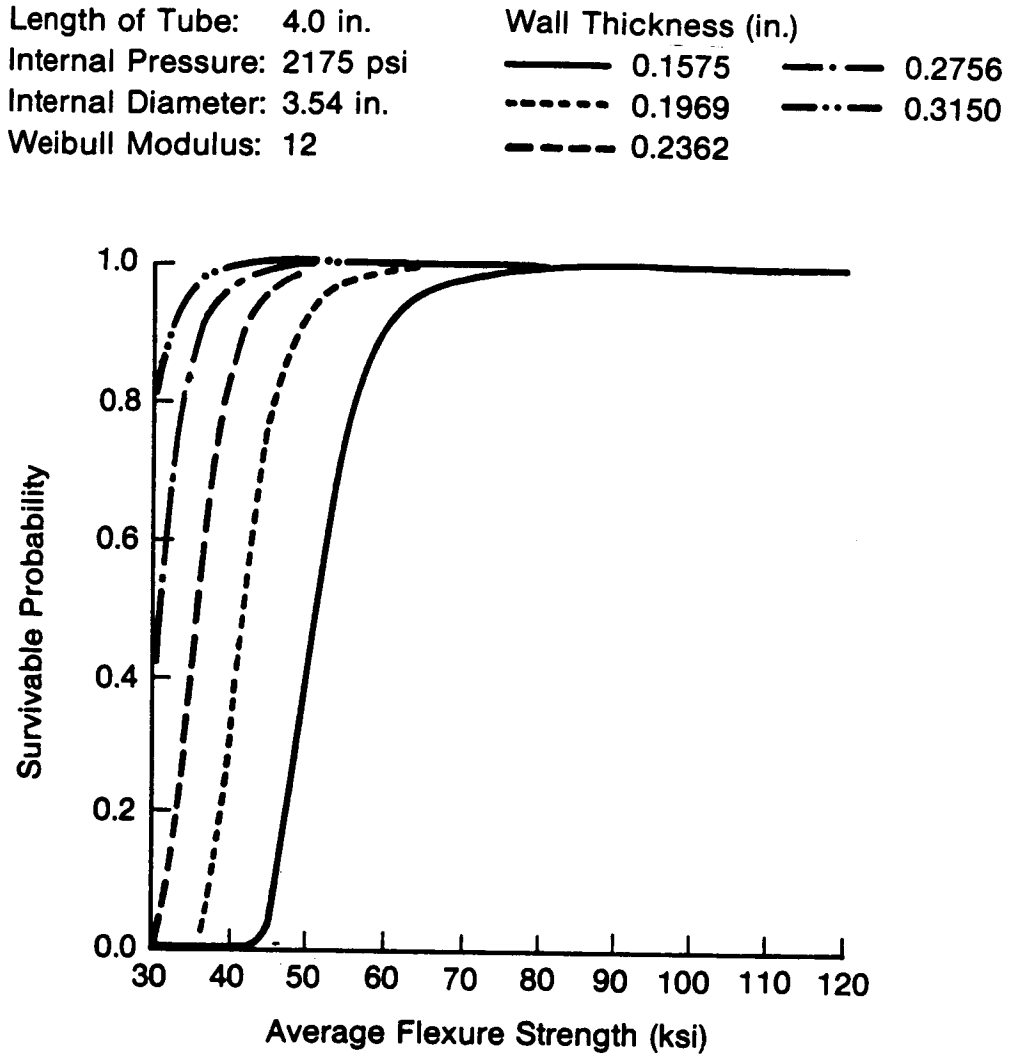


Figure 2-8 Estimate of Survival Probability

was subjected to an internal pressure of 2175 psia. Weibull modulus of 12 and strengths greater than 30 ksi were assumed.

Here, the required strength for a given wall thickness can be determined, or vice versa. Data sheet properties of 67 ksi and a Weibull of 12 for sintered alpha silicon carbide (SASC) would yield over a 95% survival property with the thinnest wall and 99% for each of the other wall thickness.

Conversely, a strength of ~75 ksi with a Weibull modulus of 12 would be required to assure a 99% survival probability with the 0.1575 in. wall thickness.

In order to accurately predict the survivability of a specific component a complete finite element analysis must be completed which takes into account all thermal, mechanical, and transient stresses.

Various iterations can be made with various strengths, Weibull moduli and wall thicknesses until an optimal combination of properties and design is achieved.

When a high volume automotive application is involved, both cost and weight become important factors. Therefore, the thinner wall is a better choice if adequate survivability can be predicted. In addition, minimizing the conduction of heat through these components to the lower part of the engine is critically important. Keeping wall thickness to a minimum helps to meet this objective as well.

Figure 2-9 shows the aforementioned simple component assuming a 0.1575 in. wall thickness. Survival probabilities at various Weibull moduli and strengths have been plotted.

As can be seen, a low Weibull modulus (i.e., 6) cannot achieve adequate survivability even with a strength of 120 ksi. However, Weibulls of 12-18 achieve high survivability even with a strength of 72-50 ksi, respectively.

Figure 2-10 is a diagram that shows how combinations of stengths and Weibull could be matched to achieve a 99% survival probability. Further finite element analysis could accurately predict the reliability of each specific component.

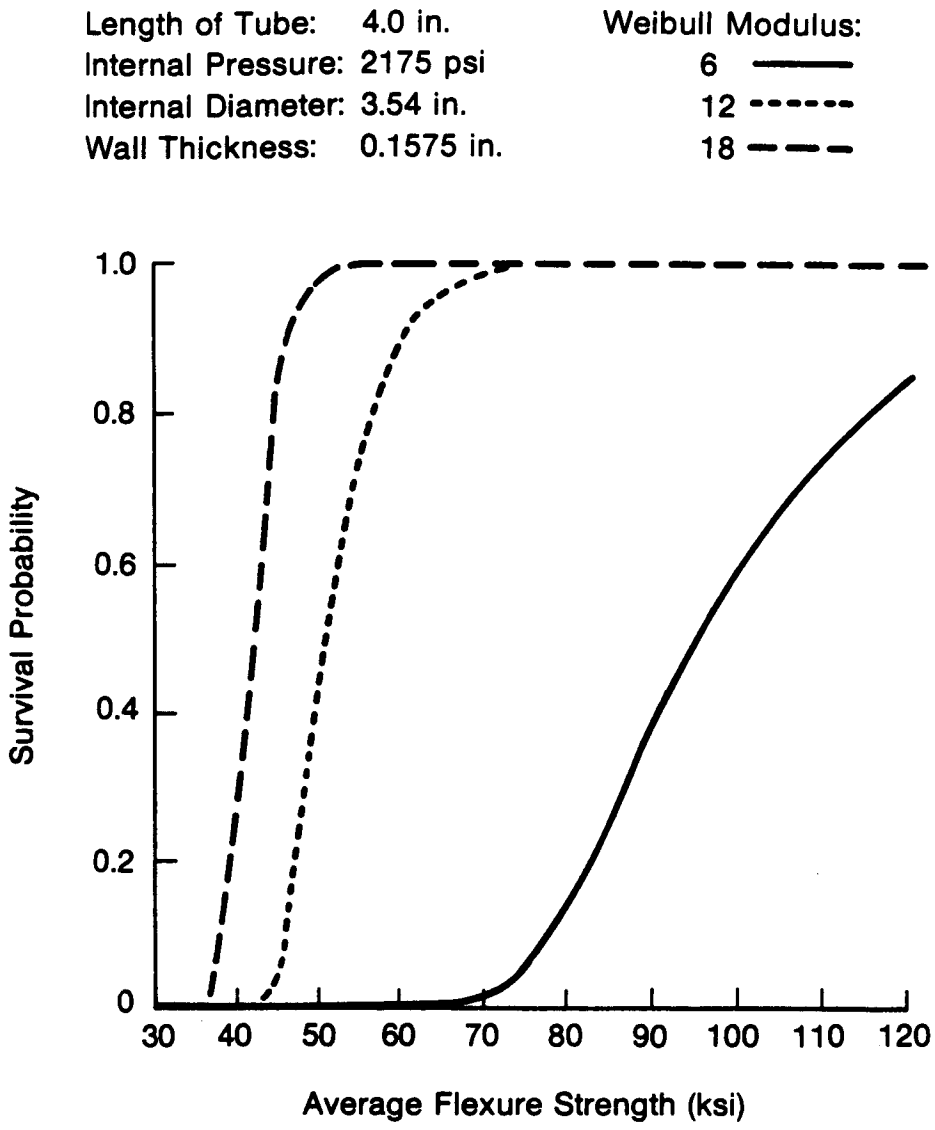


Figure 2-9 Estimate of Survival Probability

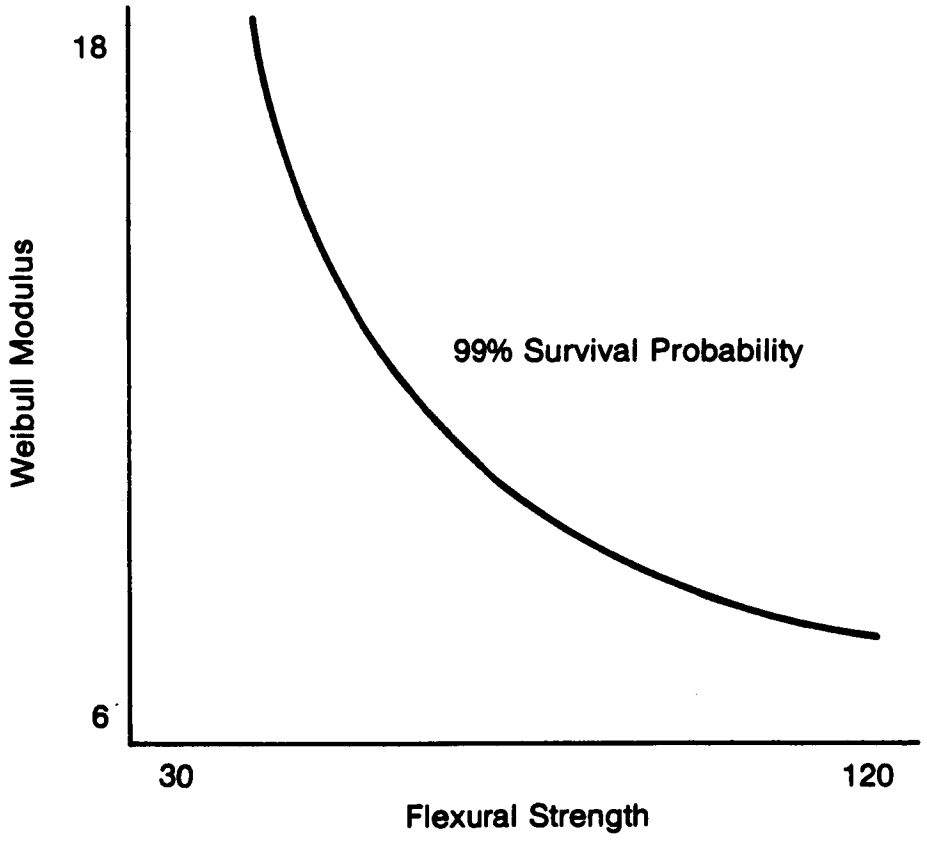


Figure 2-10 Required Combination of Weibull Modulus and Strength Required for 99% Survival Probability

Higher degrees of reliability would be required for components subjected only to nondestructive examination. However, proof testing will yield high reliability within the surviving population.

2.4 Preliminary Design Concepts

2.4.1 Design Considerations

Based on the program objectives, a check list of design considerations was generated to help in identifying an appropriate design of a Stirling engine with ceramic components.

In keeping with the philosophy of this investigation, reliability was weighed highest on this list since the reliabilty of ceramic components, or the lack there of, has been the reason why ceramics have not been used more extensively. This being true even though they often have the potential for improved performance and/or reduced manufacturing costs. Such considerations as geometric complexity, number of joints, vibration sensitivity and the potential for thermal gradients were evaluated in an attempt to maximize the reliability of the prime components.

Performance was weighed almost as heavily as reliability since, without additional performance achieved in the form of thermal efficiency, there would be little incentive to develop ceramic engines outside of the strategic metal issue.

Less important, however still considered in the evaluation of the design, were physical characteristics such as weight and envelope size. The final CASE engine had to be interchangeable with an all metal engine in order to isolate and evaluate the effects of material changes. The 1981 RESD design was chosen as the reference engine, and changes were minimized and made only when required to make ceramic construction feasible. Auxiliaries, drivetrain and all other cold systems remained the same.

2.4.2 Existing Ceramic Heater Head Conceptual Designs

There has been an effort at MTI to design a ceramic heater head suitable for use in the ASE program. As a result of these efforts, a variety of heater head concepts have been developed.

2.4.2.1 Concept A - Six Tower Design. This design (Figure 2-11), has excellent structural simplicity, however, would require extensive alteration of the existing EHS. As shown, each heater head consists of a main body which is the pressure vessel and contains the piston and annular regenerator. Six tower caps open into the pressure vessel and slide over six protruding fingers at the top of an inner ceramic cylinder, which divides the expansion space from the regenerator. Internal longitudinal finning in the tower pieces lies in contact with the cylinder's fingers. Located on the mean radius from the cylinder's center are two divider lands which split each tower assembly into two separate flow passages, one inner and one outer. The inner passage is up from the expansion space, and the outer passage is down to the annular regenerator. At the top of these six towers are caps which establish an open area which connects these two flow passages. The outside surfaces of the towers are enhanced with fins which are integrally formed with the tower and are taller towards the back side of the tower to make up for falling gas temperature. Flow guides are fitted behind the towers to keep the flow near their backsides as long as possible. These towers are symmetrically located on top of each cylinder to form four separate rings of heat-transfer area.

Assembly of all the pieces would be completed in their green unfired state, and sintered as a unit to form a monolithic heater head.

2.4.2.2 Concept B - Cast Volute Design. In this design (Figure 2-12), an attempt was made to reduce the number of joints thus increasing its reliability which, as previous stated is a major design consideration. The heat-exchanger section and the main pressure vessel are cast (or injection molded) as a single piece, with only a continuous, ring-shaped cap plate required to complete the assembly. The outside surfaces of the projecting involute tubes are not enhanced by fins, although are designed so as to provide a contracting flow stream between them, thus improving the heat transfer. The limited surface enhancement of this concept is based on a more conservative approach to ceramic fabrication. While incorporating structural simplicity, this heat exchanger design represents a high risk, possibly resulting in a higher exhaust temperature to the preheater, and higher air handling (blower) power. Also, because of the single piece construction and thick wall design, this concept will have relatively high conduction losses.

2.4.2.3 Concept C - Horizontal Tube Tower Design. The design (Figure 2-13) is an attempt to maximize the heat-transfer effectiveness of the heater head by using a

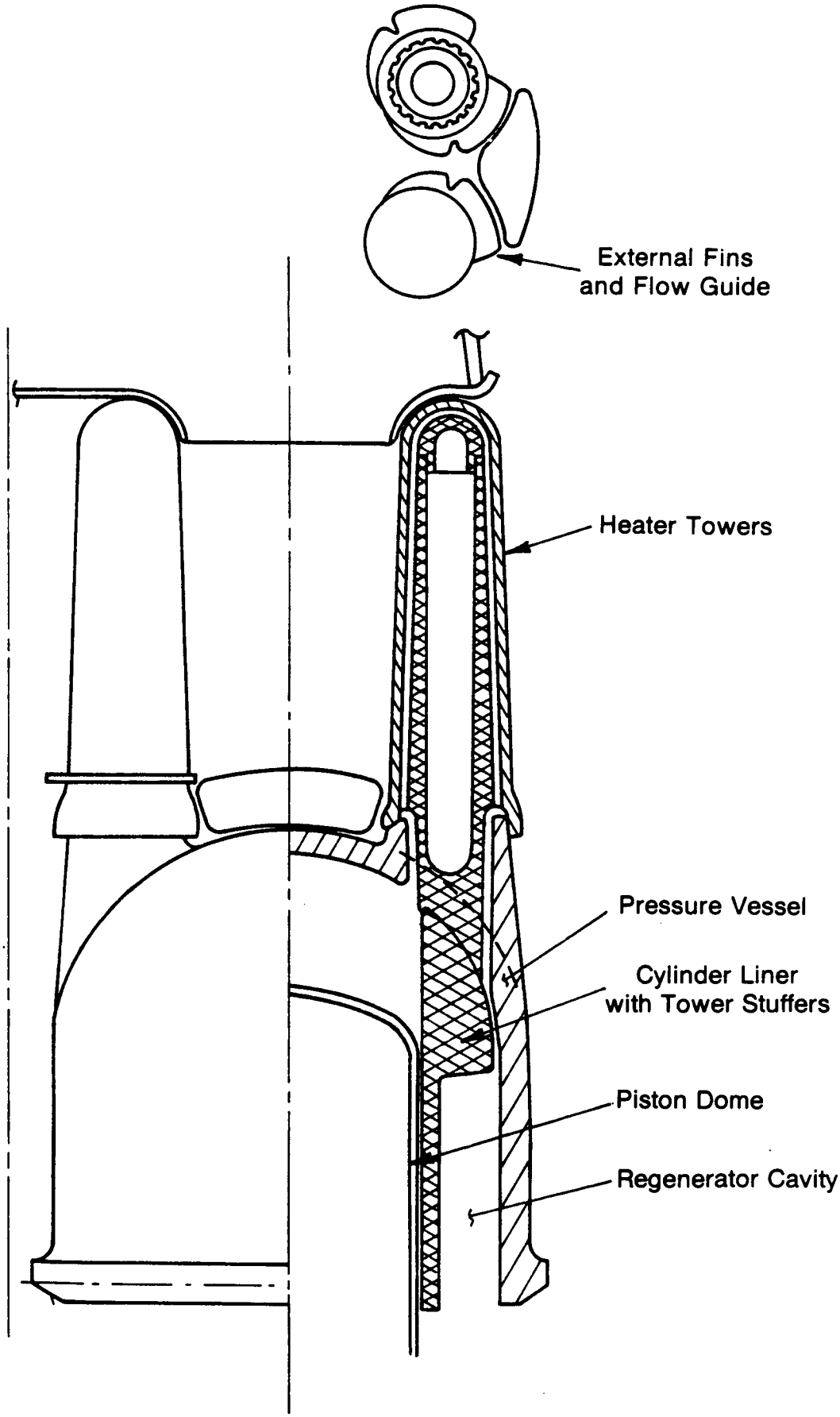


Figure 2-11 ASE Ceramic Heater Head Concept A - Six-Tower Design

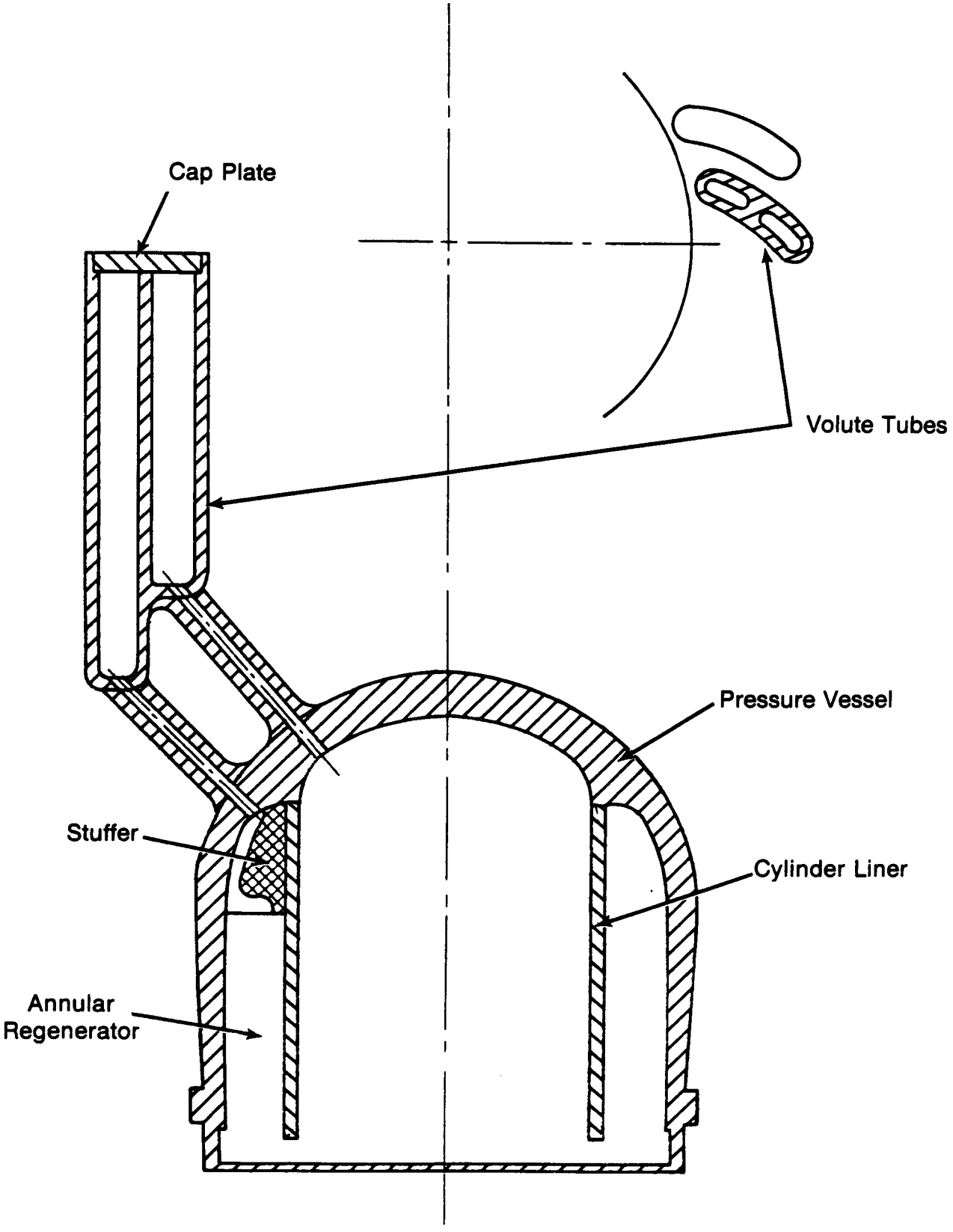


Figure 2-12 ASE Ceramic Heater Head Concept B - Cast Volute Design

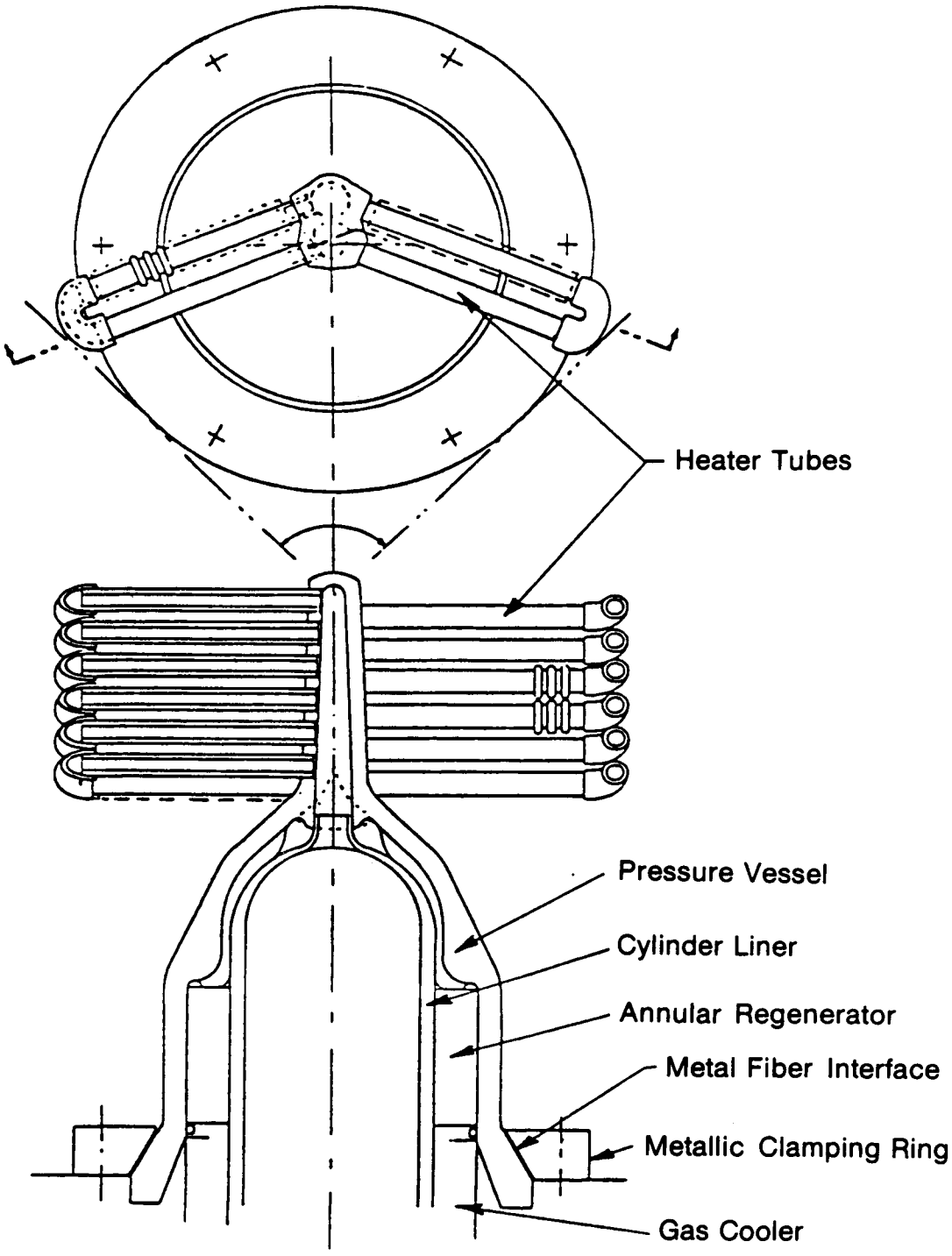


Figure 2-13 ASE Ceramic Heater Head Concept C - Horizontal-Tube-Tower Design

tube and fin geometry currently employed on the Mod I and Mod II ASE designs. This design represents the lowest-risk thermal design resulting from available heat-transfer area and material optimization. With the individual components being separately molded, the heat-transfer area of the tubes and fins could be made of highly conductive SiC while the pressure vessel can be made of a lower conductive material like mullite.

The design shows a near-axisymmetric pressure vessel with a single tower projecting vertically from its dome. This tower, which has two internal ducts, supplies the working fluid to the horizontal tubes and then collects the same and returns it to the annular regenerator. The tubes are fin-enhanced on the rear side and arranged so as to define a single combustor/heater. The tubes are straight sections inserted horizontally into the tower and joined with elbows to create out- and in-passages. As with the previous designs, all parts are assembled in their green state and co-sintered to unify the various pieces into a single unit.

A unique feature of this design is the concept of bonding a fiber-metal interface between the ceramic and a metal clamping ring. Conventionally-clamped or directly-bolted flanges impose high localized loads that increase the likelihood of failure initiation in brittle materials. The design, by virtue of the semi-compliant interface, assures that the compressive load on the ceramic is evenly distributed. In addition, the main vessel wall is flared out from the thin regenerator section to an angle of $\sim 30°$. Due to the axial pressure loading, this results in a compressive load on the ceramic and puts the bending and shear loads in the ductile metal flange. A positive seal is made on the inside surface of the heater head which is far removed from areas of high stress and flooded by cooling water.

2.4.2.4 Concept D - APSE Design with Ceramic Component. The concept, (Figure 2-14), is similar in construction to Concept B in that it consists of individual heater rings integral to each main pressure vessel and forms separate combustion zones.

More importantly though, is the fact that each of these combustion zones are pressurized via a turbocharger. This reduces the required total combustion volume, thereby minimizing the hot mass of the system.

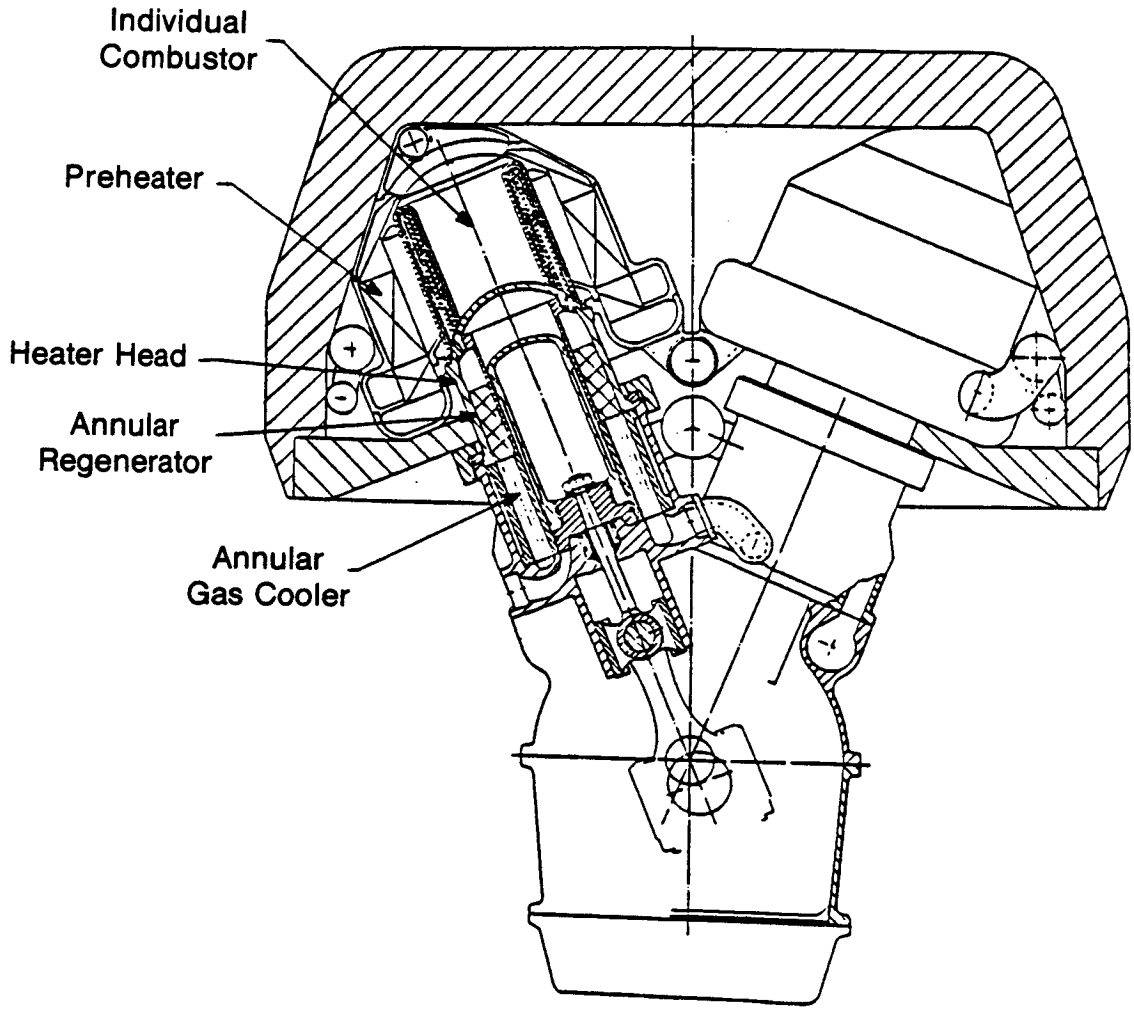


Figure 2-14 Advanced Production Stirling Engine (APSE) with Ceramic Components

2.5 Final Design Concept Description

Although a wide variety of design concepts were considered, after discussions with Carborondum and other ceramic vendors regarding forming and processing techniques, a design incorporating an annular heater head and conventional manifolds was found to be suitable from a manufacturing standpoint. Accordingly, this design approach was chosen for the preliminary design concept since it was judged as offering the best performance while representing a potentially manufacturable configuration.

2.5.1 Heater Head

The overall engine configuration (shown in Figure 2-15) is that of a four-cycle, double-acting engine with annular style regenerators and coolers. It has a twin-crankshaft and a U-drive similar to that of the 1981 RESD engine.

The heater head concept (one quadrant shown in Figure 2-16) incorporates horizontal manifolds feeding 22 verticial tubes which form a heat exchanger. The elimination of towers, as proposed in previous designs, makes available heat transfer area which would otherwise be occupied by the tower. The heater quadrants are arranged in a circular array which provides for the most efficient use of envelope space. This arrangement also lends itself nicely to use of single combustor. Multiple combustion chambers are inherent complex since they require independent temperature control and ignition systems.

The manifolds (items 2,3,4, and 5 in Figure 2-16) define the inner diameter of the combustion chamber and supply working fluid to the inner row of heater tubes. Each heater tube (item 6 in Figure 2-16) connects this set of inner manifolds with a outer set of manifolds which correspondingly defines the outer diameter of the combustion chamber. This outer row of flow ducts then collects the working fluid from the tubes and returns it to the heater head.

The heater tubes are formed in a U-shape to provide for a double-pass heat-exchanger system as they connect the inner manifold to the outer manifold. The design shows the inner row of tubes as being unfinned with an effective length of $\sim$148 mm. The outer row of tubes are finned to enhance the heat-transfer area and

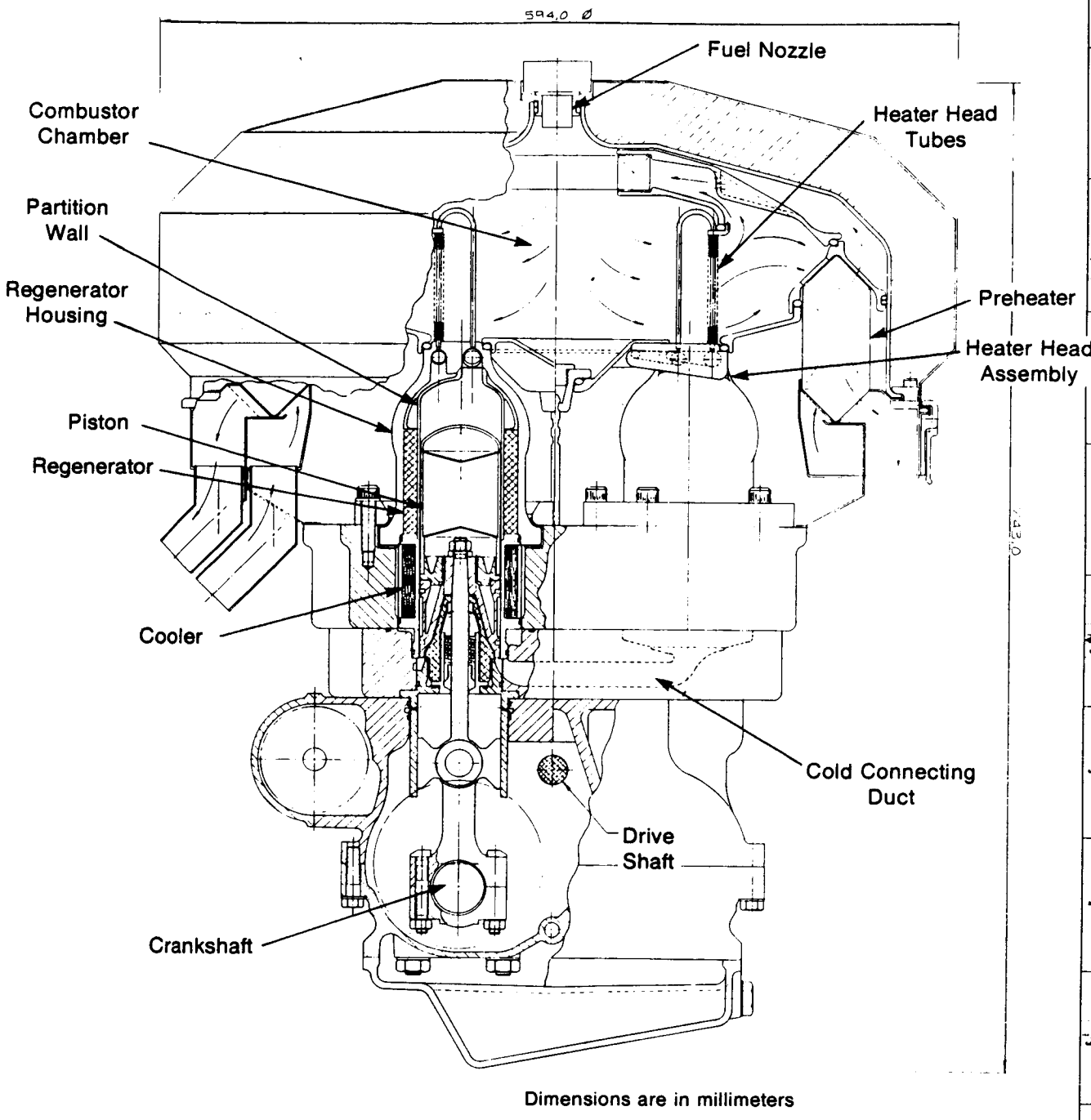


Figure 2-15 CASE Layout

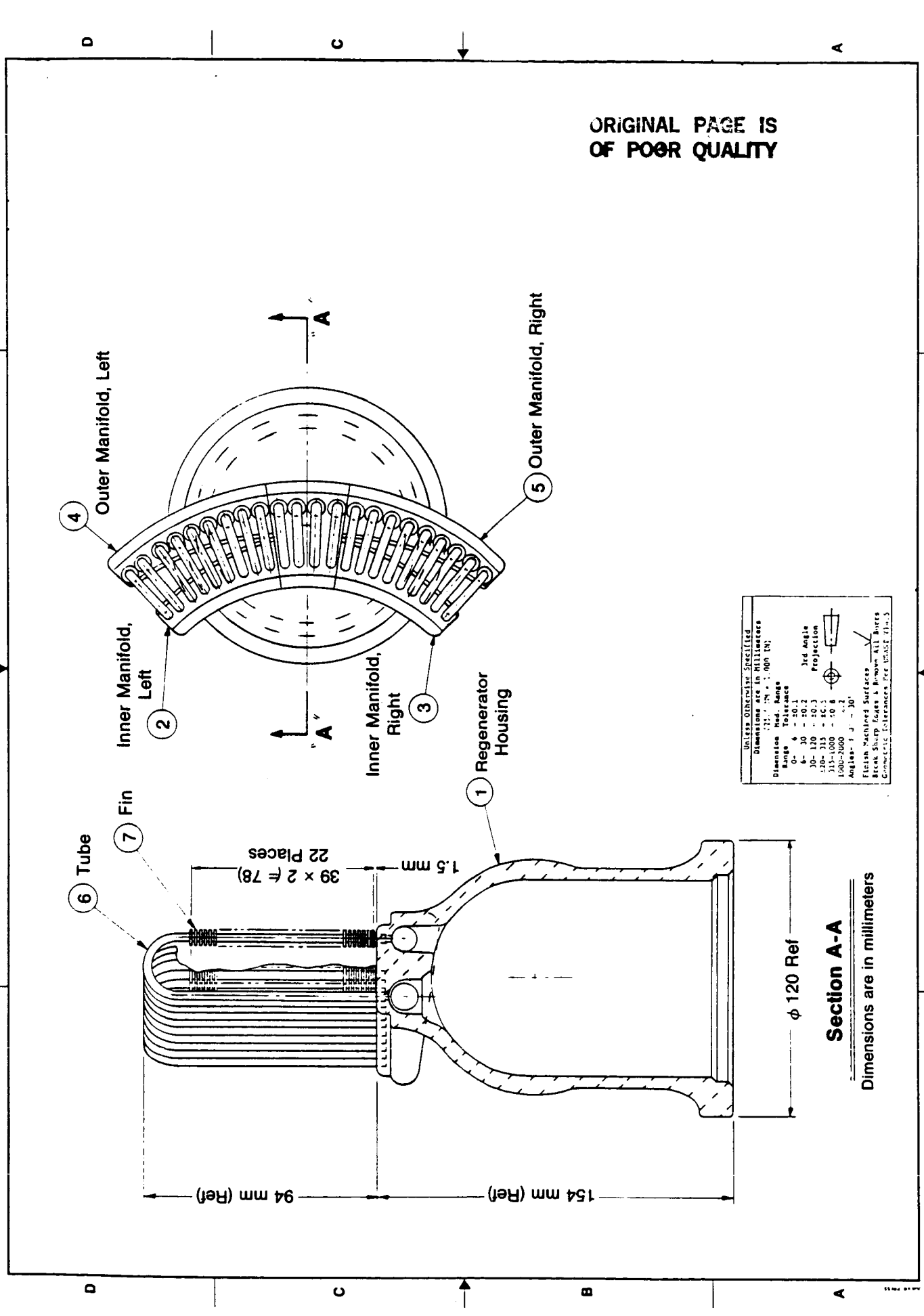


Figure 2-16 CASE Heater Head

provide for a more uniform tube temperature between the front and rear rows of tubes.

The fins (item 7 in Figure 2-16) have an 8.0-mm outside diameter (O.D.) and a 4.5-mm root diameter. Each fin is 1.00-mm thick with 1.00-mm spacing between fins. Uniform spacing between fins is obtained by a pair of dimples which are cast integral with the fin. Properly placing the fin on the tube so that these dimples are directly between the two adjacent tubes when assembled on the heater head, creates a flow blocking channel which forces the combustion gas to flow closer to the root of the fin thus increasing the overall fin efficiency. Fin density and the resulting enhancement is an extension of current technology in metal heat exchangers. Detail drawings of the heater head components are included in Appendix A.

The four heater heads and cylinders are dimensionally arranged so as to be adaptable directly to the 1981 RESD engine. This configuration utilizes the existing lower drive and allows direct efficiency and performance comparisons. Since conventionally clamped or bolted flanges are impractical with ceramic (brittle) materials, the design incorporates a concept which decreases the likelihood of failure of the heater head due to high localized loads. This is accomplished by the use of a fiber-metal interface between an annular clamping ring and the heater head thereby assuring an evenly distributed load on the ceramic. Sealing is taken on the inside surface of the heater head by an O-ring which is far removed from areas of high stress and located near the water-cooled jacket.

2.5.1.1 Preliminary Heat Transfer Analysis (Tube/Fin Geometry). Prior to completing a final design optimization together with a vehicle performance projection, it was necessary to evaluate the preliminary design in terms of its heat-transfer effectiveness from the combustion gas side. The design was evaluated on the basis of current manufacturing capabilities concerning tube diameters and wall thicknesses, and a realistic fin geometry. The analysis was intended to show whether there was sufficient available heat-transfer area on the combustion gas side based on present flow rates at a tube temperature of 1020°C and bulk combustion gas temperature at various points. It should be noted that the configuration evaluated was a preliminary design which had minor dimensional variations from the final optimized version shown in Figure 2-15. A comparison of these two geometries is shown in Table 2-6.

TABLE 2-6

GEOMETRY COMPARISON

	Preliminary	Optimized (OP-302)
Number of Tubes/Cycle	22	22
Tube I.D. (mm)	3.0	2.5
O.D./I.D.	1.5	1.5
Length of One Tube (mm)	295.7	207
Effective Length/Total Length	.94	.86
Front-Row Gap (mm)	1.85	2.75

TABLE 2-7

SUMMARY FOR PRELIMINARY TUBE/FIN GEOMETRY

	Front Row	Rear Row
Flow Rate (kg/s)	.138	.138
Flow Area (m^2)	.0241	.019
Flow Velocity (m/s)	37.23	33.63
Film Temperature (°C)-T_f	1510	1381
Re_f	465.37	324.28
h (W/m^2 °C)	293.21	324.28
Q (kW)	52.9	127.0
T_{bulk} after Row (°C)	1741.3	1053.0
ΔT (°C)	980.0	721.3
Heat Transfer Area (m^2)	.184	.543

The result of the analysis is shown in Table 2-7 and indicates that the geometry is adequate in available heat-transfer area. For the calculations the flame temperature was assumed to be 2000°C and the amount of recirculated combustion gases (CGR) was based on an assumed heat input ($Q_{in.}$) of 170 kW.

2.5.2 Other Hot System Components

A ceramic dome is attached to the reciprocating metal piston base with an epoxy-type adhesive. This bond is located at the base of the pistons in a low temperature area. Carborundum has identified a select group of these adhesives which exhibit lap shear strengths in excess of 8000 lb/in.^{2} with the only constraint that temperatures do not exceed 350°F. The ceramic dome also incorporates two ceramic radiation shields which are separately formed and sintered as a unit with the dome.

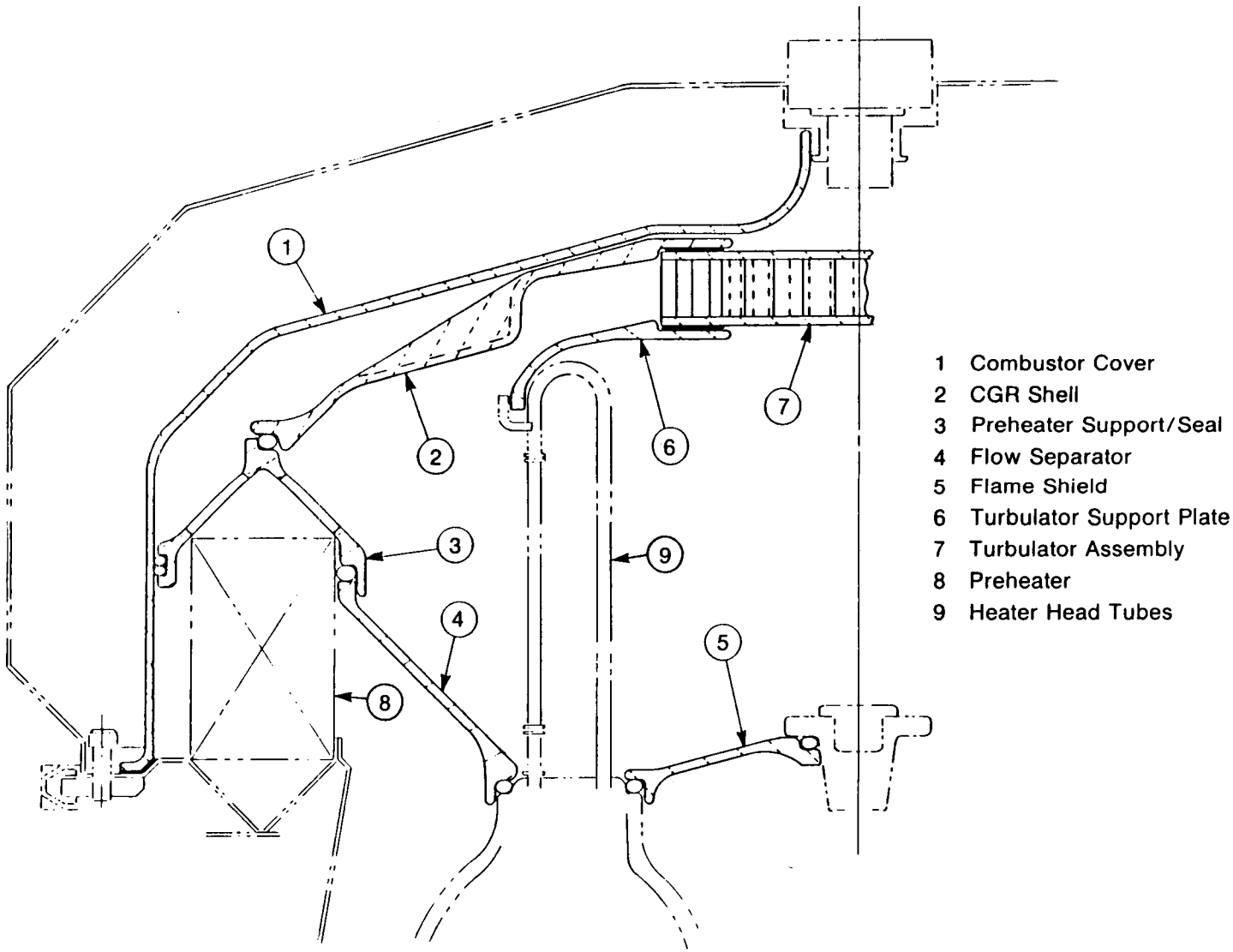
Separating the expansion space above the piston and the annular regenerator is a ceramic partition which also acts as the piston cylinder wall. The material selected for this component would be the same as that selected for the piston itself to ensure a controlled and uniform appendix gap down the length of the piston. The partition is seated into and located, at the bottom end, by the annular cooler, and forms a seal with the heater head at the top end.

The gap between the O.D. of the partition wall and the inside diameter (ID) of the heater head forms a volume for the annular regenerator. It is envisioned, due to the higher operating temperatures, that the regenerator will also be of a ceramic material. Woven and sintered Nextel fiber has been identified as the prime candidate for this application.

The final ceramic component in the hot engine system is an annular stuffer which is located on the outside of the partition wall and the hot end of the regenerator.

2.5.3 EHS

The EHS, shown in the overall engine drawing (Figure 2-15) and shown separately in Figure 2-17 is similar in principle to the system presently used on the Mod II. The function of the EHS is to provide heat to the internal working cycle via the heater head.



1 Combustor Cover
2 CGR Shell
3 Preheater Support/Seal
4 Flow Separator
5 Flame Shield
6 Turbulator Support Plate
7 Turbulator Assembly
8 Preheater
9 Heater Head Tubes

Figure 2-17 Inner Combustor Assembly

For control of emissions, the system utilizes a combustion gas recirculation (CGR) design. The CGR shell (shown in Figure 2-18) creates a low pressure area in front of the turbulator (Figure 2-19), thus drawing up and recirculating ~60% of the combustion gases.

Due to the increased combustion gas temperature and the resulting high preheated air temperature from the recuperator, several other components in the EHS are designated as being converted from metal parts to ceramic. On the metal RESD, flame temperatures of 1800-2000°C are present in the combustor, and preheater entrance temperatures are ~900°C (close to heater head temperature). If the heater head is to use the potential of ceramics like SiC, temperatures to the preheater may reach 1200-1300°C, implying flame temperatures approaching 2400°C. Thus, all exposed combustor parts, as well as the preheater, must be made of highly heat-resistant materials. Oxidation resistance is required, and thermal dimensional stability to assure proper gas flow and flame distribution. Thermal shock resistance is necessary for start-up transients. The only clear candidate materials for such demanding service are low-expansion ceramics.

The preheater is proposed for this design and is composed of many plates, sintered together to form a counter flow heat exchanger. It is shown in Figure 2-20. This is the same configuration that is currently being developed at Coors Porcelain and tested at MTI. It is a single pass, counterflow heat exchanger currently being manufactured out of cordierite ($MgO + Al_2O_3 + SiO_2$).

2.6 Heater Head Stress Analysis

2.6.1 Introduction

As part of the CASE study, Task I (conceptual design of a Stirling engine), a preliminary stress analysis of the ceramic heater head was performed to ascertain the stress levels. The purpose of this stress analysis was to establish the basic feasibility of utilizing ceramic components in an automotive Stirling environment. The following operating modes were considered:

- Engine life of 4000 hours over the combined Federal driving cycle
- Operation at full power for 100 hours
- Transient operation, including start and shutdown.

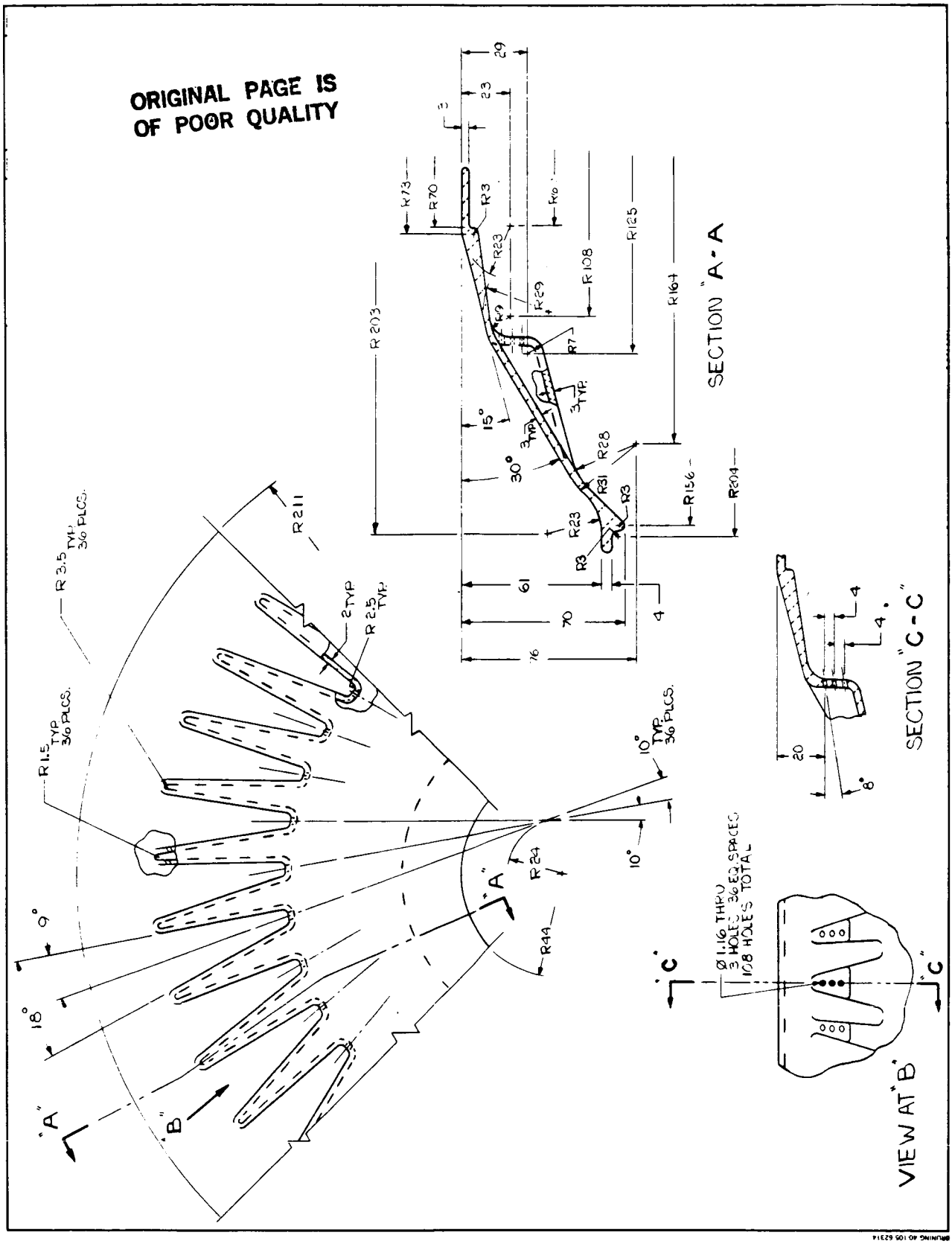


Figure 2-18 CGR Shell

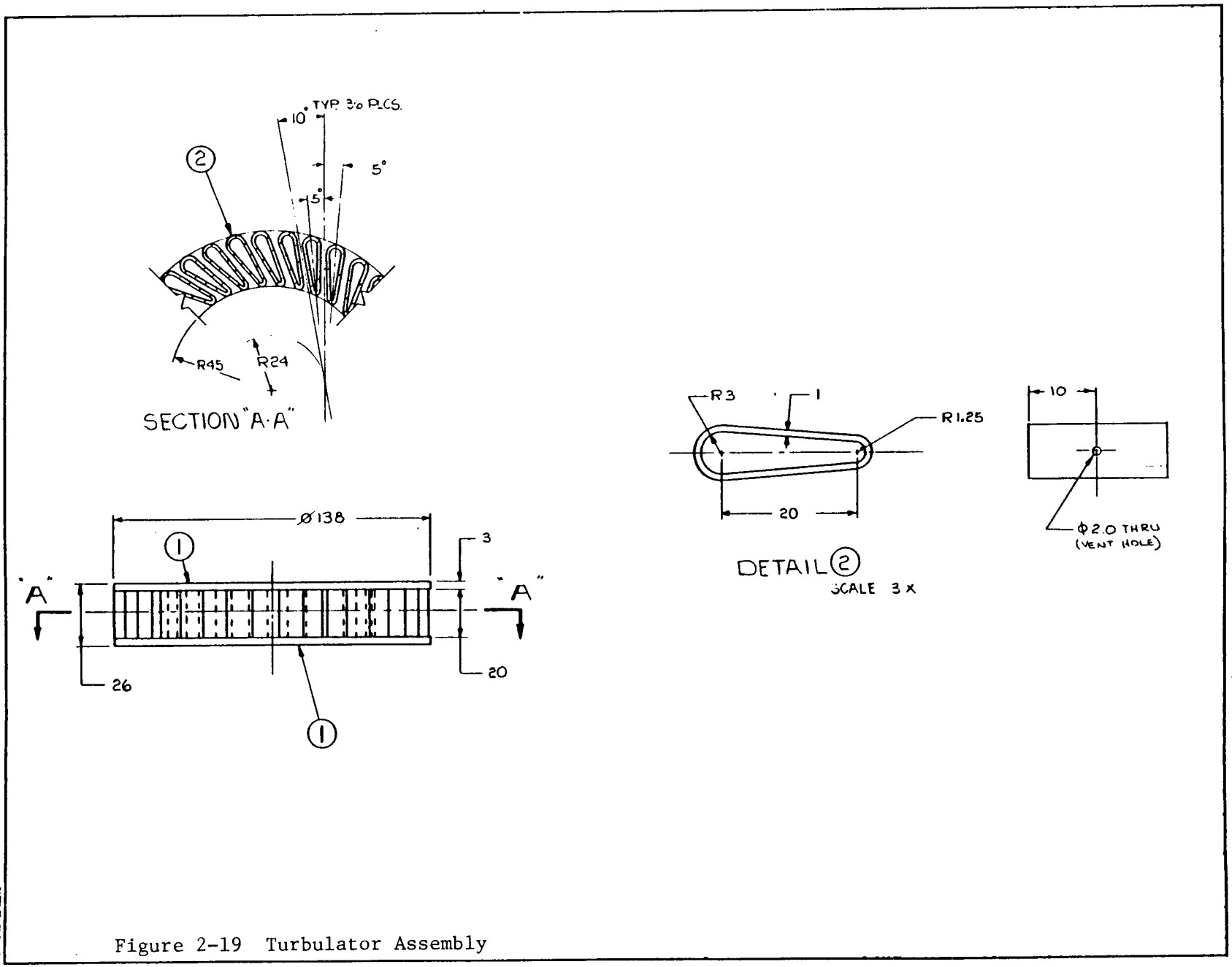


Figure 2-19 Turbulator Assembly

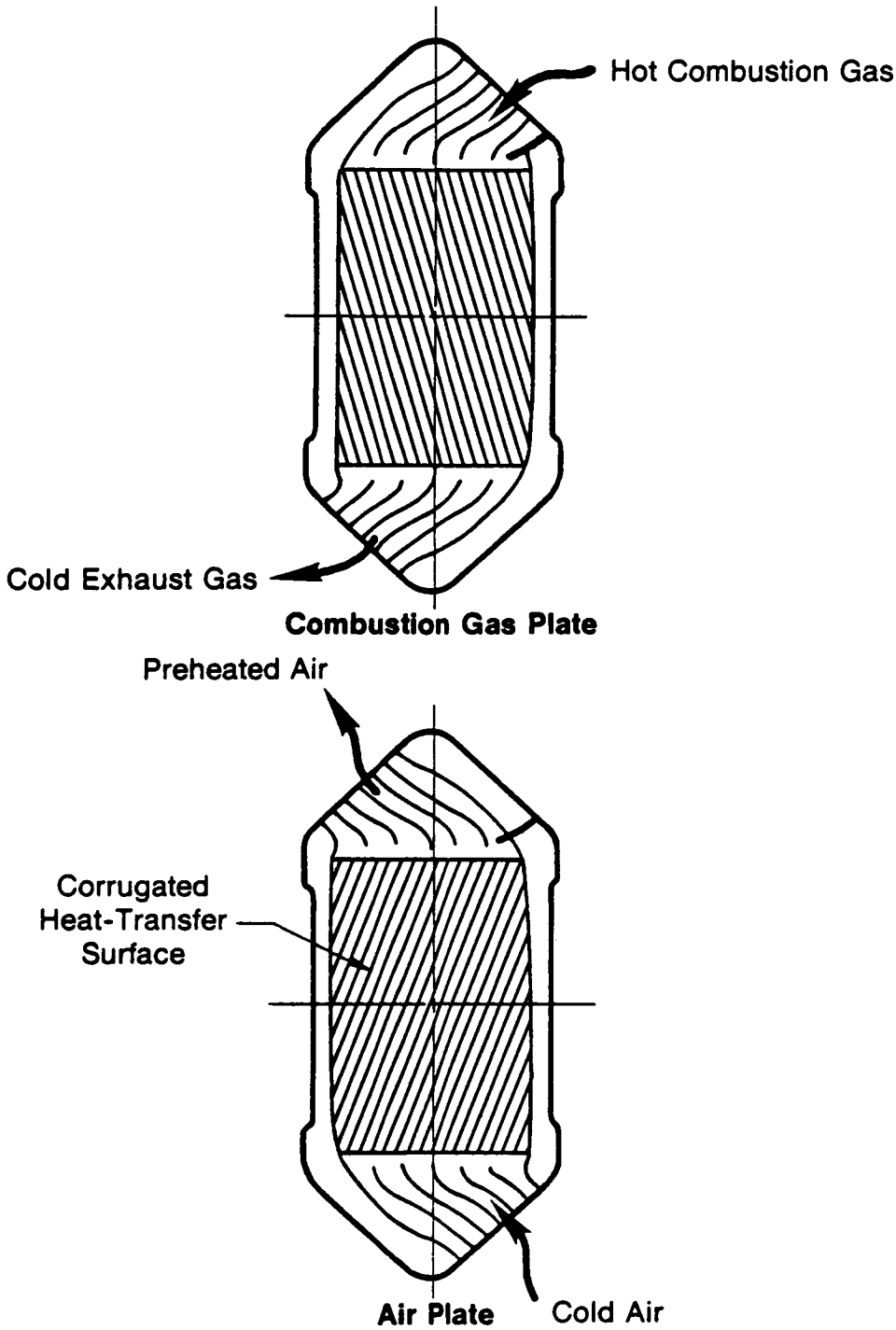


Figure 2-20 Ceramic Heat Exchanger Plates

This section of the report presents the results of the heater head stress analysis. The analysis has concentrated on the heater head manifolds and cylinder housings, since these parts operate at high temperatures, contain the working gas pressure and are subject to thermal gradients and transient thermal stresses. The heater head tubes do not represent a stress problem since they are small diameter tubes with an O.D./I.D. ratio at 1.5. The geometrically complex cylinder housing/manifold has been shown to be the critical component in similar Stirling engine designs, thus the analysis has concentrated on this component.

The study is based on three different groups of ceramic materials. Group 1 represents ceramic materials available today; Group 2 represents what is available approximately five years from now; and, Group 3 represents a future ceramic material available 10-15 years from now.

2.6.2 Stress Analysis Procedure of Ceramic Components

The flow diagram in Figure 2-21 shows a stress analysis procedure for a ceramic component. This design process can be described step by step in the following way:

1. The acceptable failure probability (F) during operation conditions (OC) must be specified.

2. All basic material data, including the Weibull modulus (m) and the ultimate strength values (SU), must be known.

3. Size effects must be taken into account.

4. A stress analysis based on the finite element method will give the stress distribution in the component during normal operating conditions. A statistical approach based on this stress distribution will then give the safety factor SF corresponding to a certain failure probability F. The SF can be defined as the allowable flexural strength divided by some nominal stress in the component. After some iterations (with the wall thickness as a parameter) the relation between the failure probability and the SF (F) during normal operating condition is known. Consequently,

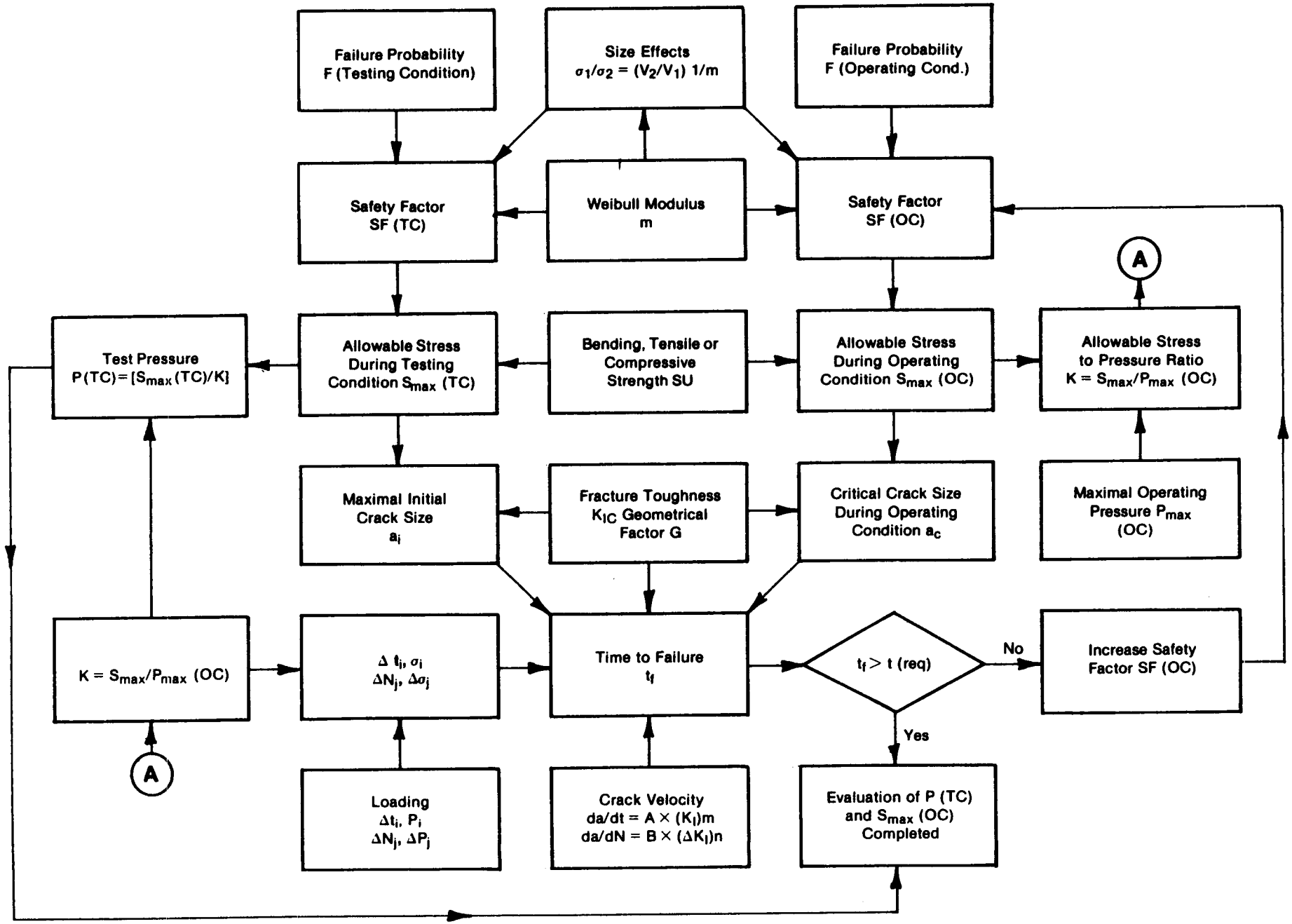


Figure 2-21 Flow Diagram Showing the Stress Analysis Procedure of Ceramic Components

the SF (OC) corresponding to the specified failure probability F (OC) is evaluated.

5. As the SF (OC) is known, also the allowable stress during operating conditions S_{max} (OC) is known.

6. The maximal operating pressure P_{max} of the component is specified, and consequently the allowable stress to pressure ratio K can be evaluated.

7. The acceptable failure probability F during proof testing condition (TC) must be specified.

8. By going through the procedure described in Nos. 2 through 5, the SF during testing condition SF (TC) can be evaluated and, consequently the maximal allow stress S_{max} (TC) during TC is evaluated.

9. Based on S_{max} (TC) and the stress to pressure ratio K, the maximal proof testing pressure P (TC) can be evaluated.

10. The components, which survive the proof testing pressure P (TC), will have a maximal initial crack size less than a_i. This crack size can be evaluated based on the stress distribution in the component during TC and the fracture toughness K_{IC} of the material. An assumption concerning the crack shape must also be completed before the geometrical shape factor G can be evaluated.

11. The critical crack size during operating condition a_c can be evaluated based on the stress distribution in the component during operating condition.

12. The loading conditions during normal operation can be specified in the following way:

$\Delta t_i, p_i \quad i = 1, imax$
$\Delta N_j, \Delta p_j \quad j = 1, jmax$, where:

Δt_i = the time fraction during which the component is exposed to the

$$\text{internal pressure } p_i \left(\sum_{i=1}^{imax} \Delta t_i = 4000 \text{ hrs} \right)$$

ΔN_j = the number of cycles corresponding to the pressure range Δ_{pj}.

13. The stress to pressure ratio K is known, and consequently p_i and ΔP_j can be transformed to stress levels σ_i and stress ranges $\Delta\sigma_j$.

14. In order to evaluate how long the component will survive during the specified loading conditions, it is necessary to study how long it will take to propagate the crack from initial size (a_i) to critical size (a_c). This evaluation can only be completed if time dependent material properties are available. Subcritical crack growth rate data can usually be expressed in the following form:

$$\frac{da}{dt} = A \cdot (K_I)^m \quad , \quad \frac{da}{dN} = B \cdot (\Delta K_I)^m$$

The first expression represents the crack growth per time unit as a function of the stress intensity factor K_I. The second expression represents the crack growth per load cycle (N) as a function of the stress intensity range (ΔK_I). A, B, m, and n are constants, dependent on material, temperature, environment etc.

15. The evaluated time to failure t_f is then compared with the specified service time t_s of the component. If $t_f < t_s$ it is necessary to increase the safety factor SF (OC), which means a jump back to No. 4. The SF (OC) can be increased by several different means, (i.e., an increased material thickness, removal of stress concentrations or material change). An increased SF means a decreased allowable stress, and consequently the allowable stress to pressure ratio K will decrease. For the same material, this results in an increased test pressure P (TC). A reduction of the allowable stress level S_{max} (OC) corresponds to a larger critical crack size a_c, and obviously it will take longer for any initial crack to reach the critical size.

16. The iteration procedure must continue until $t_f > t_s$.

The design procedure shown in Figure 2-21 represents a statistical approach combined with a fracture mechanical approach. To make life predictions of a ceramic component a fracture mechanical approach is necessary. A pure statistical approach can only give the failure probability at the time when the component for the first time is put into service. However, this approach is not realistic if the ceramic material has time dependent strength properties, and since most ceramic materials are susceptible to creep and fatigue at higher temperature, a combined approach is necessary for a thorough analytic evaluation.

2.6.3 Material Data

This study is based on three different groups of ceramic materials. For the heater head these material groups are:

1. Reaction bonded SiC (Carborundum)
2. Sintered $Si_3 N_4$ (GTE SNW1000)
3. Mullite + 20 volume % SiC whiskers.

The material data for these groups are given in Section 2.2.

Unfortunately, no creep or fatigue properties are known or available for these materials. Similarly, crack velocity data (da/dt and da/dN) are unknown for these materials.

2.6.4 Simplified Analysis Approach

The lack of load cycle and time dependent material properties made it impossible to perform any life predictions of the heater. Consequently, it is not possible to consider the long term effects of 4000 hours over the combined Federal driving cycle from a fatigue or creep standpoint. The stress analysis of the heater head can only be based on a pure statistical approach. This means that only certain parts of the design procedure shown in Figure 2-21 could be used. This simplified approach will now be described.

The Carborundum Company has recommended a survival probability of 85% during proof testing of a ceramic heater head component. This survival probability has been used and combined with a proof test factor of 1.5, which corresponds to a test

pressure of 30 MPa (for the ASE-based CASE). Consequently, this criteria was used to determine the wall thickness of the housing.

During the thermodynamic optimization of the engine, it was necessary to prescribe how the wall thickness of the heater housing depends on different parameters, such as pressure, temperature, pressure vessel diameter, etc. The following procedure was developed to describe these relationships. The heater housing was considered as a cylinder with a length equal to the regenerator length plus the inner radius of the housing. The wall thickness could then be evaluated after some iterations by the following expressions:

$$P_f = 1 - \exp\left[-\left(\frac{1}{m}!\right)^m \cdot \left(\frac{S2}{S1}\right)^m \cdot \frac{V2}{V1}\right]$$

$$S2 = \frac{p\,(D + t)}{2t}$$

$$V2 = \frac{\pi \cdot L}{4} \cdot [(D + 2t)^2 - D^2]$$

$$S1 = S0\left[\frac{m+2}{4 \cdot (m+1)^2}\right]$$

P_f = failure probability (15%)
m = Weibull modulus
S2 = primary membrane stress in the cylinder
V2 = volume of cylinder
V1 = test specimen volume
S1 = tensile strength of the test specimen
S0 = flexural strength of the test specimen (4 point bending)
p = internal pressure
D = inner diameter of the cylinder, L = length of the equivalent cylinder
t = wall thickness of the cylinder

This procedure represents a simplified statistical approach. However, the approximations are acceptable since the materials have a rather high Weibull modulus. This means that parts with relatively low stresses will not contribute significantly to the stress-volume integral. The manifolds and heater tubes are such parts, in which the relative wall thickness is thicker due to manufacturing reasons. Also, in this simplified approach the principal stresses in the radial

and axial direction were neglected, because they are considerable lower than the hoop stresses.

At the time when the stress analysis work in this study started, the final dimensions as a result of the engine optimization work were not yet evaluated. By this reason the I.D. of the housing was kept constant for all material Groups. The fixed geometry was based on drawing No. SK-D-7302 (Figure 2-15) which means an I.D. of 90 mm.

Figure 2-22 shows the failure probability P_f as a function of the wall thickness t for the different material Groups. A survival probability P_s of 85% at the proof testing pressure p = 30 MPa requires a wall thickness of 6-6.5 mm for the material Groups 1 and 3. The same survival probability requires a wall thickness of $\sim$3.5 mm for material Group 2.

2.6.5 Stress Analysis of the Heater Housing

2.6.5.1 Finite Element Models. The heater housing analysis was based on a simplified axi-symmetric finite element model. The elements are isoparametric with eight nodes. The flange geometry corresponds to drawing No. SK-D-7302 (Figure 2-15). For the material Groups 1 and 3 a wall thickness of 6.5 mm was used, for Group 2 a thickness of 3.5 mm was used. The finite element models are shown in Figure 2-23.

2.6.5.2 Loading Conditions. The following stationary temperature distribution in the housing was assumed, namely 950°C in the dome shaped top and 50°C in the lower part of the flange. The axial force in the housing due to the internal pressure was balanced in the model by a surface pressure on the flange as shown in Figure 2-23. Four different load cases were analyzed:

1. Load case A: stationary temperature distribution (T)
2. Load case B: maximal operating pressure, p = 20 MPa
3. Load case C: proof testing condition, p = 30 MPa
4. Load case D: temperature combined with p = 20 MPa.

2.6.5.3 Stress Distribution. Figure 2-24 shows the stress distribution (equivalent stress according to von Mises) along the inner surface for material Group 1

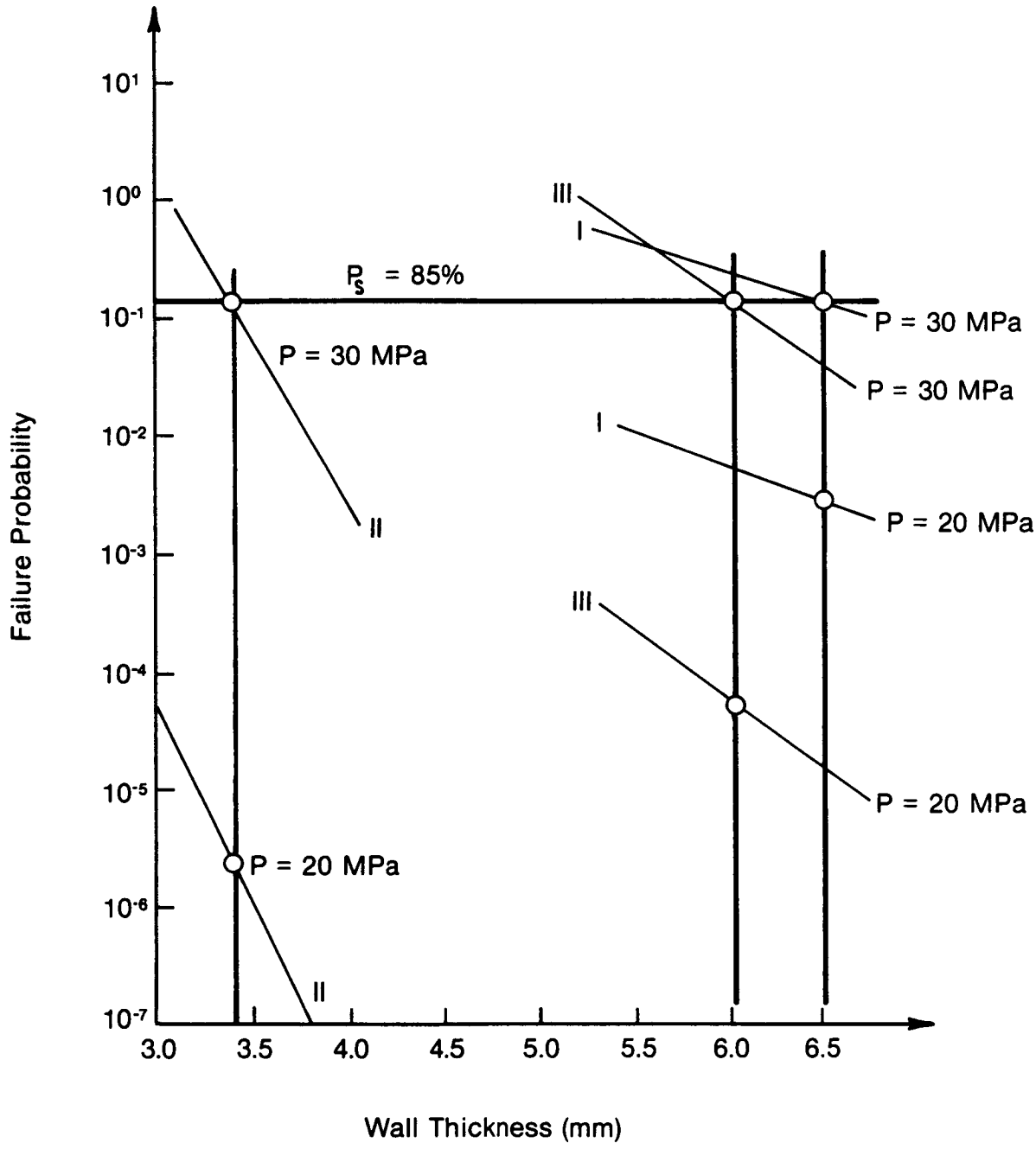


Figure 2-22 Failure Probability for CASE Materials

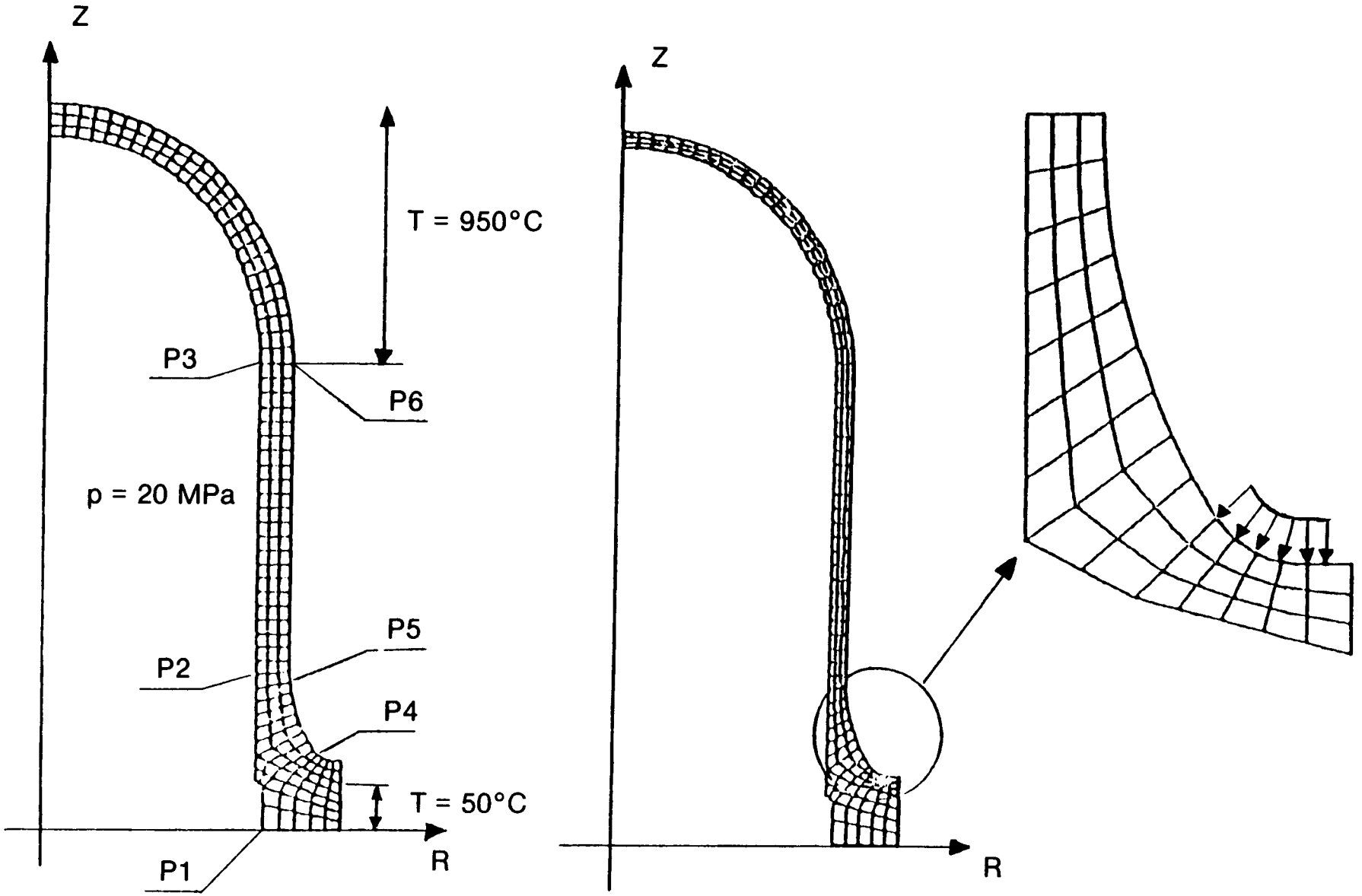


Figure 2-23 Finite Element Model of the Heater Housing

(t = 6.5 mm). For load case C the maximal tensile stress is 280 MPa (hoop stress in point P2). For case D the maximal tensile stress is 169 MPa (hoop stress in point P2).

Figure 2-25 shows the stress distribution along the outer surface for material Group 1. In load case C the maximal tensile stress is 265 MPa (maximal principal stress in point P5). For load case D the maximal tensile stress is 189 MPa (maximal principal stress in point P6).

Figure 2-26 shows the stress distribution along the inner surface for material Group 2 (t = 3.5 mm). In load case C the maximal tensile stress is 453 MPa (hoop stress in point P2). In load case D the maximal tensile stress is 281 MPa in the same point.

Figure 2-27 shows the stress distribution along the outer surface for material Group 3. In load case C the maximal tensile stress is 462 MPa (hoop stress in point P5). In load case D the maximal tensile stress is 281 MPa in the same point.

2.6.5.4 Failure Probability. The failure probability of the housing was evaluated based on the finite element analysis. The total failure probability P_{tot} was calculated based on the following expression:

$$P_{tot} = 1 - \exp\left[-\left(\frac{1}{m!}\right)^m \cdot \frac{1}{V_o} \cdot \Sigma\right]$$

$$\Sigma = \sum_{i=1}^{n} \left[\left(\frac{\sigma_{i1}}{\sigma_o}\right)^m + \left(\frac{\sigma_{i2}}{\sigma_o}\right)^m + \left(\frac{\sigma_{i3}}{\sigma_o}\right)^m\right] \cdot V_i$$

where:

m = Weibull modulus

V_o = test specimen volume

n = number of elements in the finite element model (in this case n = 204).

V_i = volume of element number i

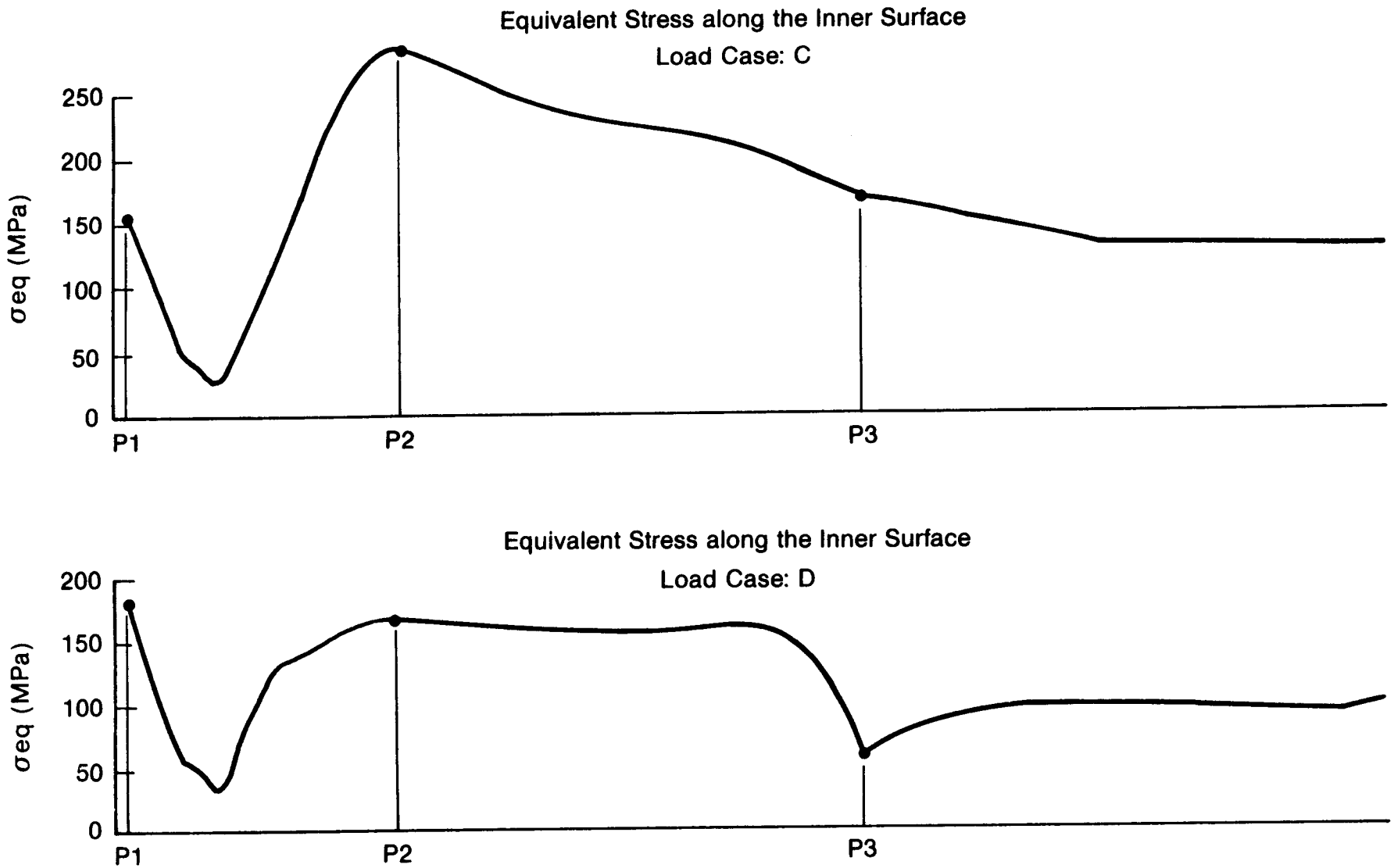
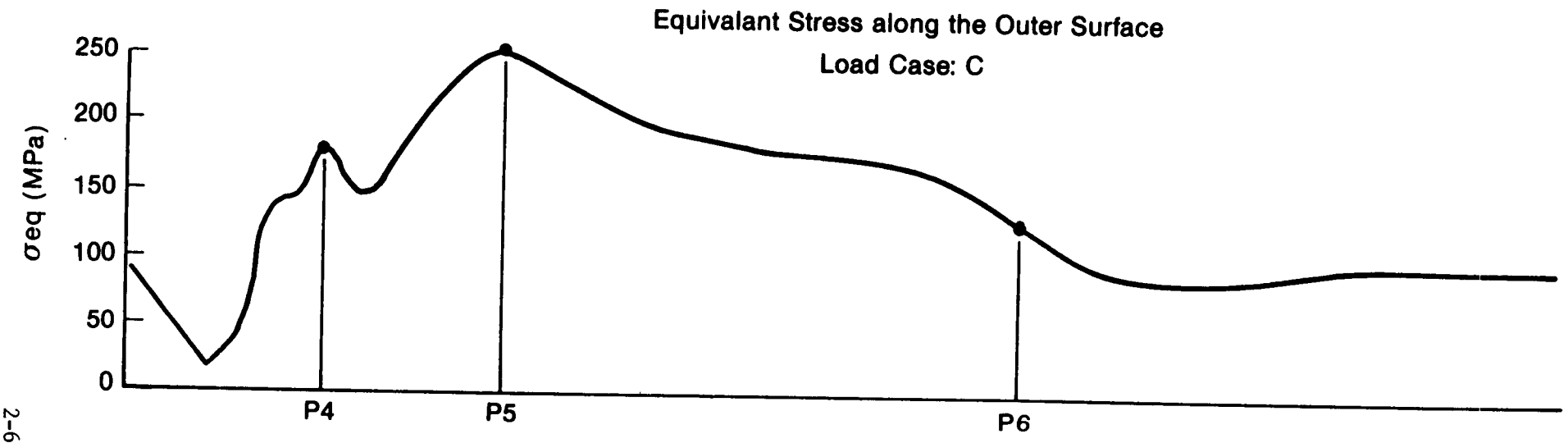


Figure 2-24 Stress Distribution Along the Inner Surface for Material Group 1



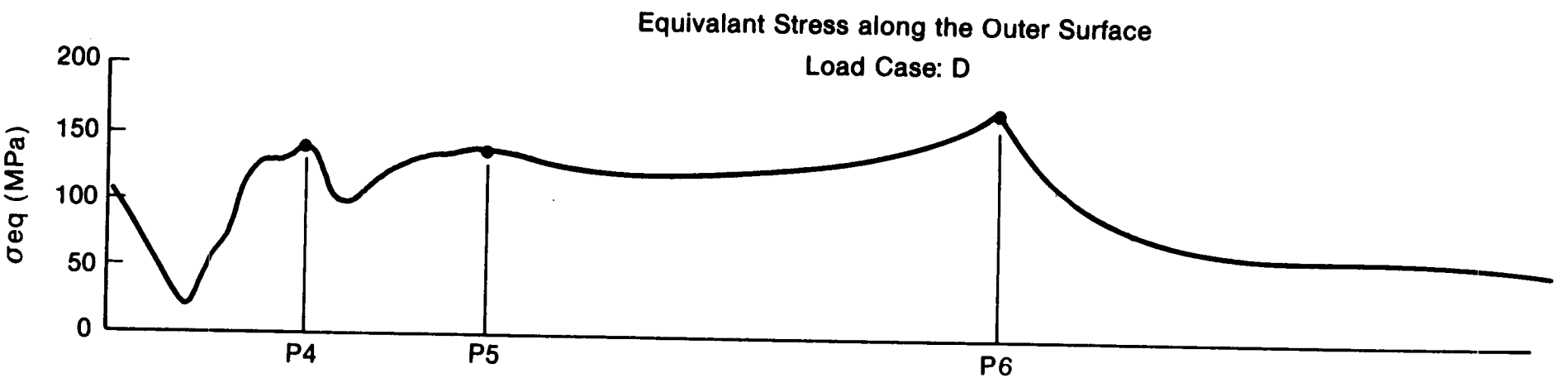


Figure 2-25 Stress Distribution Along the Outer Surface for Material Group 1

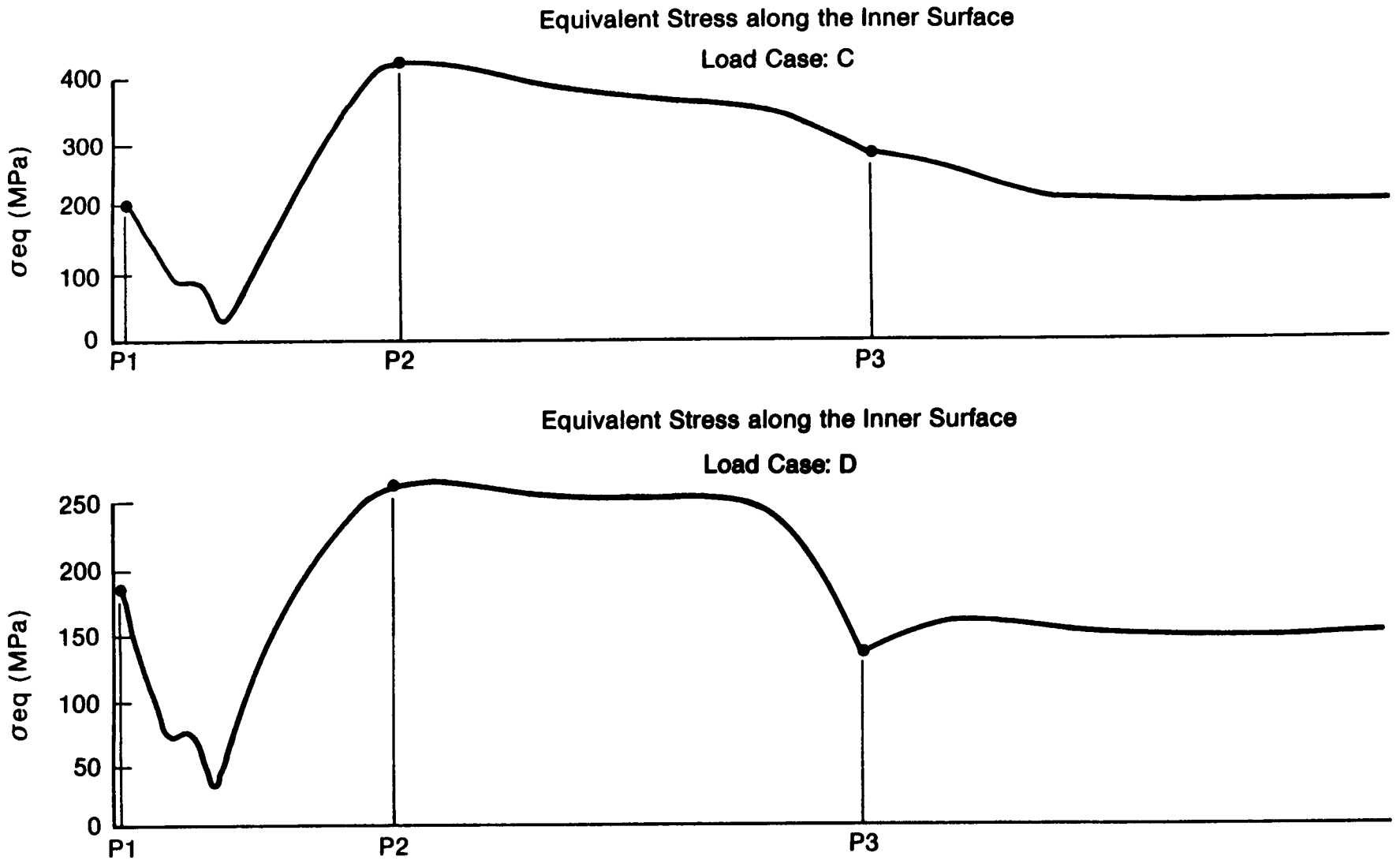


Figure 2-26 Stress Distribution Along the Inner Surface for Material Group 2

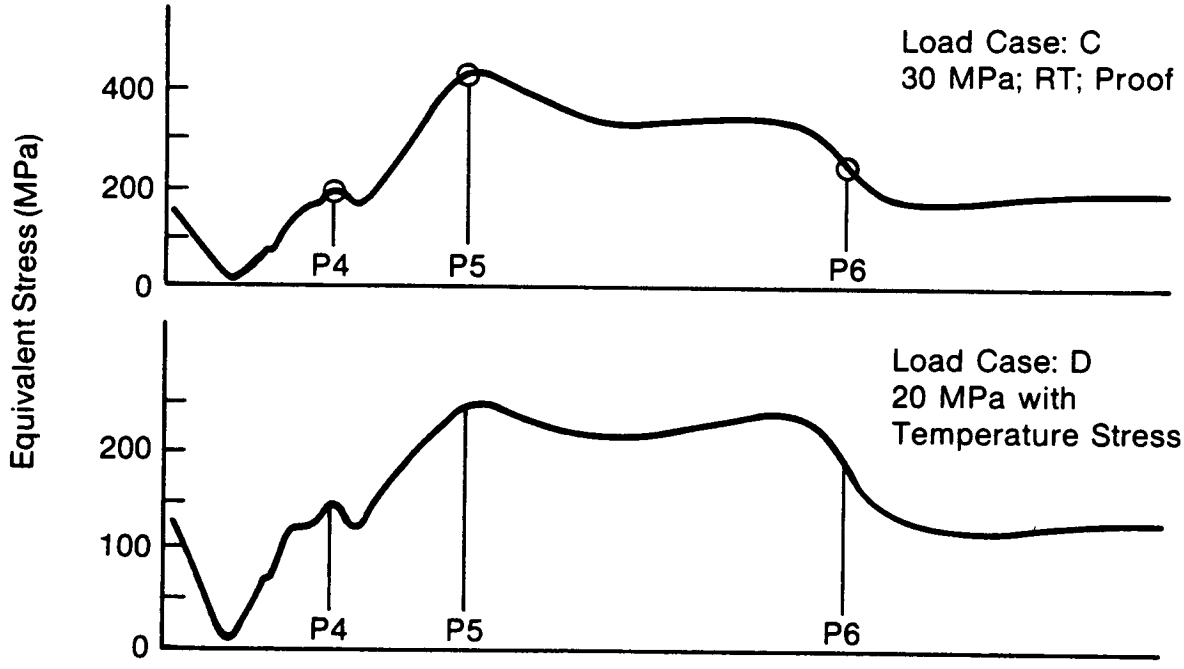


Figure 2-27 Stress Distribution Along the Outer Surface for Material Group 3

$\sigma_{i1}, \sigma_{i2}, \sigma_{i3}$ = principal stresses in element number i

σ_o = ultimate tensile/compressive strength of the test specimen. If σ_{ij} is positive, the ultimate tensile stress is used when σ_{ij}/σ_o is calculated. If σ_{ij} is negative, then the ultimate compressive strength is used.

Based on the calculation procedure above, the failure probabilities for the different load cases and material groups were evaluated. The failure probabilities for materials Group 3 were calculated based on the stress distribution for material Group 1, which needs approximately the same wall thickness in the pressure vessel. The results are listed in Table 2-8.

2.6.6 Material Characterization from Thermal Transient Point of View

The three material groups were compared from the thermal transient point of view. This was done based on analytical expressions for the maximal stress in a flat plate exposed to a thermal shock. The temperature step ΔT was selected to 700°C and the surface heat transfer coefficient h was 2000 $w/m^2°C$. This temperature loading is assumed to represent an upper limit of what is possible during start-up of the engine. As the material properties are time dependent, the maximal stress was evaluated based on material properties at two different temperature levels (at 100°C and at 500°C). The result can be seen in Figure 2-28, which shows the maximum stress, due to the temperature step ΔT = 700°C, as a function of the wall thickness t. Evidently, the material Groups 1 and 2 show a similar response to a temperature transient. Material Group 3 differs significantly, with considerably higher stresses. This is due to the lower thermal conductivity of the Group 3 materials which results in higher gradients for a given thermal input configuration. In Figure 2-30 "S_{max}" refers to the maximal absolute value of the compressive stresses, which occur on the hot side as a result of the temperature step ΔT.

2.6.7 Stress Analysis Based on Transient Loading Conditions

2.6.7.1 Finite Element Model. Thicker walls are always worse from a thermal transient point of view. The stresses due to a thermal transient were higher for material Group 3 and approximately equal for the material Groups 1 and 2. For this reason, the transient thermal analysis was based on the finite element model, which has a wall thickness of 6.5 mm. Consequently, the analysis was performed

TABLE 2-8

FAILURE PROBABILITY FOR CASE MATERIALS

	Material Group Number		
Load Case	1	2	3
A	$6.0 \cdot 10^{-8}$	$< 10^{-10}$	$< 10^{-10}$
B	$2.0 \cdot 10^{-3}$	$2.4 \cdot 10^{-6}$	$8.7 \cdot 10^{-5}$
C	0.11	0.18	0.25
D	$1.7 \cdot 10^{-3}$	$6.0 \cdot 10^{-7}$	$4.4 \cdot 10^{-5}$

A - Steady-State Temperature (P = 0 MPa)
B - Maximum Operating Pressure (P = 20 MPa)
C - Proof Test Pressure (P = 30 MPa)
D - Combined Steady-State Temperature and Maximum Pressure (P = 20 MPa)

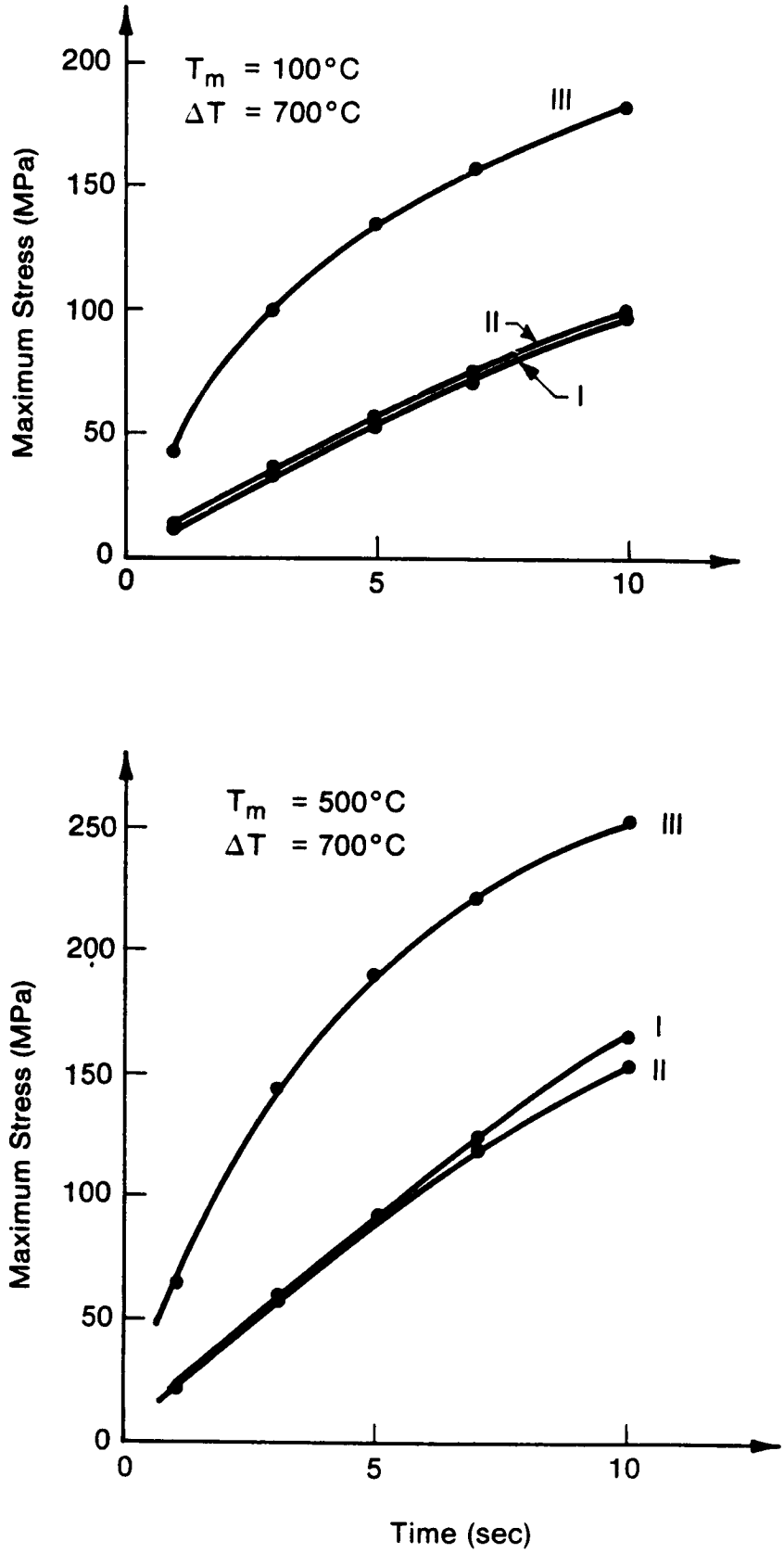


Figure 2-28 Maximal Stress as a Function of the Wall Thickness for a Flat Plate Exposed to a Temperature Step of 700°C

only for the material Groups 1 and 3. For the same temperature step the stresses were higher for a higher material temperature. Therefore, the material properties at a rather high mean temperature (Tm = 500°C) were used in the transient analysis.

2.6.7.2 Loading Conditions. The most severe loading conditions from the thermal transient point of view occur when cranking of the engine starts. At this moment the upper part of the heater housing will be exposed to the hot working gas. In this analysis the following gas temperature function has been assumed: instant temperature rise to 750°C followed by a slow temperature increase to 900°C, which is reached after 20 seconds. After this, the gas temperature is kept constant at 900°C. This gas temperature function is used together with a conservatively estimated value on the surface heat transfer coefficient (2000 $w/m^2°C$). The analysis starts with an initial temperature of 20°C in the housing. The inner surface of the dome shaped top is then exposed to the hot gas resulting in two consecutive phenomena. The first on is the "skin effect" due to a rapid temperature increase of the surface layer resulting in high compressive stresses on the surface exposed to the hot gas. The maximal stress occurs after just a few seconds. This stress is mainly dependent on the wall thickness and less dependent on the geometry of the pressure vessel. The second phenomenon occurs much later in time when the upper part of the housing has become rather hot while the lower cylindrical part is cold. This results in high bending stresses in the cylindrical part of the housing in a point where the slope of the axial temperature gradient has its maximum value. Consequently, the high stresses occurring after a few seconds depend on the temperature gradient through the pressure vessel wall and the high stresses occurring later in time depend on the axial temperature gradient in the pressure vessel.

2.6.7.3 Transient Temperature Distribution. Figure 2-29 shows the location of some points of interest in the discussion of the result from the transient analysis. In Figure 2-30 is shown the temperature as a function of time in some different points on the heater housing. "I" refers to material Group 1. Figure 2-31 shows the same thing, but for material Group 3. Figure 2-32 shows the axial temperature distribution between point B and C on the inner surface of the housing. The temperature distributions for the different material groups are shown for the time at which the stress in the cylindrical part (point E) reaches its maximum value. This occurs after 20 seconds for material Group 1 and after ~40

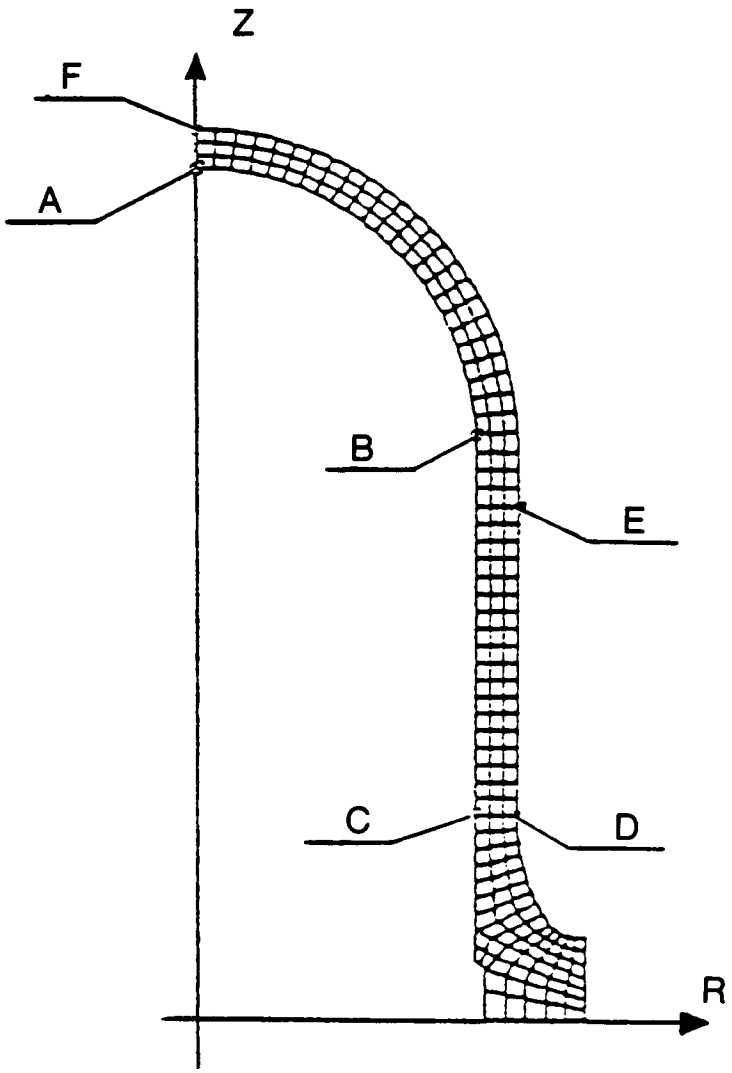


Figure 2-29 Location of Some Points Referred to in the Transient Analysis

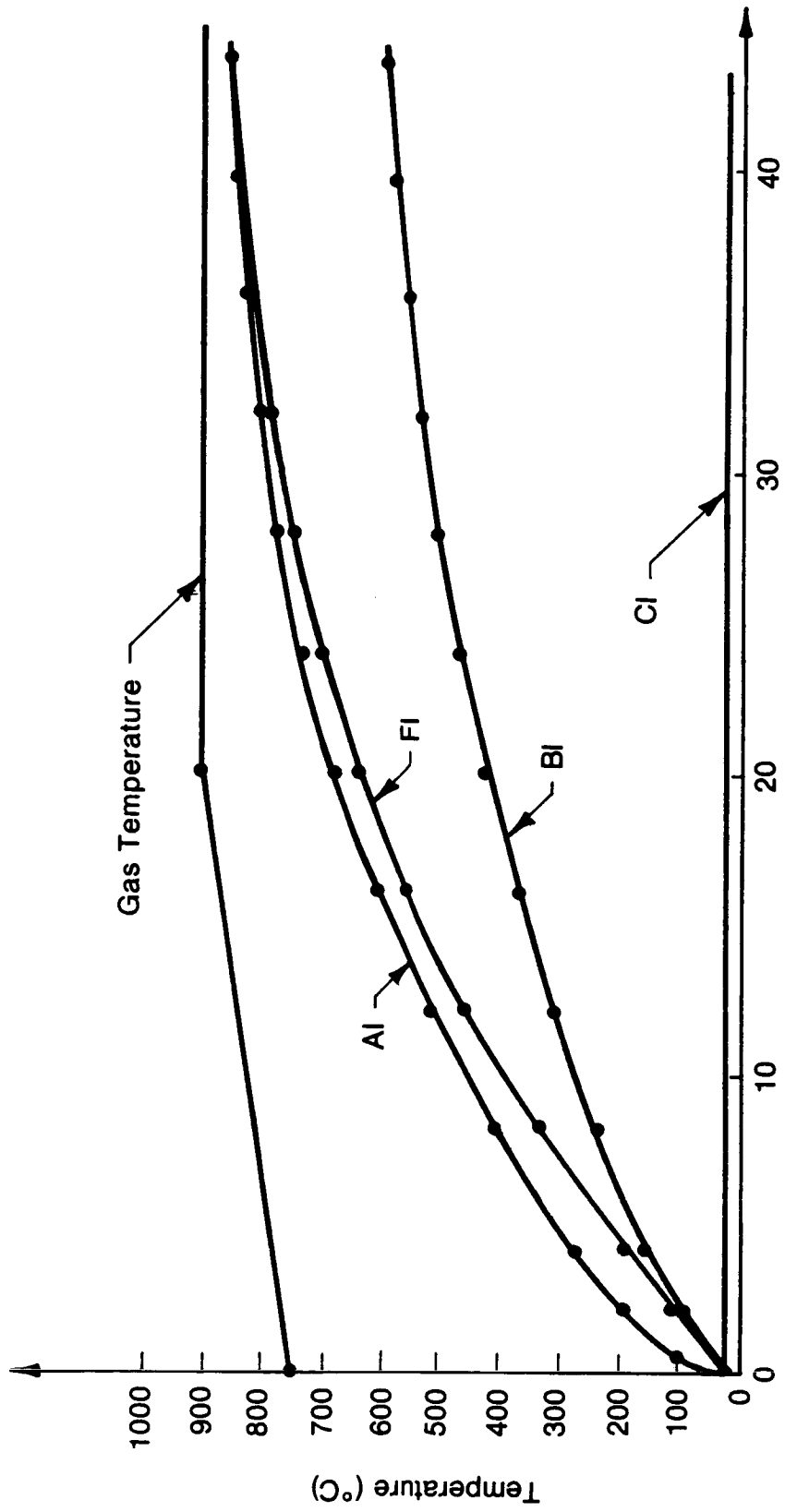


Figure 2-30 The Temperature in Some Points as a Function of Time (Material Group 1)

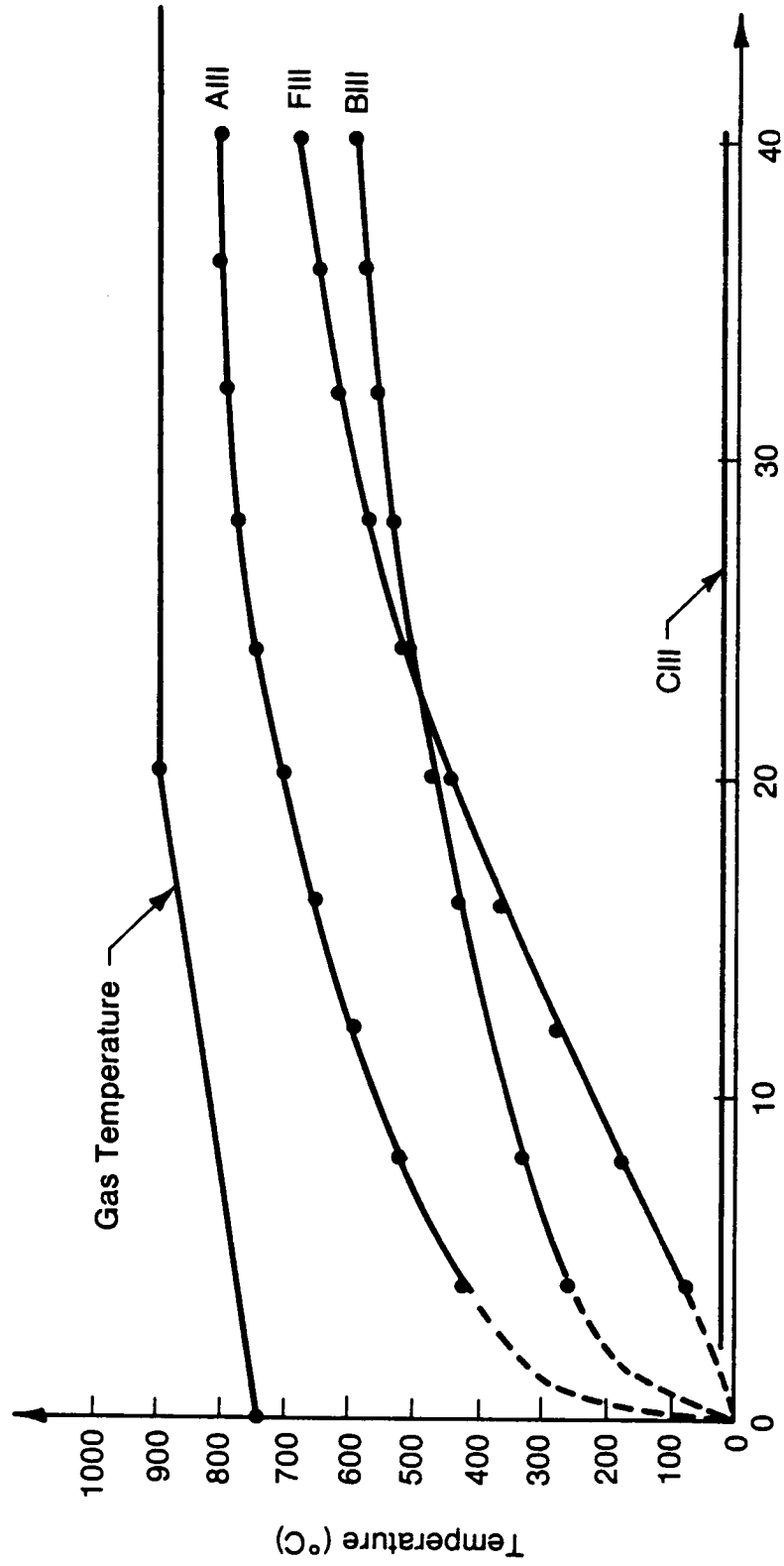


Figure 2-31 The Temperature in Some Points as a Function of Time (Material Group 3)

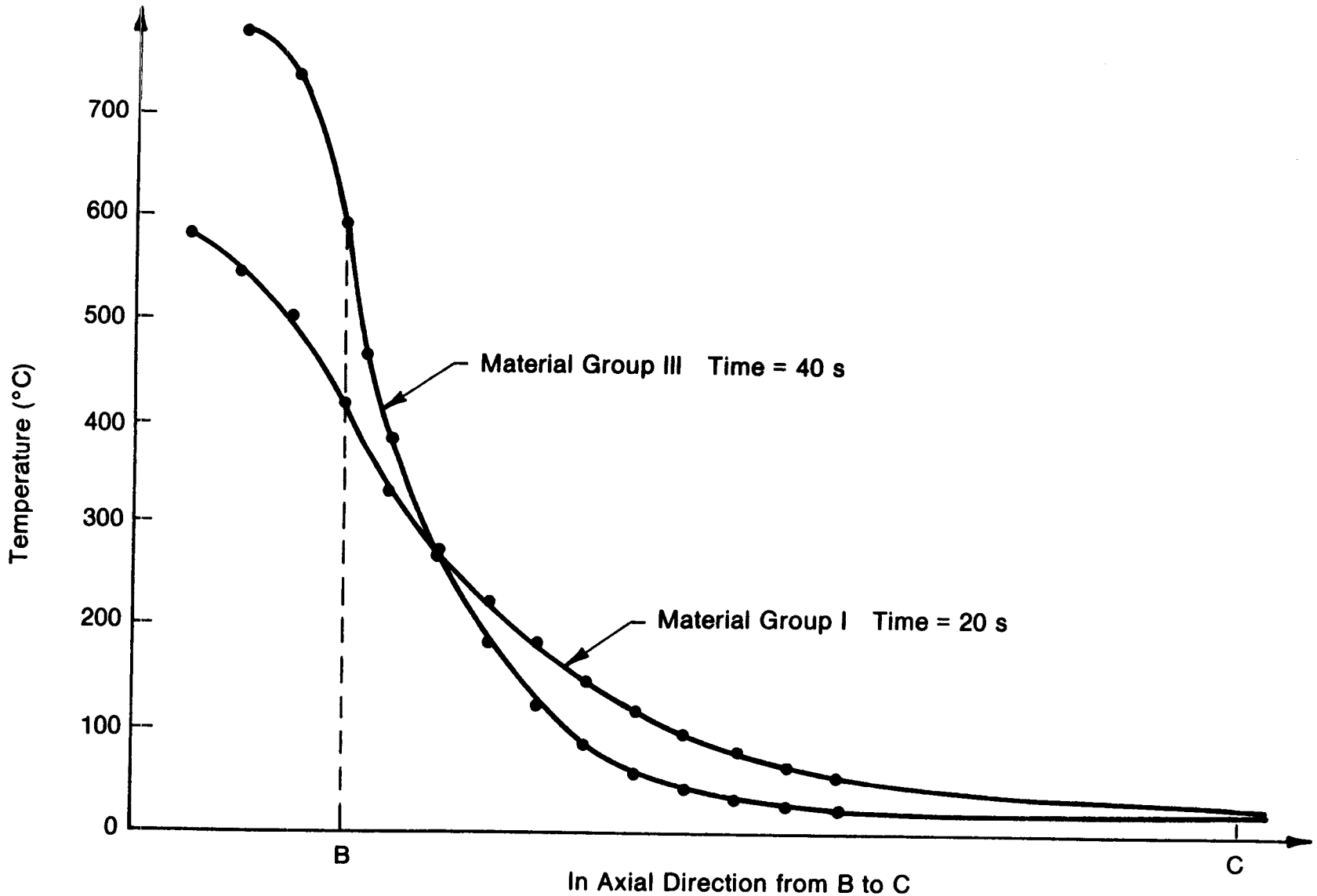


Figure 2-32 The Axial Temperature Distribution in the Housing at the Time of Maximal Stress in the Cylindrical Part

seconds for material Group 3. The axial temperature gradient is steeper for material 3 due to its lower thermal conductivity. However, the stresses due to the axial temperature gradient are somewhat lower for material Group 3. The reason is the lower value on Young's modulus, 140 GPa compared to 370 GPa for Group 1.

2.6.7.4 Transient Stress Distribution. Figure 2-33 shows the equivalent stress as a function of time for some different points on the housing. "I" and "III" refer to the different material groups. The stress in point A is a good example of the "skin effect", in which the surface layer of the material is heated up very rapidly, resulting in high compressive stresses. The maximum stress is higher for material Group 3 due to its lower thermal conductivity. The diagram shows that the maximum stress due to the axial temperature gradient (point E) occurs much later in time, after 20 seconds for material Group 1 and after ~40 seconds for Group 3.

2.6.7.5 Failure Probability. The failure probability of the housing was evaluated based on the finite element analysis in the same manner as in Section 5.4. The analysis was based on the transient stress distribution at different points in time. Naturally, the stress distributions at which the maximal stresses occur were selected. For material Group 1 the stress distribution after 1.6 seconds and after 20 seconds was used. For material Group 3 the critical stress distribution occurred after 4 seconds and after ~40 seconds. The following result in terms of failure probability P_f was evaluated.

Material Group 1, t = 1.6 seconds: $P_f - 3.0 \cdot 10^{-8}$
Material Group 1, t = 20 seconds: $P_f - 1.9 \cdot 10^{-6}$
Material Group 3, t = 4 seconds: $P_f - 10^{-10}$
Material Group 3, t = 40 seconds: $P_f - 1.3 \cdot 10^{-7}$

Evidently, the stress distributions during the first few seconds are less critical than the stress distributions corresponding to the axial temperature gradient, which has its maximal slope later in time. The reason is that the high stresses during the first few seconds are compressive and will therefore contribute much less to the failure probability.

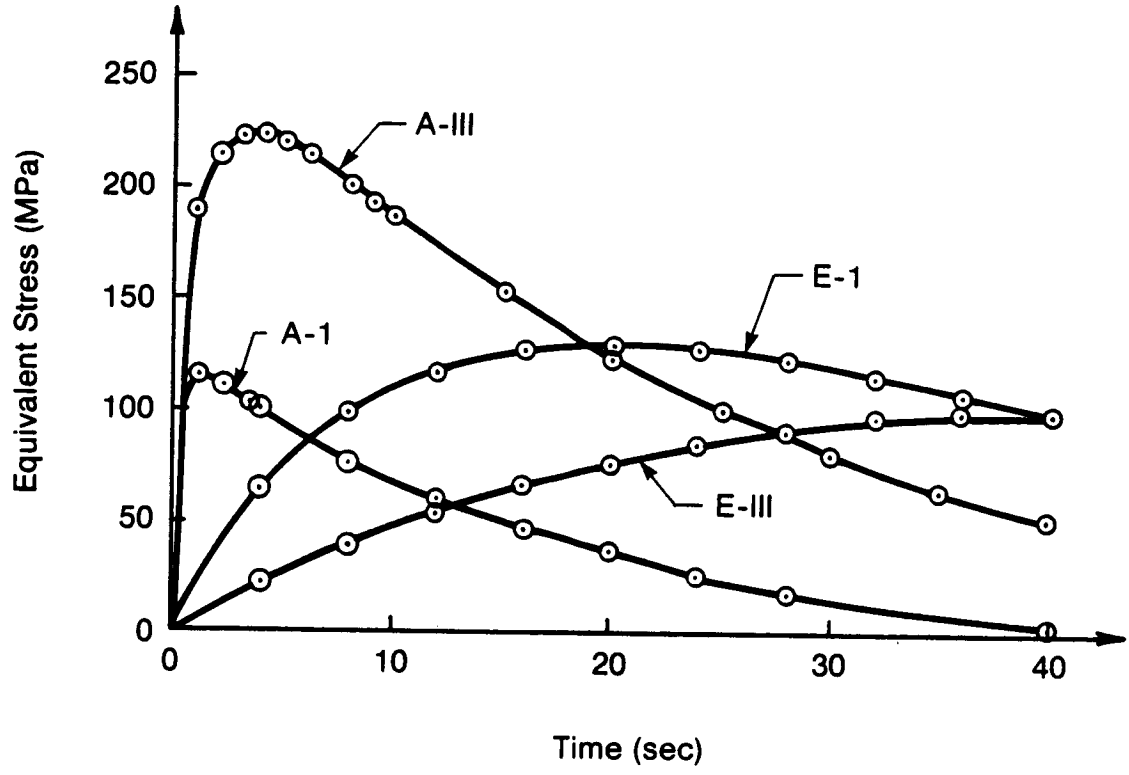


Figure 2-33 Stress as a Function of Time for Various Points on the Heater Head Housing

2.6.8 The Manifolds from the Stress Point of View

In this simplified stress analysis, it has been assumed that the stress distribution in the manifolds will not contribute significantly to the total failure probability of the heater. In the first approximation, this is probably an acceptable assumption for the following reason. Due to manufacturing constraints, the relative wall thickness of the manifolds will be greater than the relative wall thickness of the housing although the absolute wall thickness of the manifolds is actually less than the wall thickness of the housing. This results in much lower manifold pressure stresses. The stress due to thermal transients in the manifolds will also be less than in the housing.

2.6.9 The Heater Tubes from the Stress Point of View

Similar to the manifold situation, it has been assumed that the stress distribution in the heater tubes will not contribute significantly to the total failure probability of the heater. The stresses due to the internal pressure and due to thermal transients will be considerably lower than in the housing for the same reasons as for the manifolds.

2.6.10 Conclusions

As previously discussed, due to the inherently brittle nature of ceramic materials, stress analysis must be performed on a probabalistic basis with the final criteria being an acceptable failure probability.

The overall conclusion of the stress analysis is that ceramic materials with the properties discussed in Section 2.2 can be used to fabricate heater heads and tubes with acceptable failure probabilities. The analysis indicates that the pressure loading is the major contributor to the failure probability (load case B). The thermal transient at start-up appears to be more severe in terms of failure probability than the steady state temperature distribution (case A) only. However, since the thermal transient occurs at a low pressure (2-3 MPa), the actual worst case operating condition is at maximum mean pressure and at steady state temperature (i.e., load case D, failure probability of 4.4×10^{-5}, Group 3 material).

The Group 2 materials have the best strength characteristics, which for a given failure probability results in the thinest wall thickness. However, due to the low thermal conductivity of the Group 3 materials the overall engine performance is best, despite the thicker wall section required. Each of the three material groups appears adequate for use as a Stirling engine heater head material based upon the material properties assumed for this study.

3.0 TASK II - PERFORMANCE EVALUATIONS

3.1 Preliminary Design Evaluations

To support the initial design and material selection for the CASE design, a set of preliminary thermodynamic performance analyses were performed over a range of heater head temperatures. These evaluations involved performing an optimization of the engine design at each temperature level. The optimization process utilizes a computer code which models the engine geometry and optimizes each geometric variable (i.e., bore, stroke, manifold volume, tube length, regenerator porosity, etc.) to maximize the overall engine mileage (i.e., efficiency at an average operating point modified by CSP effects) while simultaneously satisfying a maximum power requirement of 60 kW at 4000 rpm. Included in the optimization program is a calculation of the required regenerator wall thickness and conduction losses based on the physical properties of the heater head material. Similarly other engine conduction losses, such as appendix gap, piston dome conduction and partition wall conduction losses are calculated based on the geometry and specified material characteristics. The optimization code also calculates the thermal efficiency of the EHS (η_B) based on geometric and material properties, while attempting to minimize the stored thermal energy (i.e., CSP) of these components. The code also calculates frictional losses in the engine drive system based on engine speed and mean pressure. The auxiliary and control system losses (i.e., blowers, water/oil pump, etc.) are also calculated based on engine speed and mean pressures as is discussed in the 1981 RESD report (Reference 1).

For the initial set of optimizations, the baseline engine losses (drive friction, auxiliaries, and EHS efficiency) were set equal to the 1981 RESD losses. Such secondary effects as the effect of heater head temperature and CGR requirements on combustion blower power and EHS efficiency were not initially included. The objective of the preliminary set of optimizations was to model the initial engine design concept using silicon carbide material properties for the heater head, tubes, piston dome, and EHS components. The regenerator was assumed to be metallic screen and the preheater performance was derived from the ceramic preheater currently under development for Mod II. The engine performance was optimized at six temperature levels: 820, 920, 1020, 1120, and 1220°C, with 1220°C being the upper range with silicon carbide. The results of this initial evaluation as well

as the 1981 RESD results are shown in Table 3-1. The table also contains a preliminary estimate of the combined mpg based on the engine map and the estimated CSP. This initial group of performance evaluations was disappointing, resulting in both efficiencies and mileage less than the 1981 RESD at all heater head temperatures up to 1220°C. The conclusions of this optimization were that the CSP was very high, and the conduction loss was very large (3 kW was assumed radial wall conduction loss). In addition, the efficiency of the EHS decreased as the heater head temperature increased due to limitations of preheater effectiveness. It was apparent from this initial optimization that silicon carbide is not well suited for use in this type of Stirling engine design as heater head material. The conduction losses, neglecting the assumed radial loss associated with the annular design (not present in the 1981 RESD) are much larger than the metallic 1981 RESD engine due to the combination of high thermal conductivity and required wall thickness associated with silicon carbide. The CSP values are all in the range of 2-3 times the 1981 RESD value.

Subsequent to the initial optimizations, three heater head material groups were identified based on the concept of investigating materials with better strength/conductivity properties. The material groups included: Group 1 - silicon carbide, Group 2 - silicon nitride, and Group 3 - silicon carbide whisker reinforced mullite. The engine optimizations were repeated utilizing the engine material properties for each of the groups. In addition, the Stirling engine optimization code was updated to incorporate the following features:

- The radial partition wall conduction losses was revised and calibrated based on actual annular engine design test results
- The CSP modeling was improved by better specific heat curve fitting
- The regenerator housing wall thickness was calculated based on Weibull failure theory, applied on an 85% survival rate at 30 MPa internal pressure
- The piston stroke was allowed to vary as an optimization parameter.

In addition to these features, it was determined that the EHS components would be fabricated of porous silicon carbide material with a leak tight "skin" on one side. This approach greatly reduced the material density, thus reducing the stored energy in the EHS and therefore the CSP.

TABLE 3-1

CASE SiC PRELIMINARY RESULTS

Optimization Results

Quantity	1981 RESD	SiC CASE				
	344-00	3-00	5-00	6-00	7-00	8-00
Heater Head Temp. (°C)	820	820	920	1020	1120	1220
Combined mpg	37.6	28.3	28.8	28.6	28.3	27.8
Part-Load Efficiency (%)	37.6	30.5	31.6	32.1	32.2	32.1
Hot Energy (MJ)	9.8	15.6	16.9	18.1	19.5	20.9
CSP (g)	134	261	282	303	326	350
Q_{cond} (kW)	1.6	7.3	7.0	7.3	7.5	7.7
Swept Volume (cc)	106	116	105	93	85	79
Cylinder Diameter (mm)	63	66	63	59	56	54
Part-Load (η_B)	91.7	92.1	91.0	89.9	88.8	87.7
Full-Load Efficiency (%)	34.2	30.0	32.3	34.8	36.9	38.1
Full-Load Power (kW)	60	60	60	60	60	60

Based on the preliminary optimization of the Group 1 materials, each of the three material groups was optimized at 1020°C since the effect of temperature on mileage appeared relatively "flat" at temperatures above 1020°C. To confirm the effect of heater head temperature performance, the Group 3 design was optimized at 920, 1020, and 1120°C. The results of these performance analyses are shown in Table 3-2.

Although the improvements in modeling and the reduction of the hot mass in the EHS improved the performance of the Group 1 design, it was still not as good as the 1981 RESD in terms of mileage or efficiency. The Group 2 design showed some performance improvement over the 1981 RESD. This was primarily due to the reduction in conductivity losses down the regenerator housing caused by the lower thermal conductivity of silicon nitride and the reduced wall thickness due to its excellent high temperature strength properties. The Group 3 materials at 1020°C showed a clear improvement over the 1981 RESD performance. Mileage improved from 36.5 to 39.9 mpg, with a corresponding improvement in part-load efficiency from 37.6 to 39.2%. It should be noted that only the Group 3 design included a Nextel (lithium aluminum silicate from 3M Corp.) regenerator matrix which helped increase efficiency relative to metallic matrices. The results of the material group comparisons clearly indicated that the Group 3 material approach would offer the best performance for a ceramic ASE. Accordingly, the final stages of engine performance optimization concentrated on the Group 3 material design.

3.2 Final Engine Design Optimization

The final optimization was performed using the Group 3 materials, at a heater head temperature of 1020°C. Although higher temperatures could be considered for the mullite materials, the insensitivity of mileage to temperature above 1000°C did not warrant pursuing these temperatures.

The model used in developing the final optimization included a blower power correction to account for the increased CGR required to prevent excessive NO_x production in the combustor (see Section 3.3). The remaining engine auxiliary and frictional losses were as in the 1981 RESD. A comparison of the performance and loss breakdown for the 1981 RESD and the optimized CASE Group 3 design is shown in Table 3-3. The 1983 V-4, annular regenerator RESD is also shown in Table 3-3 for comparison with the latest metallic technology. The overall engine map is shown

TABLE 3-2

CASE PERFORMANCE RESULTS

Optimization Results

Quantity	1981 RESD	Group 1	Group II	Group III		
	344-00	103-00	201-00	302-00	303-00	304-00
Heater Head Temp (°C)	820	1020	1020	1020	920	1120
mpg	37.6	35.2	38.5	39.9	39.4	40.1
Part-load Efficiency (%)	37.6	34.5	37.7	39.2	38.4	39.9
Hot Energy (MJ)	9.8	9.3	8.7	8.5	7.9	9.2
CSP (g)	134	126	117	116	107	126
Q_{cond} (PL) (kW)	1.6	4.7	2.4	1.5	1.4	1.6
Part-Load η_B (%)	91.7	89.7	89.4	89.3	90.5	88.1
Full-Load Efficiency (%)	34.2	33.3	35.2	36.9	34.9	38.4
Swept Volume (cc)	106	98.7	98.5	97.1	105.7	92.7
Regenerator Data	Metal	Metal	Metal	Nextel	Nextel	Nextel

TABLE 3-3

PERFORMANCE OF OPTIMIZED CASE GROUP 3
1981 and 1983 RESD ENGINES

Power in kW, efficiency in %, and speed in rpm

Operating Point		1981 RESD 34-00	1983 RESD V4AR 723-00	CASE 1984 Material Group 3 305-00
Full-Load Point	p = 15 MPa n = 4000 rpm			
Indicated Power		73.3	69.8	72.7
Friction		9.8	6.3	9.0
Auxiliaries		3.4	3.4	3.6
Net Power		60.1	60.2	60.0
EHS Efficiency		90.5	90.3	89.0
Net Efficiency		34.2	34.6	36.5
Part-Load Point	p = 12 kW n = 2000 rpm			
Indicated Power		14.9	14.3	14.8
Friction		2.1	1.4	1.9
Auxiliaries		0.8	0.9	0.8
Net Power		12.0	12.0	12.0
EHS Efficiency		91.7	92.3	89.3
Net Efficiency		37.6	37.3	39.1
Heat Conduction Loss		1.6	2.6*	1.5*
Max Efficiency Point	p = 15 MPa			
Engine Speed		1100	1350	1300
Indicated Power		24.8	28.1	27.8
Friction		2.3	2.0	2.5
Auxiliaries		0.4	0.6	0.6
Net Power		22.1	25.5	24.7
EHS Efficiency		92.4	92.8	90.5
Net Efficiency		43.5	42.2	44.4
Low-Load Point	p = 5 MPa n = 1000 rpm			
Indicated Power		7.9	7.2	7.4
Friction		0.9	0.6	0.8
Auxiliaries		0.4	0.4	0.4
Net Power		6.6	6.2	6.1
EHS Efficiency		89.8	90.7	86.6
Net Efficiency		36.4	33.9	36.7

*Conduction loss redefined since 1981 RESD

in Figure 3-1. The CASE design incorporating the Group 3 materials achieved a peak efficiency of 44.4% at 15 MPa and 1300 rpm. The conduction losses have been minimized and the cycle efficiency (ratio of heat input to the cycle to P-V power delivered to the pistons) is 55% or ~73.3% of the Carnot cycle efficiency at this temperature. It should also be noted that at the higher heater head temperature there is a tendency for the EHS efficiency to drop due to practical limits on the preheater effectiveness.

The sensitivity of the final CASE optimization to heater head temperature is shown in Figure 3-2. Mileage, part load and full load efficiency are plotted against heater head temperatures from 820 to 1220°C. As can be seen from this figure, combined mileage peaks in the range of 1100°C, although it is essentially flat over the range of ~1000-1200°C. At temperatures above 1200°C despite the fact that part-load engine efficiency is increasing, the mileage begins to decrease due to increasing CSP and decreases in EHS efficiency. The net result of this effect is that although higher heater head temperatures may lead to marginal improvements in part-load engine efficiency, corresponding increases in CSP and conduction losses, and reduced EHS efficiency outweigh any net efficiency gains at temperatures above 1200°C.

It should be noted that the combined mileage predictions discussed thus far in this study are based on the latest USAB vehicle performance code. This code, as well as the MTI vehicle performance code have been extensively modified since 1981 when the original 1981 RESD mileage predictions were published. The use of the latest USAB vehicle simulation model results in the 1981 RESD engine map producing a combined mileage of 37.6 mpg (134 g CSP) versus the original 1981 RESD estimate of 41.1 mpg based on 94 g CSP. The USAB code predicts a 1.6 mpg or 4.3% improvement for the optimized CASE over the 1981 RESD.

To confirm the USAB mileage predictions, the 1981 RESD and optimized Group 3 engine maps were run through the MTI vehicle simulation code. The MTI simulation code, which is slightly different than the USAB code, predicted an 1981 RESD mileage of 39.3 mpg (134 g cold start) and a CASE mileage of 40.7 mpg or a 1.4 mpg (3.5%) improvement. Although there is more than a 1 mpg difference between the two codes, the relative performance between the two designs is quite consistent (3.5 versus 4.3%). A summary of the MTI mileage results is shown in Table 3-4. A

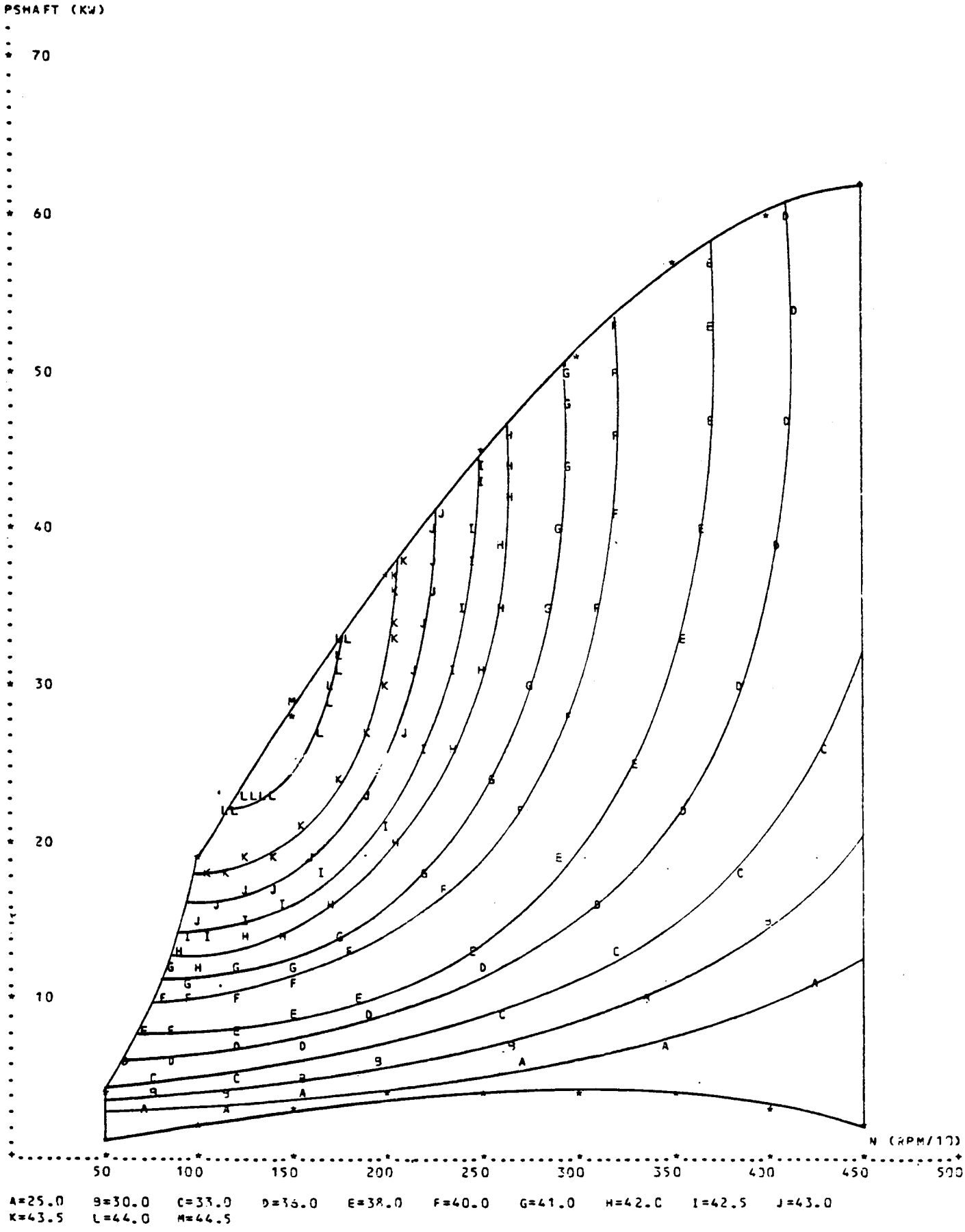


Figure 3-1 CASE Performance Map

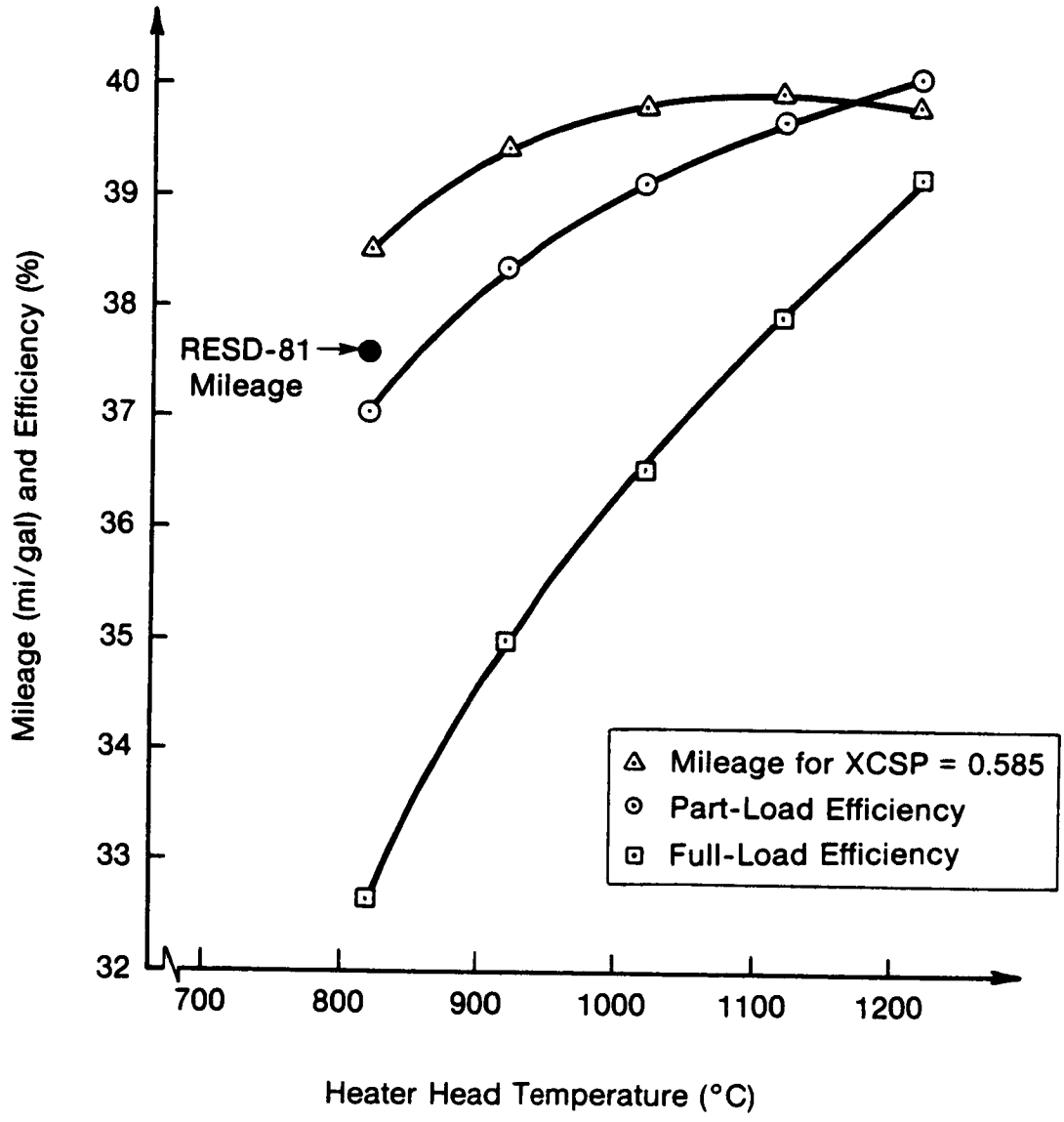


Figure 3-2 CASE Mileage and Efficiency as a Function of Heater Head Temperature

TABLE 3-4

CASE VEHICLE PERFORMANCE (MTI CODE)
(Unleaded Gasoline)

	CASE 305-01	1981 RESD 344-01
Urban Mileage (without CSP)	39.4	39
CSP (g)	115	134
Urban Mileage (with CSP)	32.4	31.2
Highway Mileage	59.1	57.4
Combined mpg	40.7	39.3
0-60 mph (s)	15.5	14.8

TABLE 3-5

1981 RESD/CASE VEHICLE SPECIFICATIONS

	EPA Cycles
Vehicle Mass	3125 lb
Engine Inertia	6.07 lbm/ft^2
Torque Converter Inertia	.54 lbm/ft^2
Transmission Inertia	.19 lbm/ft^2
Wheel Inertia	45.40 lbm/ft^2
Drag Coefficient	.419
Rolling Friction Coefficient	.0110
Air Density	.0727 lbm/ft^3
Fuel Density	6.17 lb/gal
Frontral Area	21.34 ft^2
Idle Speed	600 rpm
Engine	CASE 305-01
Transmission Gear Ratios:	
First	2.91
Second	1.55
Third	1.00
Fourth	.71
Accessory Loads	PS/FP
Lockup Speed	30 mph
Drop Out Speed	25 mph
Transmission Efficiency	Ricardo Polynomial
Torque Converter	GM THM 125
Axle Ratio	3.77

summary of the vehicle specification used in the simulation model is shown in Table 3-5.

The geometric characteristics of the final CASE optimization (305-00) are shown in Table 3-6. These values were used to develop the final engine design discussed in Section 2.0.

3.3 CASE Emission Considerations

Since the ultimate objective of the CASE design is to meet the requirements of an automotive application, a preliminary analysis was performed to evaluate the emission control requirements for a Stirling engine operating at heater head temperatures in the range of 1000-1050°C.

Currently, the engines developed under the ASE Program, operating at 820°C are able to meet the EPA emission requirements mandated by the Clean Air Act. Since the combustion in a Stirling engine is continuous, and takes place external to the engine cycle, the formation of pollutants such as CO, hydrocarbons, and particulate emissions is not a problem except under transient conditions. However, the control of NO_x, due to the high flame temperatures, requires special considerations. The Mod I and Mod II engines utilize two systems to control NO_x emissions; exhaust gas recirculation (EGR) and combustion gas recirculation (CGR). Both systems recirculate combustion products into the combustion zone to reduce the flame temperature and, hence the NO_x level. The only difference between the two systems is that CGR is internal to the combustor, while EGR reinjects cooled exhaust gas from the exhaust exit to the air inlet. By properly sizing the amount of CGR or EGR, the NO_x emissions can be controlled below the EPA 0.4 g/mi limit. However, the use of CGR or EGR has an adverse effect on blower power, thus it is important to determine the level of CGR or EGR required and factor this level into the blower power requirement. It should be noted that the CASE combustor design incorporates CGR, however, the analysis addresses both CGR and EGR.

Analytical and experimental data was used to estimate the amount of EGR or CGR needed for a CASE vehicle to achieve 0.4 g/mi NO_x over the urban CVS cycle.

The calculations were based on the following assumptions:

TABLE 3-6

FINAL CASE ENGINE GEOMETRY

All Dimensions in mm

Engine Type: CASE Type U4AR Optim 305-00 with Heater Temperature 1020°C

Expansion Cylinder	
Cylinder Diameter	61.7
Crank Radius	16.2
Stroke	32.4
Displacer Dome Height Cylinder Part	106.
Radial Gap Cylinder Wall Dome	0.40
Clearance Dome Cylinder Top	1.0
Cylinder Wall Thickness	2.0
Dome Wall Thickness	2.0 (min)
Duct Expansion Cylinder-Heater	
Volume (cc)	12.8
Heater	
Number of Tubes Per Cycle	22
Tube Inner Diameter	2.5
Outer Diameter/Inner Diameter	1.5
Length of One Tube	215
Effective Length/Total Length	0.86
Duct Heater-Regenerator	
Volume (cc)	20.5
Regenerator	
Matrix Type	Nextel Gauze
Matrix Cross Sectional Area Per Cycle (cm^2)	23.0
Matrix Length	77.6
Filling Factor	0.29
Wire Diameter	0.055
Housing Wall Thickness	5.7

TABLE 3-6

FINAL CASE ENGINE GEOMETRY (Continued)

Duct Regenerator-Cooler	
Volume (cc)	1.2
Cooler	
Number of Tubes Per Cycle	220
Tube Inner Diameter	1.0
Outer Diameter/Inner Diameter	1.7
Length of One Tube	70.4
Effective Length/Total Length	0.773
Relative Pitch	1.86
Duct Cooler Compression Cylinder	
Volume (cc)	59.9
Compression Cylinder	
Cylinder Diameter	61.7
Piston Rod Diameter	12.4
Crank Radius	16.2
Clearance Piston-Cylinder Bottom	1.0
Connecting Rod Length	90.5
Regenerator Housing Dimensions	
Housing Inner Diameter	85.2
Regenerator Matrix Width (Radially)	9.7
Partition Wall Thickness	2.0
Heater Height	94.0
Front Row Heater Tube Gap	2.12

1. Unleaded gasoline fuel approximated by octane, $C_8 H_{18}$.

2. CASE parameters:

   a. heater head temperature = 1020°C
   b. preheat air temperature (Tin) = 1100°C
   c. urban CVS mileage = 31.7 mpg (preliminary estimate)

3. NO_x:

   a. 100% prompt + thermal (e.g., no fuel bound nitrogen)
   b. formation occurs at stoichometric
   c. residence time = Upgraded Mod I and Mod I
   d. rate defined by "flames and combustors" (Figure 3-3)

4. Flame temperature:

   a. NASA equilibrium, Tin = 800°C
   b. empirical effect of Tin
   c. empirical effect of EGR.

Since NO_x emissions are a function of combustor design as well as stoichometry and cycle parameters, the estimates are only approximate especially in light of the large number of assumptions made. For fuels without nitrogen, such as gasoline, NO_x is a function of residence time and temperature via the Zeldovich mechanism. With a turbulent diffusion flame, as in a Stirling, combustion occurs in a thin layer at stoichometric (λ=1) conditions where diffusing fuel vapor and air meet. Assuming temperature and time are independent then it can be shown that the ratio of NO_x at two different flame temperatures, T and T' is:

$$NO_x'/NO_x = e^{-45380\ (1/T' - 1/T)} \qquad (1)$$

Flame temperature, T, at equilibrium conditions was calculated from a NASA computer program as a function of λ and EGR at Tin = 1073°K, Figure 3-3. Using an empir-

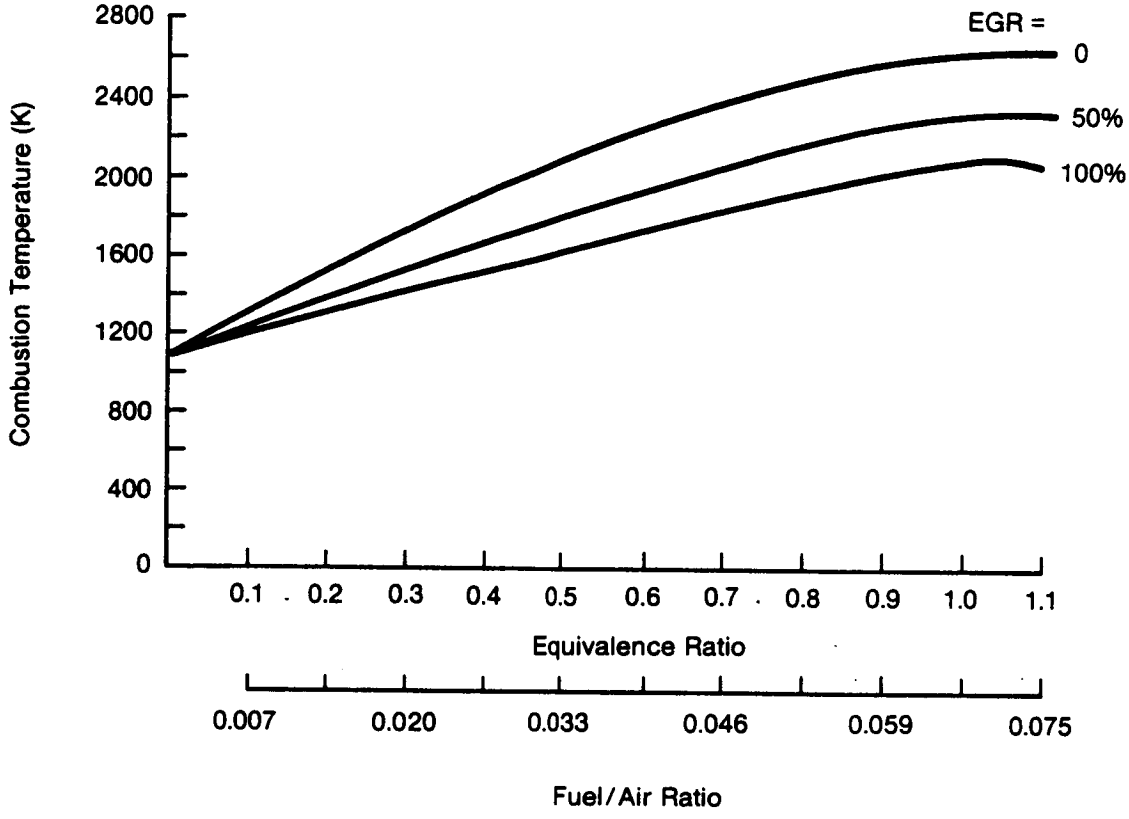


Figure 3-3 Equilibrium Flame Temperature for C_8H_{18} at T_{in} = 1073°K

ical relationship to account for variations in Tin* and Figure 3-3, the following equation was derived:

$$T = 3235 - 605\ \lambda + 1/2\ (Tin - 1073) - EGR\ (6.9 - 0.014\ EGR) \qquad (2)$$

where:

Tfl, Tin = °K

$0 \leq EGR \leq 100\%$

4

$1 \leq \lambda$

Equation (2) will predict Tfl within 1% except at the extreme condition of $\lambda = 1.6$ and 100% EGR (2%).

Equations (1) and (2) were then used with existing Mod I and Upgraded Mod I emissions data to determine the required levels of EGR and CGR for CASE. Before making CASE estimates, the validity of the technique was verified (Table 3-7) using Upgraded Mod I data. The data in Table 3-7 represents specific fuel flows. For an entire CVS cycle NO_x emissions are integrated as a function of fuel flow using a 12-point simulation (Reference 5). CVS cycle NO_x emissions were determined as follows:

1. Upgraded Mod I engine data was used to determine the NO_x emissions and average EGR or CGR** for the urban CVS cycle.

2. T was calculated from Equation (2) at $\lambda = 1$ and the results of 1 and 2 plotted (Figure 3-4).

3. $$\text{CASE } EINO_x = \frac{(.4\ g/mi)\ (1000\ g/kg)\ (31.7\ mpg)}{2845\ g/gal}$$
$$= 4.45\ g/kg$$

4. The amount of EGR/CGR is calculated by determining the T for 4.45 g/kg NO_x (Figure 3-4) and then using Equation (2).

---

* $\Delta T = 1/2$ Tin

**CGR and EGR are equivalent with regard to their effect on flame temperature.

TABLE 3-7

COMPARISON OF MEASURED AND CALCULATED UPGRADED MOD I NO_x EMISSIONS

			Measured			Calculated	
Ttube (°C)	Tin (°C)	mf (g/s)	EGR (%)	$EINO_x$ (g/kg)	NO_x Ratio	T (°K)	NO_x Ratio
720	800	2.2	0	16.3		2630	
			15	8.4	.515	2530	.506
720	800	2.0	0	16.9		2630	
			36	4.05	.240	2400	.191
820	900	.7	31	13.4		2480	
720	800			9.15	.683	2430	.686
820	900	2.0	0	21.4		2680	
			13.25	13.8	.645	2591	.559
720	800	2.0	0	18.8		2630	
			13.25	9.9	.526	2541	.546
820	900	2.0	0	21.4		2680	
720	800			18.8	.878	2630	.725

Notes:

1. T per Equation (2) at $\lambda = 1$
2. Calculated NO_x ratio per Equation (1)

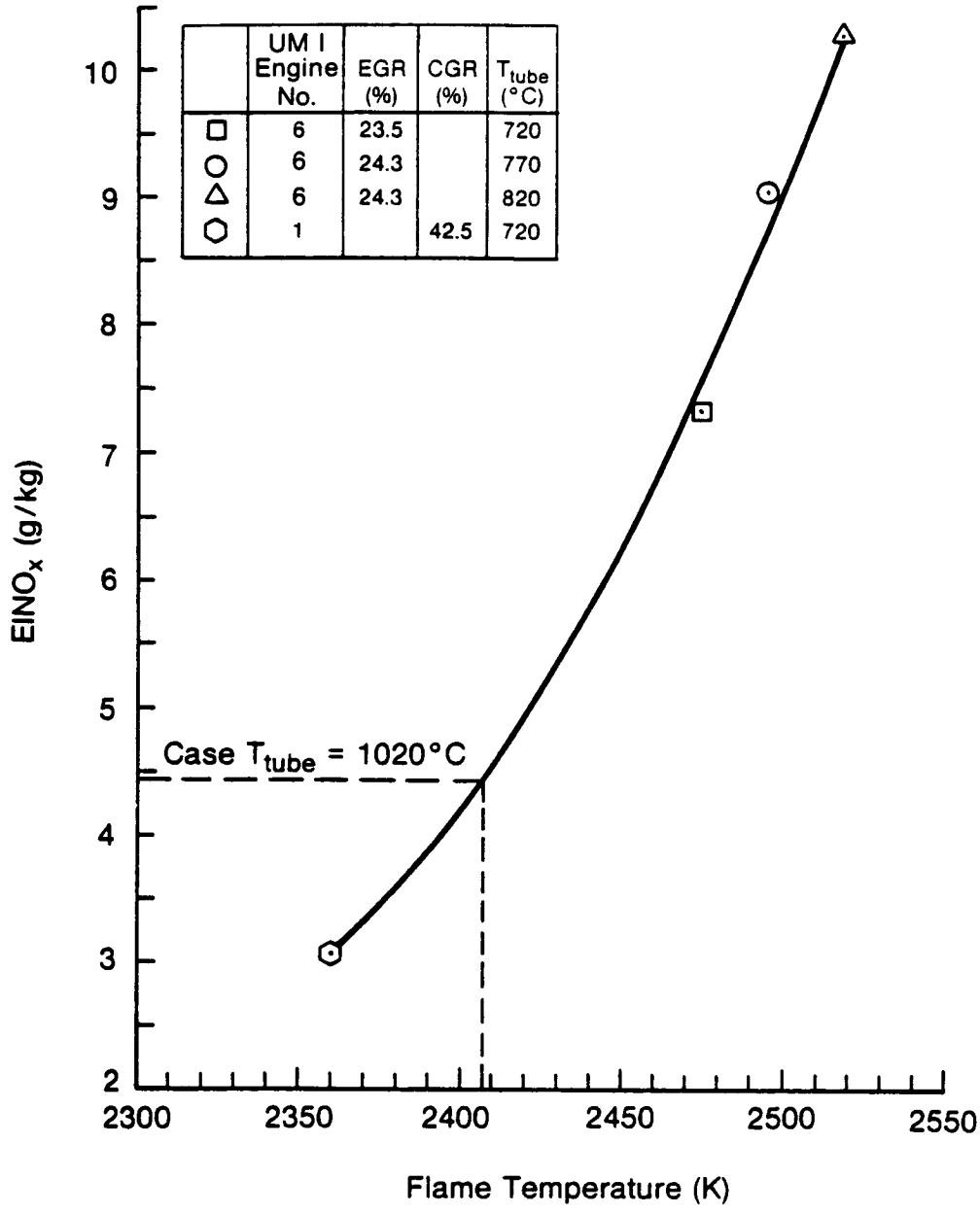


Figure 3-4 Estimated CVS Cycle NO_x Emissions

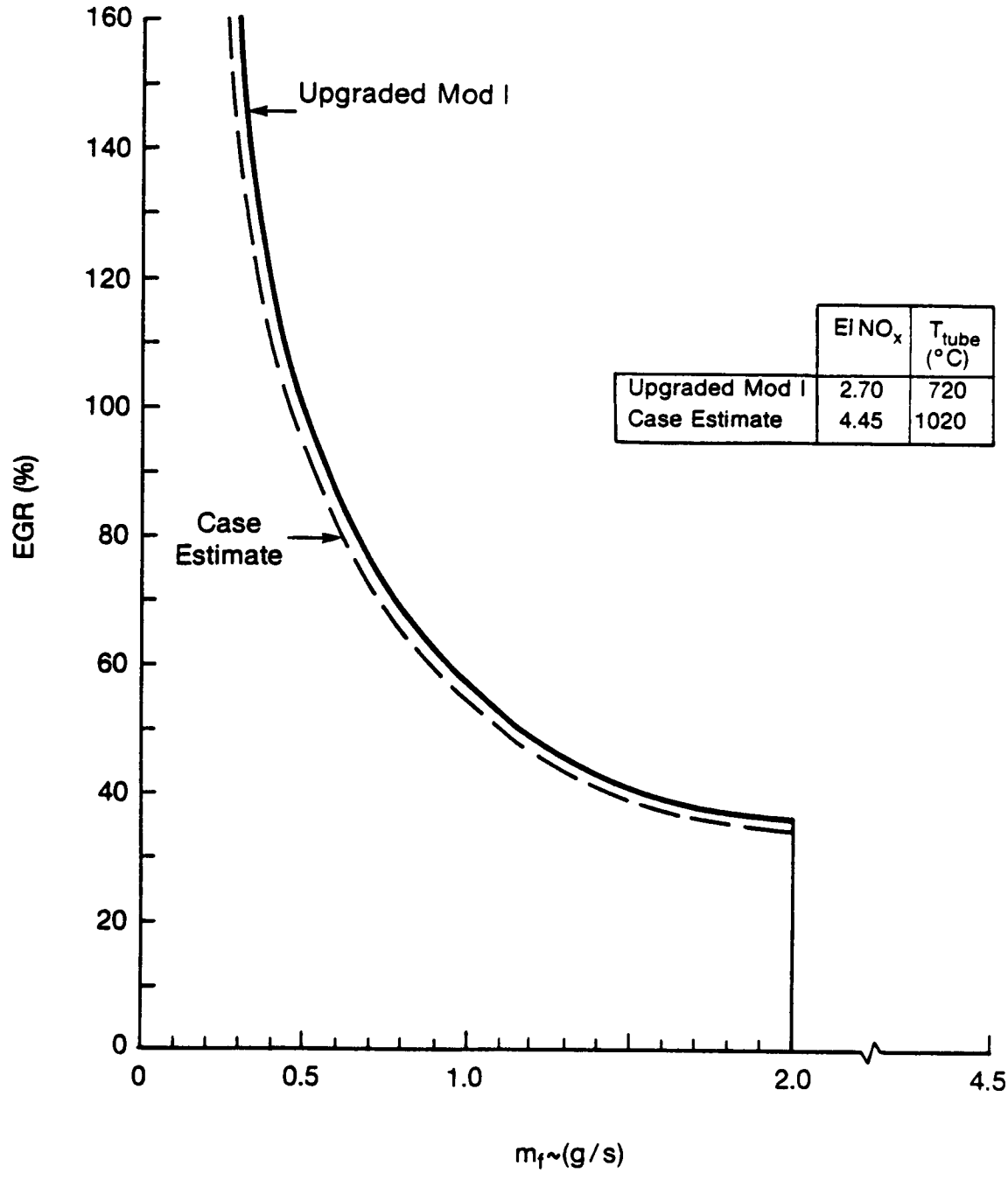


Figure 3-5 Estimated EGR for CASE

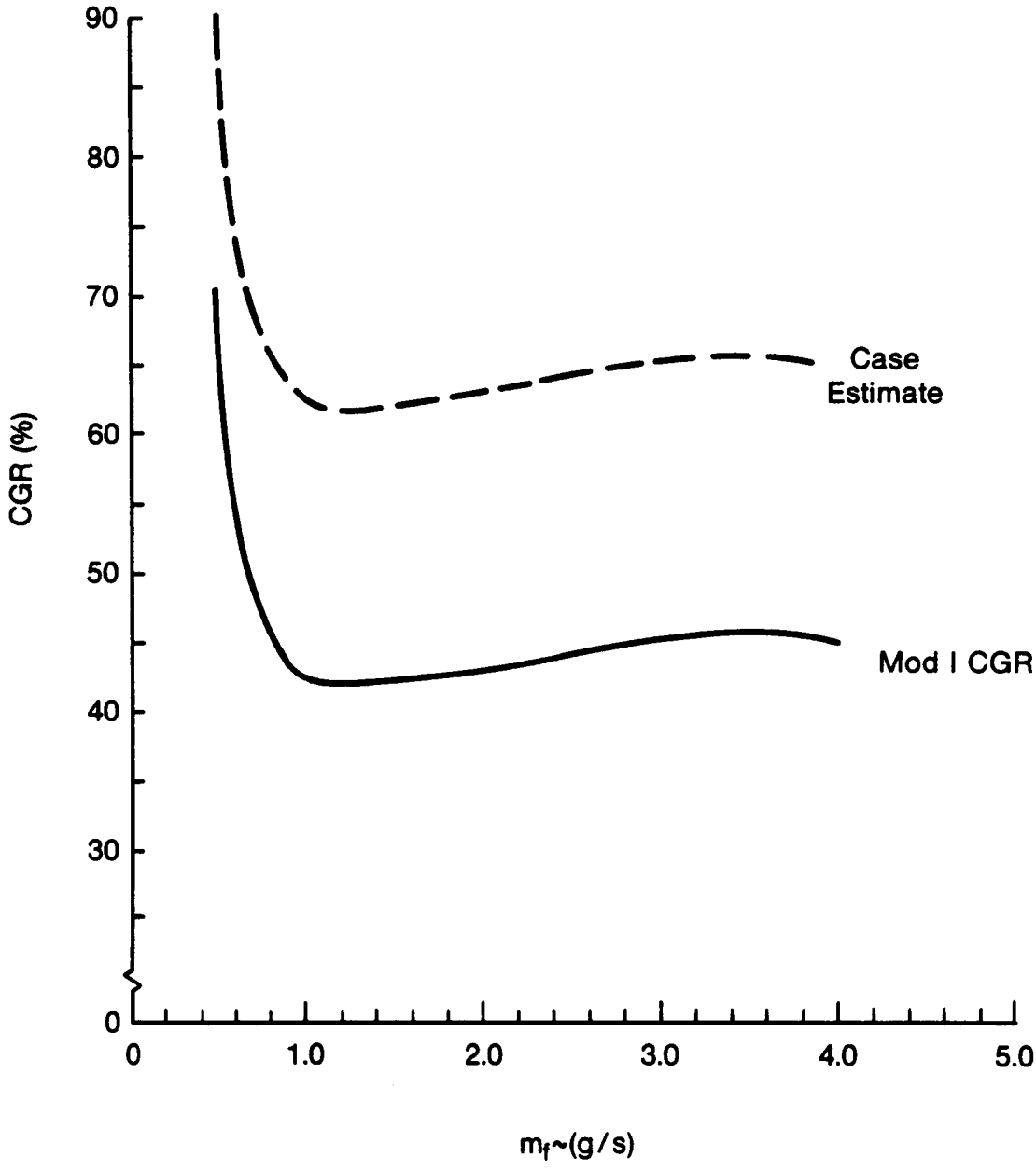


Figure 3-5 Estimated CGR for CASE

The final step is to use the recirculation calculated above, 62%, at a CVS cycle average fuel flow while duplicating the shapes of the existing EGR and CGR curves of the Mod I/Upgraded Mod I (Figures 3-5 and 3-6). The implicit assumption is future CASE CGR combustors or EGR characteristics will duplicate present designs.

The conclusion of this preliminary assessment is that a CASE design operating at 1020°C tube temperature will require ~30-35% more CGR than a conventional engine at 820°C. At this condition, the engine will be able to meet the ultimate objective of the EPA emission requirements, which have yet to be implemented. This increase in blower power has been included in the blower power requirement used for performance calculations.

4.0 MANUFACTURING COST STUDY

4.1 Objective

The objective of the CASE manufacturing study is to evaluate the feasibility of mass production of ceramic components based on the CASE design. Once the feasibility of mass production was established, an OEM cost estimate for the production of 300,000 units/year was developed. The ceramic assemblies included in the estimate include: combustor, heater head, displacer, partition wall, and regenerator. A ceramic matrix preheater was also included in the CASE estimate, however, the costing for that component has been previously developed in the RESD cost estimate. After the CASE manufacturing cost estimate was developed, the costs were compared with the 1981 RESD and conventional IC engines. The manufacturing cost of individual components were compared to identify the specific components offering significant cost advantages due to the use of ceramics.

4.2 Cost Analysis Data

The manufacturing cost analysis information is based upon the following sources for raw material costs:

- Reaction Bonded Silicon Carbide - SOHIO Engineered Materials Company (Carborundum)
- Nextel Fiber - 3M Company
- Mullite - Kyanite Mineral Company
- Silicon Carbide Whisker - Atlantic Richfield Company (ARCO).

The actual manufacturing (mixing, molding, green machining, sintering, and testing) costs were developed by SOHIO Engineering Materials Company for ceramic components. The metallic engine components were based on the 1981 RESD cost estimate performed by Pioneer Engineering and Manufacturing Company. As discussed, the ceramic estimate was based on the production of 300,000 engine units/year which justifies the use of specialized and highly automated production equipment. The manufacturing costs developed in this study were adjusted to a 1984 economic base.

4.3 Basis of Cost Analysis

The manufacturing cost analysis was developed based on the inclusion of the following factors:

- Material and inbound freight
- Labor - direct and indirect
- Manufacturing scrap
- Machine set-up
- Expendable production tools and liquids
- Rework factors
- Standard factory overheads
- Depreciation of capital equipment and tooling
- Maintenance, repairs and other facility related items.

Conversely, several categories of potential expenses were not included in the cost estimate since they were judged to be outside the normal definition of manufacturing cost. These items included:

- R&D amortization
- Sales and general administration
- Packaging and shipping
- Profits
- Start-up costs
- Inventory costs
- Interest on work-in-progress.

4.4 Manufacturing Cost Estimate

4.4.1 Ceramic Material Costs

Based on contacts with the material suppliers identified in Section 4.2 and the quantities required for 300,000 engines/year the following bulk material cost and consumption rates were developed for use in this study:

Material	Cost/lb ($)	Annual Consumption Million lb	lb/ engine
Reaction-bonded silicon carbide (RBSic)	2.00	9.38	31
Silicon carbide whiskers and mullite matrix composite 20:80	1.66	1.57:6.30	26
Nextel fiber	20.00	2.25	7.5

4.4.2 Cost Summary for CASE Components

Table 4-1 tabulates the "mature" manufacturing cost for the ceramic components (excluding the ceramic preheater, which was estimated in the 1984 RESD). The manufacturing costs are again based on 300,000 units/year.

4.4.3 Comparison of CASE and 1981 RESD Manufacturing Costs

An item by item cost comparison of the CASE ceramic components and the equivalent metallic components in the 1981 RESD is presented in Table 4-2. As can be seen from the comparison, certain ceramic components offer significant manufacturing cost advantages over the equivalent metallic components. However, this situation is not universally true and is a function of the size, function, and dimensional requirement of the component. Many of the large, thin combustor components are less expensive to manufacture as metallic forms due to the inherently low cost of manufacture (stamping, deep drawing). The use of ceramics in these parts is more costly due to the difficulty of fabricating, and firing of large, thin, fragile ceramic components. Although it should be noted that the ceramic combustor components have temperature capabilities which far exceed the metallic components identified in the 1981 RESD.

In the case of heater heads and other physically smaller components, the ceramics generally have a cost advantage for two basic reasons. One primary factor is that the base material cost of ceramics tends to be much lower than metal parts, particularly those metals used for high temperature applications. A second factor is the method of manufacture. Ceramic components utilize injection molding to manufacture the "green" ceramic components which are then

TABLE 4-1

COST SUMMARY OF CASE COMPONENTS

	Quantity/ Engine	Manufacturing Cost
Combustor Assembly		
Inner Combustor Shell	1	$136.21
EGR Shell	1	71.84
Preheater Support/Seal	1	92.83
Flow Separator	1	57.88
Flameshield	1	12.42
Turbulator Support Plate	1	16.05
Turbulator Assembly	1	19.94
TOTAL		$407.17
Heater Head Assembly		
Heater Housing (green forming)	4	31.35
Manifolds (green forming)	16	9.62
Heater Tubes with Fins (green forming)	88	18.48
Assembly and Sintering Cost	4	93.64
TOTAL		$153.09
Displacer Dome Assembly	4	24.06
Displacer Cylinder	4	29.24
Stuffer	4	11.52
Regenerator Matrix		166.00
Grand TOTAL-CASE Components Estimated Cost		$791.08
CASE Component MATURE* Cost		$672.42

*It is assumed that the estimated cost will "mature" by 15% once production has commenced and production and field experience have contributed to cost improvement.

TABLE 4-2

MANUFACTURING COST COMPARISON OF COMPONENTS/ASSEMBLIES OF CASE RESD

CASE Part/Assembly Title	Mfg Cost 1984 $	1981 RESD Equivalent Part/Assembly Title	Mfg Cost 1984 $
1. Inner Combustor Shell	136.21	Inside Sheet Casing Sheet Ring Sheet Cone	28.60
2. EGR Shell Turbulator Support Plate Turbulator Assembly	107.83	Combustion Chamber Assembly Assembly - Outer Cone Outside Sheet Steel Cone Jet Tubes Turbulator Guide Vane	60.49
3. Preheater Support Seal	92.83	Lower Sub Assembly - Preheater Matrix Inside Tightening Plate Assembly Ring - Inside Tightening Plate Notched Ring - Inside Tightening Plate Lower Ring - Weldment Assembly Tightening Ring - Bottom Pan Tightening Ring - Side Wall Flange	66.0
4. Flow Separator	57.88	Insulation Cover - Outer Insulation Cover - Inner	48.31
5. Flow Shield	12.42	Flame Guard Assembly Cover Casing Plate - Middle Plate - Bottom Dowel Insulation	17.80
6. Heater Head Assembly Heater Housing Heater Head Inner Manifold, L.H. Heater Head Inner Manifold, R.H. Heater Head Outer Manifold, L.H. Heater Head Outer Manifold, R.H. Heater Tubes Heater Fins	153.09	Heater Assembly Cylinder Housing Regenerator Housing Heater Tubes Fins - Heater Tubes Sheet Boss Plug - Angle Clip - Cylinder Housing	575.23

TABLE 4-2

MANUFACTURING COST COMPARISON OF COMPONENTS/ASSEMBLIES OF CASE RESD (Concluded)

CASE Part/Assembly Title	Mfg Cost 1984 $	1981 RESD Equivalent Part/Assembly Title	Mfg Cost 1984 $
7. Dome Assembly Cylinder Cap Baffle - Lower Baffle - Upper	24.06	Dome Assembly Upper Dome Dome Sleeve Baffle - Dome Assembly	80.83
8. Cylinder (Partition Wall)	29.24	The functional equivalent part for Items 8 and 9 in regenerator housing which is included in the heater assembly cost under No. 6	
9. Stuffer	11.52		
10. Regenerator Matrix	166.00	Regenerator Matrix - Stainless Steel Woven Wire Cloth	429.56*
TOTAL	791.08		$1,307.32

*Pioneer Engineering and Manufacturing Company costed the 1981 RESD with two types of regenerator matrix materials. In their initial March 1981 costing stainless steel woven wire cloth was used. In July 1981 estimating "carbon steel wool" was used for valve engineering purpose which costs only $39.51. This is the cost which was used in the final report. However, now it is confirmed that technically it is not feasible to use "carbon steel wool" as regenerator matrix. Hence, for a true and meaningful cost comparison, for this CASE analysis, Pioneer's March 1981 costing is used.

assembled and sintered as a unit. This approach allows the use of complex shapes which are then assembled into a more complex assembly. At this state the "green" ceramics are easy to machine (if necessary) and are easily assembled. The equivalent metallic component must be initially cast into the final complex geometry and then machined and brazed into a final assembly, requiring many more steps and hence more cost.

One of the major assumptions in the ceramic manufacturing estimate that reduces the cost is that very little machining (grinding) is required after final sintering and that good dimensional control of the sintering process can be maintained such that only critical surfaces require grinding. If this assumption is not true and extensive machining of sintered parts is required, ceramic components quickly become very expensive.

Table 4-3 presents a comparison of the various CASE ceramic components and the 1981 RESD components, and includes a brief evaluation of the potential for mass production and further development. The evaluations made in Table 4-3 also take into account improvements of the RESD design from 1981 to 1984. The various components are evaluated on a scale from 1 to 10 with 10 representing the best candidates for mass production and 1 representing components where the use of ceramics is least attractive based on cost and manufacturing considerations.

From Table 4-3 it appears clear that the "hot" components of the engine (i.e.; heater head; displacer dome; partition wall; stuffer; and, regenerator) offer the greatest potential advantage for ceramic fabrication. Heater heads are clearly one of the best candidates for ceramic fabrication owing to the strategic metal (nickel, chromium) of the current metallic heads as well as the high cost of precision investment casting of metals as compared to the injection molding/sintering of ceramic. However, an item that is also an excellent candidate is the piston dome which is hydroformed and welded, and machined in the current metallic design. The concept of injection molding/sintering and utilizing high strength adhesives to attach the dome to the piston base appears very attractive even in low temperature engines. The use of ceramic piston domes may be the least developmentally difficult application of ceramics, however, aside from the potential cost benefit, the use of a ceramic dome does not offer any significant performance or technical advantages over metallic domes.

ORIGINAL PAGE IS
OF POOR QUALITY

TABLE 4-3

COMPARISON OF SUITABILITY FOR MASS PRODUCTION - CASE VERSUS 1981 RESD

Title	Material	Basic Process	Comments	Evaluation No.
Inner Combustor Shell	RBSIC	CAST	Too big, fragile, and too costly. Metal form part is much simpler to handle, assemble, store, and also inexpensive.	1
EGR Shell	RBSIC	Injection Mould	Big, fragile, and costly. Metal form part is much simpler to handle, assemble, store, and also inexpensive.	2
Preheater Support/ Seal	RBSIC	Injection Mould	Very fragile, difficult to assemble, handle, and costly. Metal stamped and formed part is very inexpensive in RESD-V4 engine.	1
Flow Separator	RBSIC	Injection Mould	In RESD-V4 engine the substitute part is a simple metal forming, very inexpensive	2
Flame Shield	RBSIC	Injection Mould	In RESD-V4 engine the substitute part is a simple flamestone, very inexpensive.	3
Turbulator Support Plate	RBSIC	Injection Mould	A metallic support plate is much less expensive.	2
Turbulator Assembly	RBSIC	Injection Mould	Competitive with metallic substitute assembly cost-wise. Performance advantages have to be evaluated.	6
Heater Head Assembly, Heater Housing Manifold, Tubes with Fins	SIC Whiskers & Mullite Matrix Composite, RBSIC	Injection Mould	The best candidate for ceramic fabrication. Eliminates use of strategic materials and many complex fabrication operations. Good saving potential.	10
Dome Assembly	SIC Whiskers & Mullite	Injection Mould	Good candidate for ceramic fabrication. Eliminates use of strategic materials. Good saving potential. This component is difficult to manufacture as a metallic component.	8
Cylinder (partition wall)	SIC Whiskers & Mullite Matrix Comp.	Injection Mould	Very good candidate. May resolve technical problems associated with metal parts. Good cost savings potentials.	9
Stuffer	SIC Whiskers & Mullite Compo.	Injection Mould	Has to be developed along with ceramic dome assembly and displacer cylinder.	7
Regenerator Matrix	Nextel fiber	Weave	A very good candidate for development since a reliable alternate material apart from stainless steel wire cloth for regenerator matrix is very essential. Cost saving potential.	10

Other components which also offer excellent potential for ceramic manufacture are the stuffer and displacer cylinder (partition wall). These parts could most easily be developed since they are not pressure containing components and are not subject to high stresses. The ability to injection mold these complex shapes contributes to their competitive advantage.

The regenerator is the final component which offers good potential. Many types of porous (i.e., foam) ceramics have been tested for use as regeneration material, however, none have been successful because they could not duplicate the geometric regularity of sintered screen. The pore size and regular spacing of screen matrix are a result of the screen weaving process. By duplicating this process with a ceramic fiber of the required diameter (≈.50 μm), it should be possible to weave the fibers into screen which are then stacked to form the matrix. As can be seen from Table 4-2 the regenerator is one of the most expensive components in the engine, and is also critical to engine performance. Thus, the development of a less expensive, but well-performing regenerator matrix would be very attractive since no inexpensive metallic alternatives have been identified.

4.5 Manufacturing Technology

In general, the fabrication of the ceramic components consists of several basic steps consisting of raw material preparation, forming, assembly (if required), sintering and final grinding. Quality control in each step of the process is extremely important to maintain a high overall yield. This is especially true for components which are subject to proof testing, since failure to meet the proof test requirement results in destruction of the part.

As discussed, the raw material preparation consists of the milling of raw materials to the proper size and insuring the purity of the materials. The raw materials are mixed with a variety of binders and liquids to form a mixture which is then formed into the required final shape. The mixture can then be formed by a variety of methods, although the processes of injection molding and slip casting have been chosen for use in the CASE study due to their versatility and potential cost effectiveness.

Injection molding consists of making parts by injecting heated and softened ceramic compound into a shaped cavity that has been built into an appropriate mold. The compound is automatically fed into the hopper of an injection molding machine where it is heated to ~300°F and softened in the barrel of the machine and injected into the cavity. In the cavity the softened material is held under pressure until it solidifies. The solid part thus formed reproduces the cavity shape in detail and is removed from the mold. Ejector pins or rings in the mold free the part from it. Softened compound is produced by heating raw material in the cylinder of the molding machines while the part is cooling in the mold. The advantage of injection molding is that complex shapes can be easily formed with excellent dimensional control and repeatability.

This overall procedure is repeated in a rigidly maintained cycle. The cycle time is determined by the rate at which heat can be removed from the cooling part. This rate is approximately proportional to the wall thickness of the part, however, cooling rates tend to be slow because of low thermal conductivity. For this reason parts are to be designed with the walls as thin as is consistent with design requirements and ease of fabrication. The configuration and dimensions of the molding tool depend on the size and shape of the part to be produced as well as the number of cavities to be employed in production. At the same time mold dimensions must be governed by the dimensions of standard molding machine. Mold costs often can be reduced by the use of a standard mold frame into which the part-forming cavities are fitted.

The part removed from the mold is knows as "green" and is relatively soft and can be damaged. However, green formed parts are easily machined if required and can be assembled together such that the parts can be joined during sintering.

Injection molding technology has been proven as a high production technology in the plastics industry, and much of the existing technology base should be adaptable to ceramics forming.

Slip Casting - The process of slip casting involves pouring of waterbase slurry of the ceramic compound into a plaster mold having the component's exterior shape. The slurry stays for a predetermined period of time (15 to 30 minutes) to allow the water to seep through the plaster mold. The period of time allowed

for seeping of the water determines the wall thickness of the final green component. The excessive slurry is poured out or removed. The component in the mold is air dried, and demolded by turning the mold. Also, instead of plaster, porous ceramic or plastic material can be used for the mold when longer mold life is desired.

Slip Casting has the limitation that only exterior contours and relatively constant section parts can be produced, but it is effective for the production of large parts such as the combustion liner.

In order to bring the green state components to their final density and strength, the components must be sintered. This sintering process consists of heating the green parts according to a well defined time-temperature schedule designed to drive off the binders and sinter the ceramic material. During sintering it is important that the components are properly fixtured to prevent dimensional distortion. It is also important that the shrinkage that occurs during sintering be accounted for in the sizing of the green state parts.

After sintering, dimensions which must be controlled to less than the sintering variation must be ground to final dimension. The grinding of ceramics is a difficult and expensive process due to the hardness of ceramic materials. Thus the number of ground dimensions must be kept to an absolute minimum.

Both during and subsequent to the final manufacturing processes quality control plays a significant role in the successful production of ceramic parts. For the most part, components will be proof tested (pressure test) to verify the overall quality of their manufacture. The proof testing must be chosen to assure the reliability of the component in production. This proof testing is the "acid test" of the quality system throughout the manufacturing process and must result in acceptable yields if the overall manufacturing process is to be economic.

Components that do not lend themselves to an effective and reliable proof test should be subjected to nondestructive examinations (NDE) such as fluorescent penetrant inspection (FPI), real time microfocus x-ray, ultrasonic, and automated measurement and profile reading. However, components which fail these nondestructive examinations must also be scrapped. Thus the quality system is

equally important in producing non-proof-tested components at acceptable yields.

4.6 CASE Costing Methodolgy

4.6.1 Cost Analysis Assumptions

The CASE cost analysis was developed based on several major assumptions regarding the detailed manufacturing methodology. These assumptions included the use of a highly automated production facility incorporating specialized equipment. Injection molding, green handling and assembly processes would be automated to the greatest extent possible. The furnace technology used for production would maximize the use of testing of components to minimize furnace size. Table 4-4 describes the general statistics of the proposed production facility.

4.6.2 Detailed Costing Methodology

An example of the costing methodology used in this study is shown for the flame-shield (drawing No. 1016C014) shown in Figure 4-1. The detailed cost sheet is shown in Figure 4-2. The breakdown identifies each step of the process, beginning with tooling, raw materials, mixing costs, forming, binding, removal, cleaning, fixturing, sintering and final quality control. Calculations relating to the number of molding machines, furnaces and fixtures required are also shown.

The detailed process sheet also indicates the anticipated yield for each step of the process, which is factored into the final cost per unit. Similar process sheets were developed for each component and assembly in the CASE estimate.

TABLE 4-4

CASE MANUFACTURING GENERAL STATISTICS

Item	Statistics
Annual production volume	300,000 engines
Overall part yields (molded parts)	80-87% range
Injection molding machine requirement	28
Sintering furnace (15 ft^3) requirement	237
Factory area	50,000 ft^2
Total capital cost	$150 million
Overhead rate (including supervision and engineering)	150%

Personnel

Direct	1225
Indirect	235
Total	1460

Machine Utilization Schedule

3 shift working - 5 days/week
24 hours x 5 days x 50 weeks/year
6000 production hours/machine/year

Manufacturing Cost Breakdown(regenerator matrix cost excluded)

Title	Cost/Engine	Ratio (%)
Material	$106.06	16.97
Labor	233.02	37.28
Overhead	286.00	45.75
Total	625.08	100.00

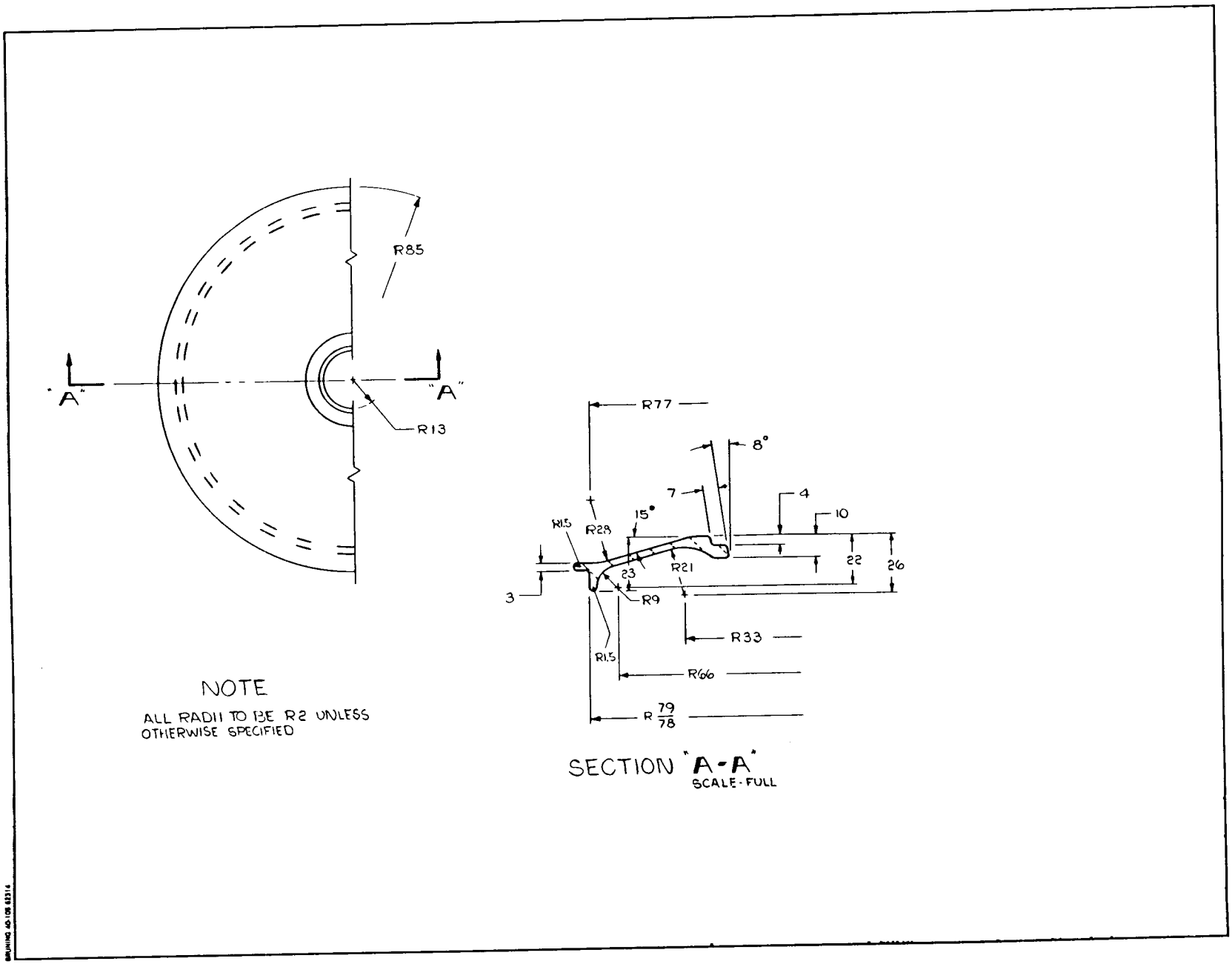


Figure 4-1 Flameshield

FLAME SHIELD
DRAWING C-014
6

	YIELD	# UNITS	UNITS PER	MATERIAL TOTAL UNITS	MATERIAL COST/UNIT	MATERIAL $	LABOR HRS	LABOR $	OVERHEAD VAR OH %	OVERHEAD VAR OH $	TOTAL COST	COST/ UNIT
TOOLING	100	353180		4	$65,000	$260,000					$260,000	$0.74
MATERIAL	100	353180	1.00	353180	$2	$706,360					$706,360	$2.00
MIX	100	353180	20.84			$0	16947	$186,419	150	$279,629	$466,048	$1.32
FORM	98	353180	120.00			$0	2943	$32,375	150	$48,562	$80,937	$0.23
BIND REMOVE	98	346116	18.75			$0	18460	$203,055	150	$304,582	$507,637	$1.47
CLEAN	98	339194	30.00			$0	11306	$124,371	150	$186,557	$310,928	$0.92
FIXTURE	100	332410	30.00	932	$60	$55,920	11080	$121,884	150	$182,825	$360,629	$1.08
SINTER	95	332410	233.00	1427	$400	$570,661			150	$0	$570,661	$1.72
QC 1	95	315789	24.00				13158	$144,737	150	$217,105	$361,842	$1.15
OVERALL YIELD	85											
SUBTOTAL											$3,625,042	$12.08
PARTS SHIPPED		300000										
MANUFACTURING COST											$3,625,042	$12.08

Molding - 4 cavity mold = 353,180 parts

- 2 min cycle 4 x 30/hr = 144,000 x 4 = 576,000
- 1 machine
- 3 tools @ $65,000 = $195,000 over 5 years $0.11

Sintering- 332,410 units: 300 days 1108/day
1108 units: 232 units/furnace run = 5 runs = 2 furnaces

Fixtures - 233 x 2 x 2 = 932 $60 each #55,920

Q.C. - In units of 4: Automated real time X-ray with color or tone.
FPI - conveyor
Dimensional gauging

Figure 4-2 Detailed Cost Sheet Example

4.7 Engine Cost Comparison; CASE, 1981 RESD, and I.C.

Title and Description	Manufacturing Cost/Unit ($)
1981 RESD basic engine All metal parts (except air preheater) with stainless steel wire cloth matrix	1,505.13
CASE - 1981 RESD basic engine with CASE components	1,066.33
I.C. Engine - 67.5 kW	610.27
1984 RESD V-4 Mark V basic engine All metal parts (except air preheater) with stainless steel wire cloth matrix	687.11

Note: Basic engine manufacturing cost does not include cost of controls and auxiliaries.

In summary, the conclusion of this manufacturing cost estimate and comparison is that the incorporation of mass-produced ceramic components in a design similar to the 1981 RESD results in a projected significant reduction in manufacturing costs. This projection is based on the development of advanced technology for the mass production of high quality, reliable ceramic components. Such ceramic technology only exists today at a laboratory scale and to develop ceramic technology into a mass production technology will require extensive and prolonged development.

The majority of the cost reductions identified in this study were associated with the heater head, piston dome, and regenerator matrix. It should be noted that the 1984 RESD, an annular V-4 all metal design , has been estimated to have manufacturing costs much lower than the CASE. Thus the cost developed in this study should be monitored against the latest developments in automotive Stirling engine design to assure that the potential cost benefits remain valid.

5.0 ADVANCED CASE DESIGN

Although the incorporation of ceramic components in the 1981 RESD resulted in performance improvements over a conventional all-metal engine, it became apparent that the advantages of ceramic materials could perhaps be best implemented in an engine design which is radically different from the 1981 RESD concept. Accordingly, several advanced CASE concepts were developed and analyzed to determine which approach offered the greatest benefits. The advanced CASE concepts developed are in some cases radically different from conventional ASE type engines, and incorporate features which are technically feasible but are clearly developmental in nature. Thus the advanced CASE concepts represent the long term potential for the use of advanced ceramic material in an ASE. The advanced CASE concepts incorporate such features as hot rings and unlubricated ceramic element roller bearings.

In reviewing the possible approaches to the advanced CASE design, three approaches were developed to explore the potential of ceramics in an automotive Stirling design.

The three advanced CASE concepts were based on Stirling engine configurations that offerred potential improvmeents due to the incorporation of unique features made possible by the use of advanced ceramic materials. The first concept incorporated an opposed piston configuration which minimized the engine dead volume, simplified the gas flow path and utilized high temperature ceramic rings. A control concept based on the use of piston phase modulation was also included in this concept.

The second concept was based on the use of an annular regenerator V-4 configuration similar to the Mod II ASE engine, except with a ceramic heater head components and turbo-compound combustion. The potential improvement associated with this approach was based on the use of a combined Brayton/Stirling cycle to maximize engine efficiency by cascading the high temperature exhaust from the Stirling heater head to the Brayton cycle turbomachinery. The third concept evaluated is an in-line single-acting engine which incorporates hot piston ring, minimum dead volumes and solid lubricated ceramic bearings.

This configuration was developed to incorporate many of the features identified in the opposed piston concept into an easily manufactured, packageable design.

5.1 Opposed Piston

The first approach was based on an engine concept which represented as near as possible a geometrically ideal configuration for a Stirling cycle. This concept is referred to as the single-acting opposed cylinder design (SAOC) and is shown in Figure 5-1. The SAOC configuration embodies a "text-book" approach to a Stirling engine. The cylinders are linearly opposed with the hot expansion space and cold compression space connected by a cooler, regenerator, and an array of straight heater tubes. Since there are no manifolds in the configuration, the dead volume in the engine is minimized. In addition the arrangement results in excellent flow distribution in the heater, cooler, and regenerator. The configuration uses hydrogen as the working fluid and the two crackcases are pressurized. Rotary seals on the crankshaft penetrations seal the crankcase pressure, which is maintained at the cycle mean pressure, from the atmosphere. Since the crankcases are completely closed, no oil is used for lubrication and rolling element ceramic bearings will be used for main, connecting rod and wrist pin bearings.

The pistons utilize solid lubrication at the piston skirts/cylinder interface to absorb the piston side loads. Also a hot ring will be incorporated into the hot side piston. The hot ring will be a ceramic ring which will seal the expansion piston near the top of the hot side piston dome thus eliminating the appendix gap losses associated with the conventional designs that utilize cold rings at the bottom of the dome. The engine utilizes two drive shafts, one for the compression side and one for the expansion side. The drive shafts will be connected together using a toothed belt drive. The drive system connecting the two crankshafts also drives an output shaft and contains several idler wheels which allow the phasing between the compression and expansion side to be controlled. This variable phasing arrangement is used to control the output of the engine, while maintaining constant engine pressure.

The engine combustion system incorporates a system of scrolls to duct the combustion products to the heater tubes, as shown in the drawing. The regenerator and cooler are in the compression side cylinder housing and are of a conventional type of construction. The cooler are of shell and tube type, while the regenerator will be a matrix of woven ceramic fibers.

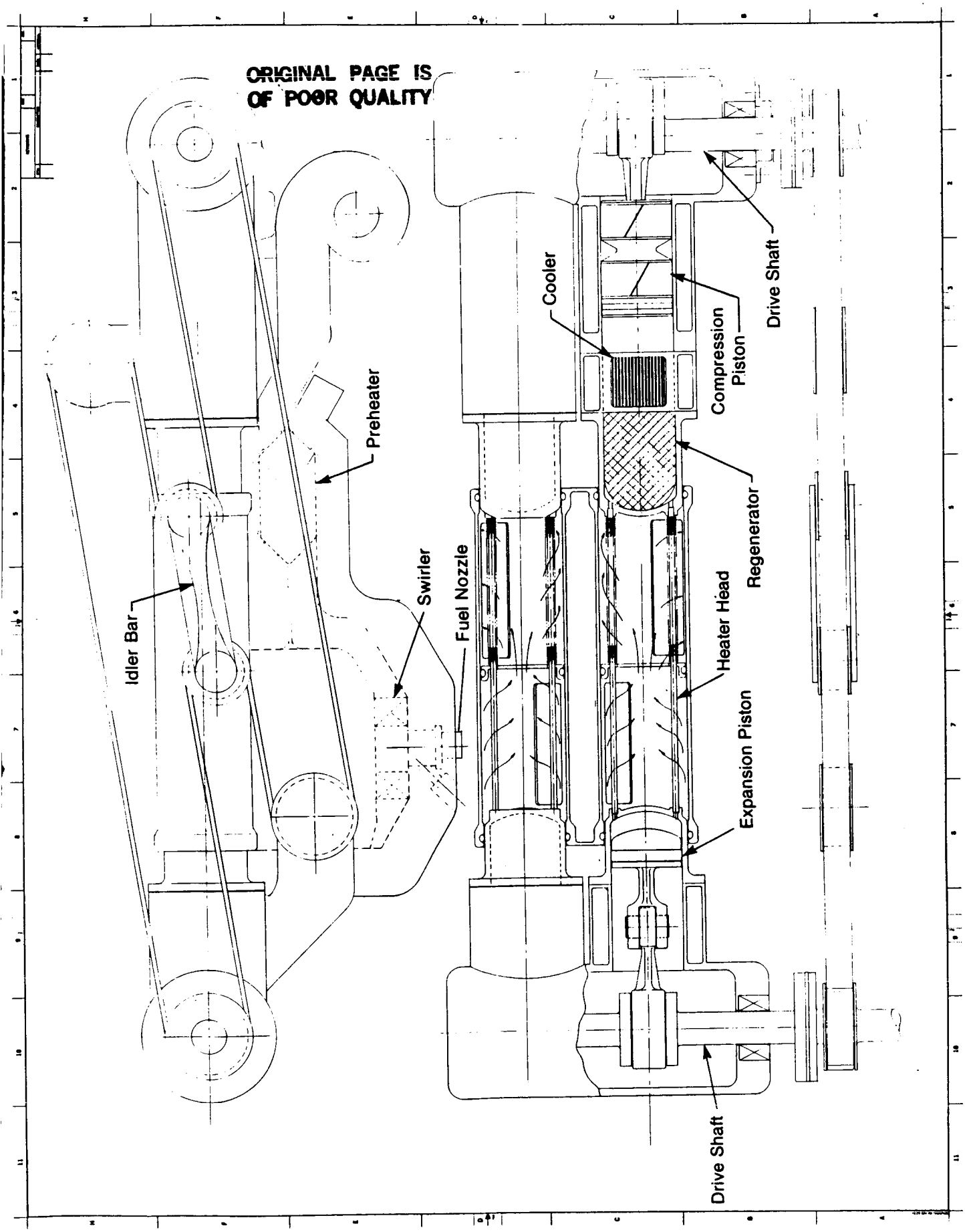


Figure 5-1 Advanced CASE SAOC Concept

The materials used in the analysis of this type of engine were based on the initial CASE study. A low thermal conductivity silicon carbide whisker reinforced mullite will be used for the cylinder housings. This material will minimize the thermal conductivity losses while providing the required strength for these parts. The heater tubes will be silicon caribide, and will be sintered to the mullite cylinder housings. The pistons will also be mullite. The crankcases will be of conventional ductile iron or steel castings. Overall the engine will be a flat four cylinder package with the combustor located near the center of the engine.

The geometry of the engine was modeled and entered in MTI's first-order analysis code. This code predicts the thermodynamic performance of the engine, calculating the indicated performance of the engine (i.e., without any frictional or auxiliary losses). The indicated power and efficiency curves are shown for this engine in Figures 5-2 and 5-3. The engine was geometrically optimized and sized to produce ~65 kW at 4000 rpm. This will result in ~60 kW once frictional and auxiliary losses are accounted for. The peak indicated cycle efficiency was ~64% at 3500 rpm.

The indicated cycle efficiency curves for several values of phase angle (relationship between compression volume variation and the expansion volume variation) are also shown in the plots. The engine peak power and efficiency occur at a phase angle of 90°, with power and efficiency falling off at lower phase angles. The phase angle is controlled by moving the idler bar (Figure 5-1) to the left and right. This movement changes the phase relationship between the compression and expansion shafts (pulley on extreme left and right) while maintaining the overall length of the belt. This control system is very attractive from a simplicity standpoint. The cycle mean pressure is maintained at constant level, all of the control system is external to the engine and only involves the mechanical positioning of the idler bar. However, the part load performance of the phase control system is not as efficient as other advanced CASE engines under consideration. This fact coupled with the shape of the efficiency curve, which peaks in the 3000-4000 rpm range, results in an engine map which is not optimal for the automotive application. The average operating point for the automotive application is approximately half maximum speed (2000 rpm), which is well below the SAOC peak efficiency speed. (The extremely short flow path of the cycle gas in this concept is responsible for the high-speed character of the map). A version fully optimized for automotive use would therefore be geared to run faster, perhaps 6000 rpm

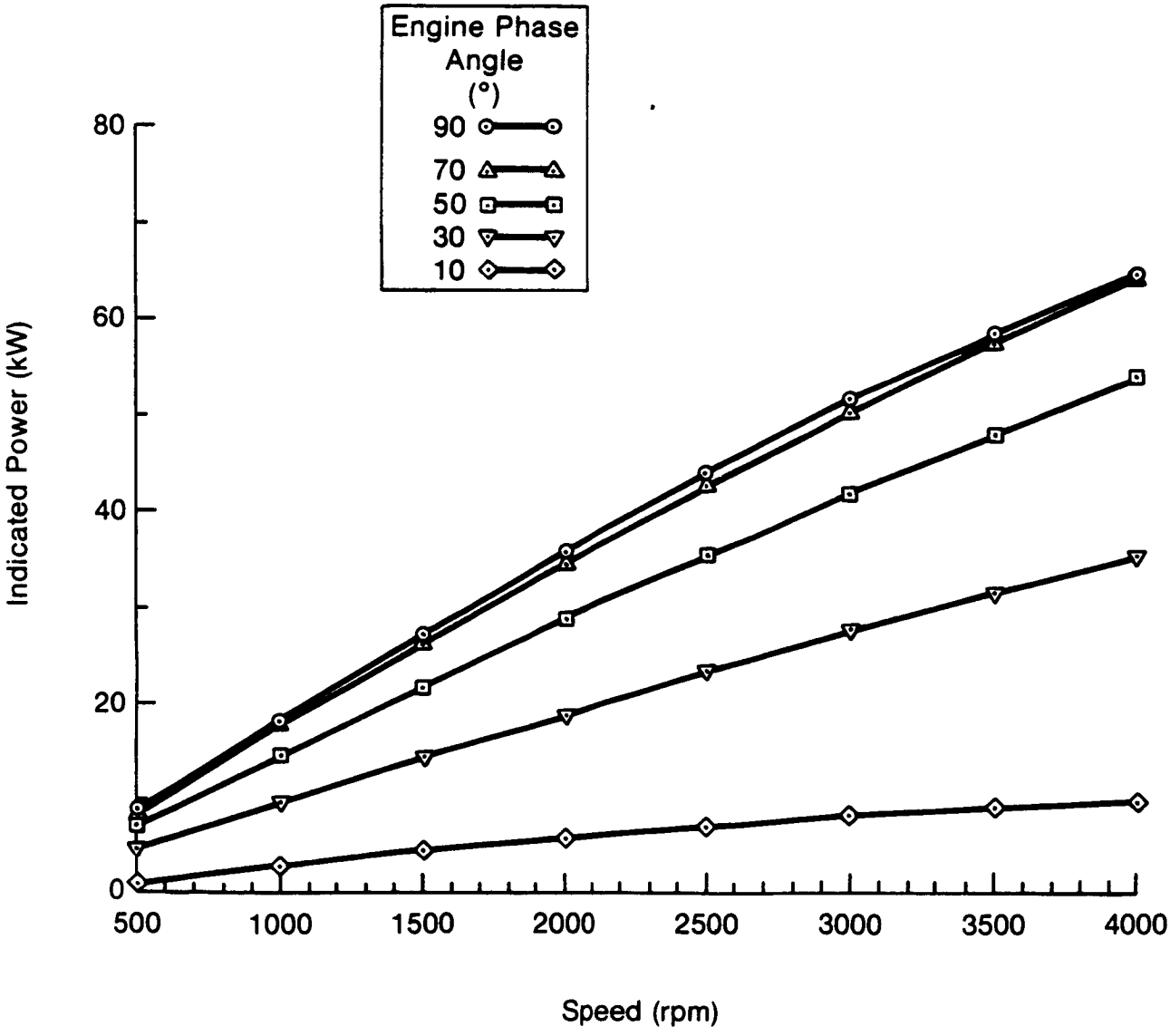


Figure 5-2 SAOC Indicated Power Curve

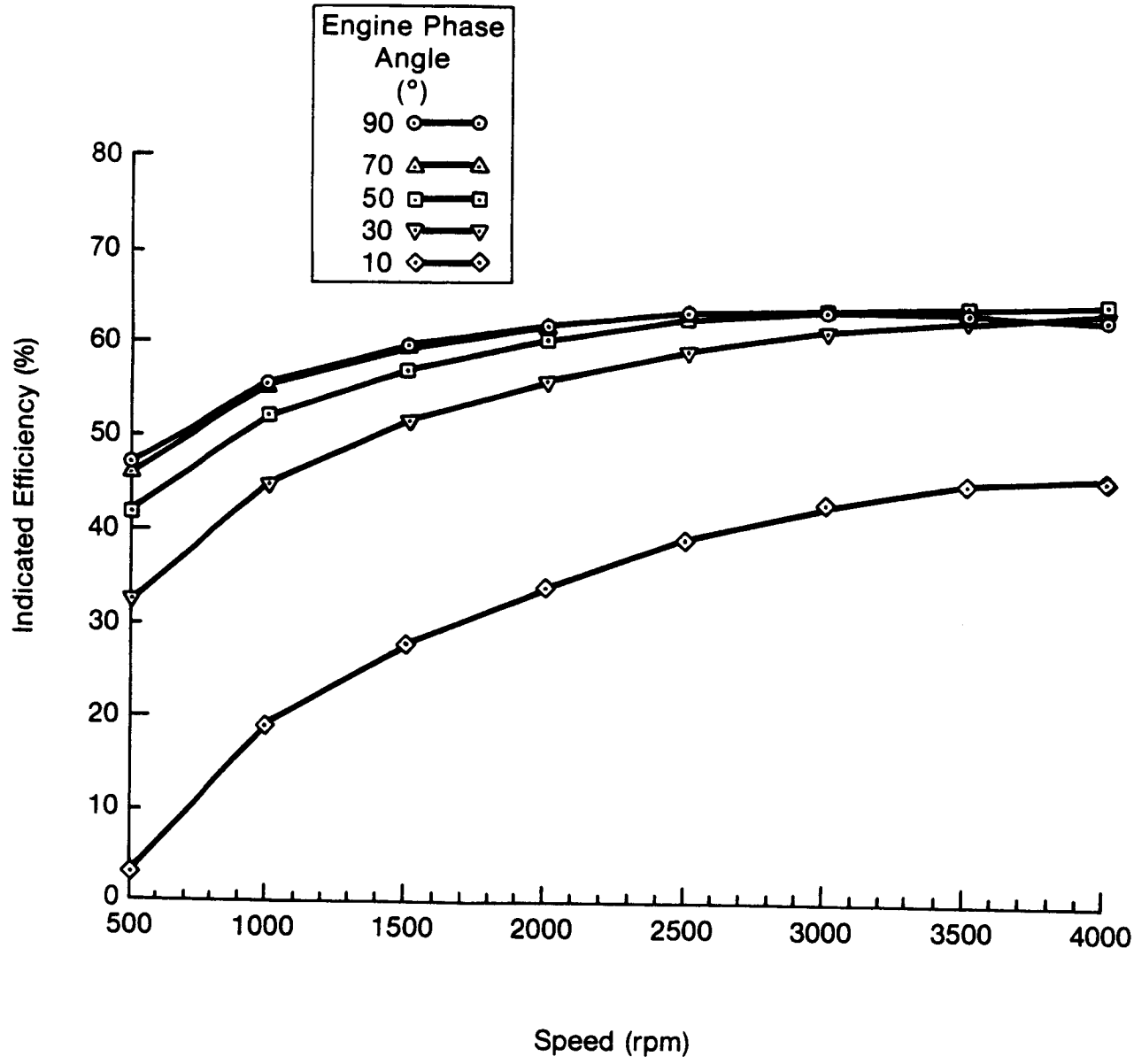
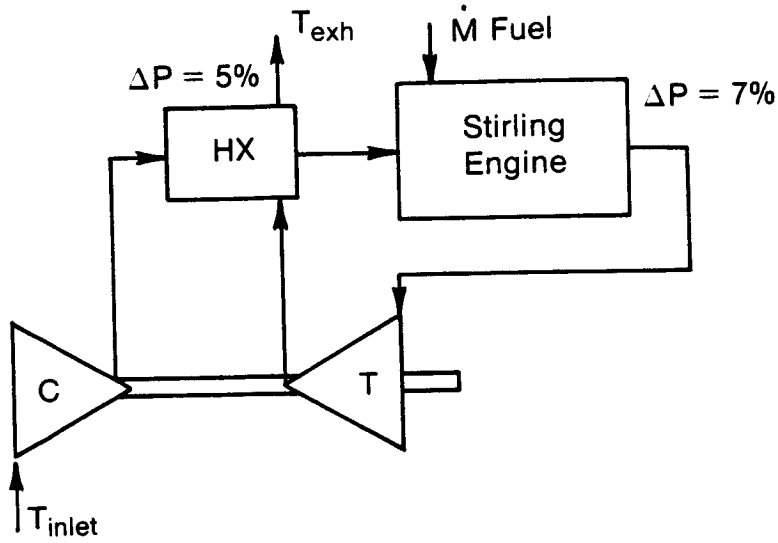


Figure 5-3 SAOC Indicated Efficiency Curve

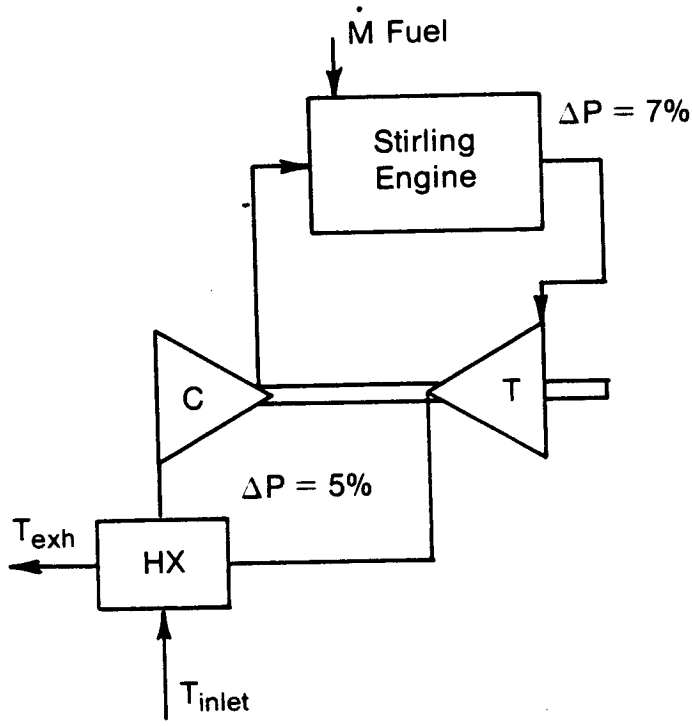
maximum to move the efficiency peak to a relatively slower point. As the power curves are still strongly rising at 4000 rpm, the 6000 rpm version would be over-powered at this size, and could then be reoptimized to smaller dimensions and lighter weight.

5.2 Turbo-compound Engine Concept

The second approach to the advanced CASE design involved the use of advanced ceramic Stirling engine design coupled with a turbine/compressor EHS blower to produce a turbo-compound Stirling cycle. The concept was to utilize the high temperature combustion products leaving the engine heater head in a combined Stirling/Brayton cycle. Conventional Stirling engine designs utilize the combustion products to recuperatively heat the inlet air to the combustor. However, at the high temperatures leaving a Stirling ceramic heater head (1100-1200°C) it would be attractive to utilize a Brayton cycle to extract useful power from the gas stream as well as performing the preheat function. The use of turbo-compounding requires a compressor to increase the pressure of the incoming air, a preheater either before or after the compressor, a pressurized combustion system, and an expansion turbine to expand the combustion gas back to atmospheric pressure. The objective is to design the turbo-compound system to produce a net output to be added to the Stirling output thus increasing the total output of the engine. Schematics of the turbo-compounding arrangement are shown in Figure 5-4. The arrangements differ in the location of the preheater. The Stirling engine itself was based on an annular V-4 design similar to the baseline CASE design except with a "V" configuration. Preliminary cycle calculations were performed to evaluate the performance of the overall combined cycle. A conceptual layout of the engine hot end is shown in Figure 5-5. The BSE performance was based on the CASE engine previously previously developed in this study. The normally aspirated version of this engine was used as a baseline for comparison to the turbo-compound engine. A heater head temperature of 1020°C was used for this evaluation and a preheater was used to recover the waste heat from the turbine exhaust. Turbomachinery efficiencies were based on the goals for the Automotive Gas Turbine (AGT) Program. Two configurations were explored, one with the preheater downstream of the compressor (i.e., between the compressor discharge and the combustor) and a second configuration with the preheater upstream of the compressor inlet.

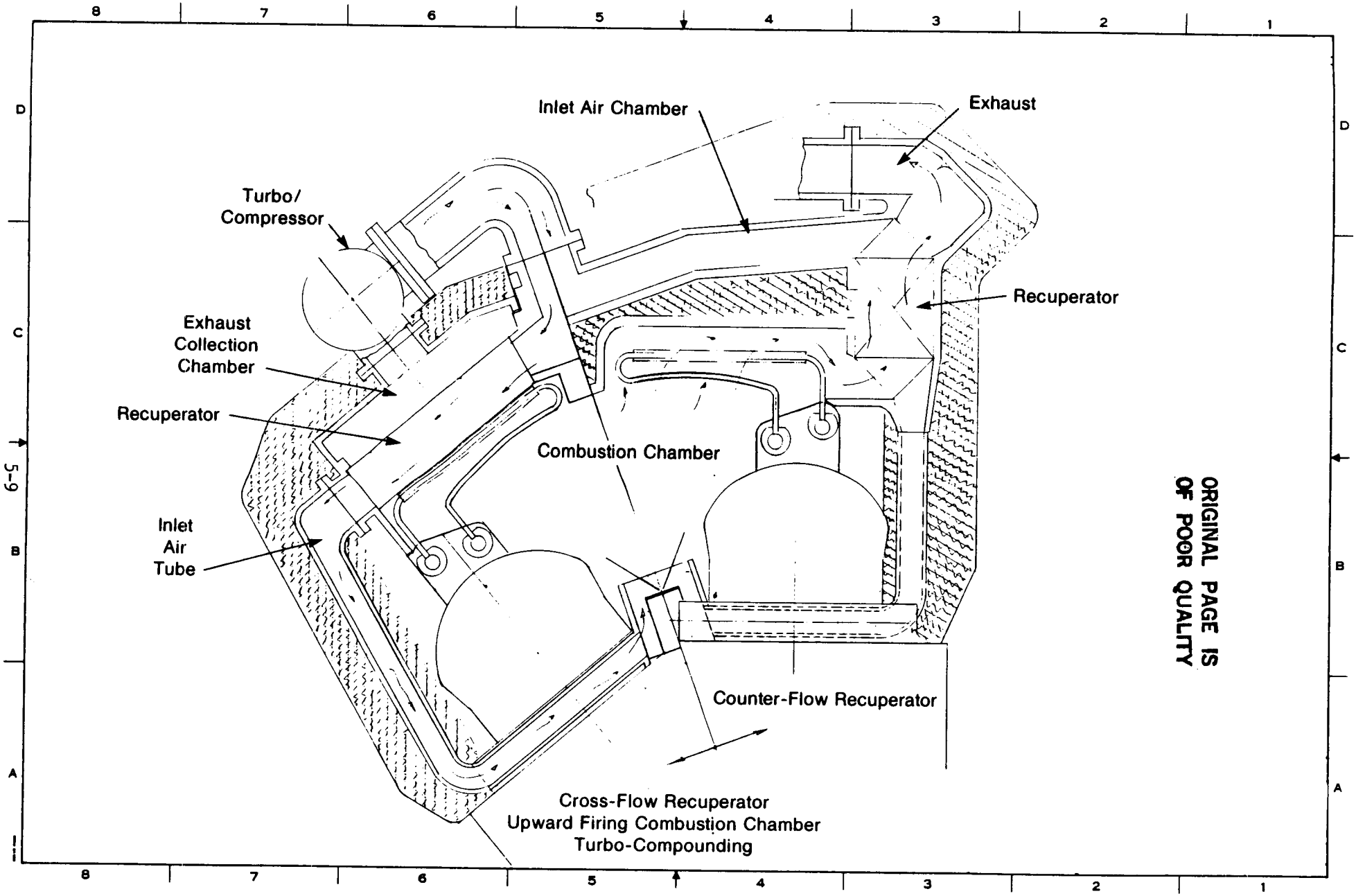


Configuration No. 1



Configuration No. 2

Figure 5-4 Advanced CASE Turbo-Compound Engine Configuration



ORIGINAL PAGE IS
OF POOR QUALITY

Figure 5-5 Advanced CASE V-4 Concept

Configuration One resulted in a slight improvement over the base engine efficiency at high speeds. However, over most of the engine speed range the turbo-compound engine efficiency is 1-2 percentage points less than the baseline engine efficiency. The power and efficiency data for this design and the baseline are shown in Tables 5-1.

In the second configuration, the turbo-compound engine efficiency was less than the baseline efficiency by ~9-12 percentage points over the entire range of the engine, as shown in Table 5-2.

The overall conclusion of the turbo-compounding study was that the possible gains are very small, and that the additional hardware and complexity required to implement the concept would be extensive.

5.3 Single Acting In-Line Concept

The third advanced CASE concept evaluated is the Single-Acting In-Line (SAIL) design. The SAIL design utilizes four in-line single-acting cylinders. The front two and rear two cylinders are paired to form the compression and expansion spaces of two Stirling cycles. The cooler, regenerator, and heater tubes are connected between the two working spaces as shown in Figure 5-6. This figure represents the initial design concept, which has been subject to further development. The engine contains two cycles, and as in the SAOC concept, a pressurized crankcase is utilized. The crankshaft penetration from the crankcase is sealed utilizing a rotary face seal. The crankcase utilizes nonlubricated rolling element ceramic bearings and the expansion pistons incorporate a "hot ring" to minimize the appendix gap loss. The housings that contain the cooler, regenerator, compression piston, and expansion piston will be manufactured of silicon carbide whisker reinforced mullite to minimize the conduction losses down the cylinder walls. The ring manifold will also be SiC-mullite and will be sintered to the cylinder housing/tube assembly to form a complete heater head. The tubes will be silicon carbide with fins on the outer row. The engine will require two combustors, one for each cycle, which presents some complication to the EHS. The EHS incorporates a scroll-type configuration to distribute the preheated air to the two combustors and return the exhaust products to the preheater. The preheater will be a ceramic plate/fin type unit similar to those being developed for the ASE Mod II program.

TABLE 5-1

COMPARISON OF TURBO-COMPOUND CASE WITH BASELINE CASE
(Pressure Ratio = 4.0, Configuration No. 1)

Speed	Pressure MPa	Turbo-Compound Net Efficiency%	Baseline Case Net Efficiency%	Turbo-Compound Net Power kW	Baseline Case Net Power kW
1000	15	41.9	44.0	23.8	18.9
2000	15	42.1	43.9	46.7	37.1
3000	15	40.3	41.0	66.1	51.4
4000	15	37.6	36.8	79.6	60.0
1000	5	36.9	36.9	8.1	6.1
2000	5	38.2	39.0	15.2	11.7
3000	5	36.4	36.8	20.4	15.6
4000	5	32.8	32.0	23.3	17.2

TABLE 5-2

COMPARISON OF TURBO-COMPOUND CASE WITH BASELINE CASE
(Pressure Ratio = 4.0, Configuration No. 2)

Speed	Pressure MPa	Turbo-Compound Net Efficiency%	Baseline Case Net Efficiency%	Turbo-Compound Net Power kW	Baseline Case Net Power kW
1000	15	34.9	44.0	14.0	18.9
2000	15	34.8	43.9	27.4	37.1
3000	15	31.9	41.0	37.3	51.4
4000	15	27.6	36.8	41.7	60.0
1000	5	28.4	36.9	4.4	6.1
2000	5	29.8	39.0	8.3	11.7
3000	5	27.0	36.8	10.7	15.6
4000	5	21.9	32.0	11.0	17.2

ORIGINAL PAGE IS
OF POOR QUALITY

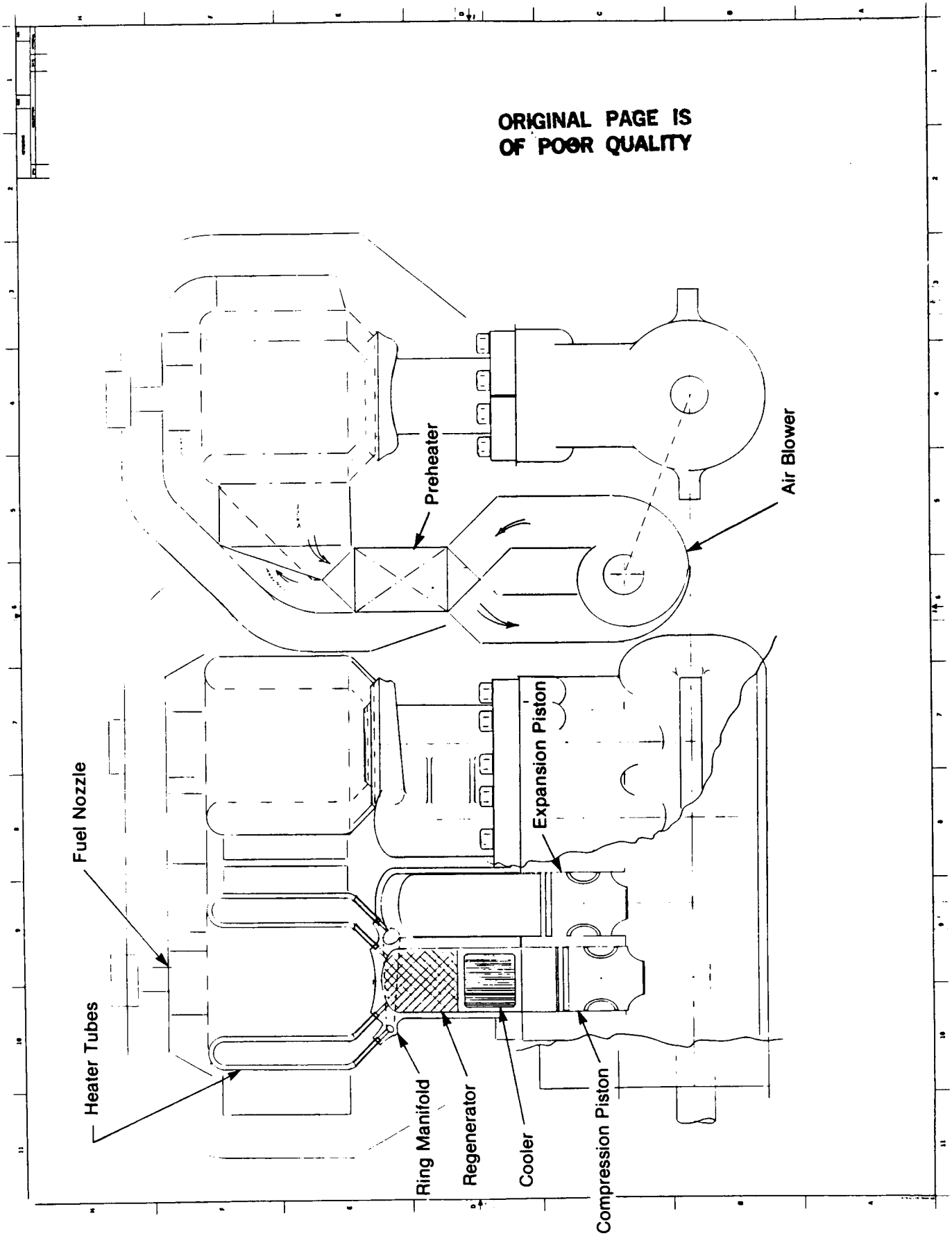


Figure 5-6 Single Acting In-Line Engine Concept

The indicated power and efficiency curves for the SAIL configuration are shown in Figures 5-7 and 5-8. The engine cycle produces excellent efficiency, with the efficiency peak occuring in the 1000-1500 rpm range. In addition, the part load curves (10 and 5 MPa mean pressure) exhibit very high performance at part load points.

As a result of the initial screening analysis of the three advanced CASE concepts, the SAIL configuration was chosen for further evaluation as the advanced CASE design. The SAIL engine concept offers excellent efficiency, good packageability and a straightforward manufacturing approach for the ceramic engine components.

As a result of the choice of the SAIL concept for further evaluation, the design and analysis of the engine was reviewed in greater detail than the initial screening application. The design was developed with additional emphasis on the manufacturing and practical aspects of the engine design. The expansion and compression cylinder housings were split to eliminate direct conduction losses from the hot space to the cold space, and the ring manifold was moved to an external location. The manifold will be formed in a green state as a partial ring and sintered to the expansion cylinder housing. The expansion pistons utilize a "hot ring" located at the top of the piston and a reduced diameter center section to minimize conduction losses to the base of the pistons. In addition, more detail regarding the size and configuration of the combustion system and crankcase have been added. The final SAIL configuration is shown in Figures 5-9 through 5-11.

To evaluate the actual performance of the engine design, estimates of the engine frictional and auxiliary losses were developed. These losses were based, where possible, on information from the 1983 RESD report. A combustion system efficiency of 90% was assumed (current Mod I combustion system efficiencies are 91-92%). A summary of the auxiliary losses is shown in Table 5-3. These losses include: water pump, blower, control system, hydrogen compressor, seal friction, and bearing friction. When these losses and the EHS efficiency are combined with the SAIL cycle efficiency, the overall net engine power and efficiency can be calculated. These final engine maps are shown in Figures 5-12 and 5-13. Those maps are based on a heater head temperature of 1100°C and 50°C cooling water temperature. The maps indicate that the peak engine efficiency of 53.4% occurs at 1000 rpm. The engine design produces a maximum power of 65 kW at 4000 rpm. A breakdown of the

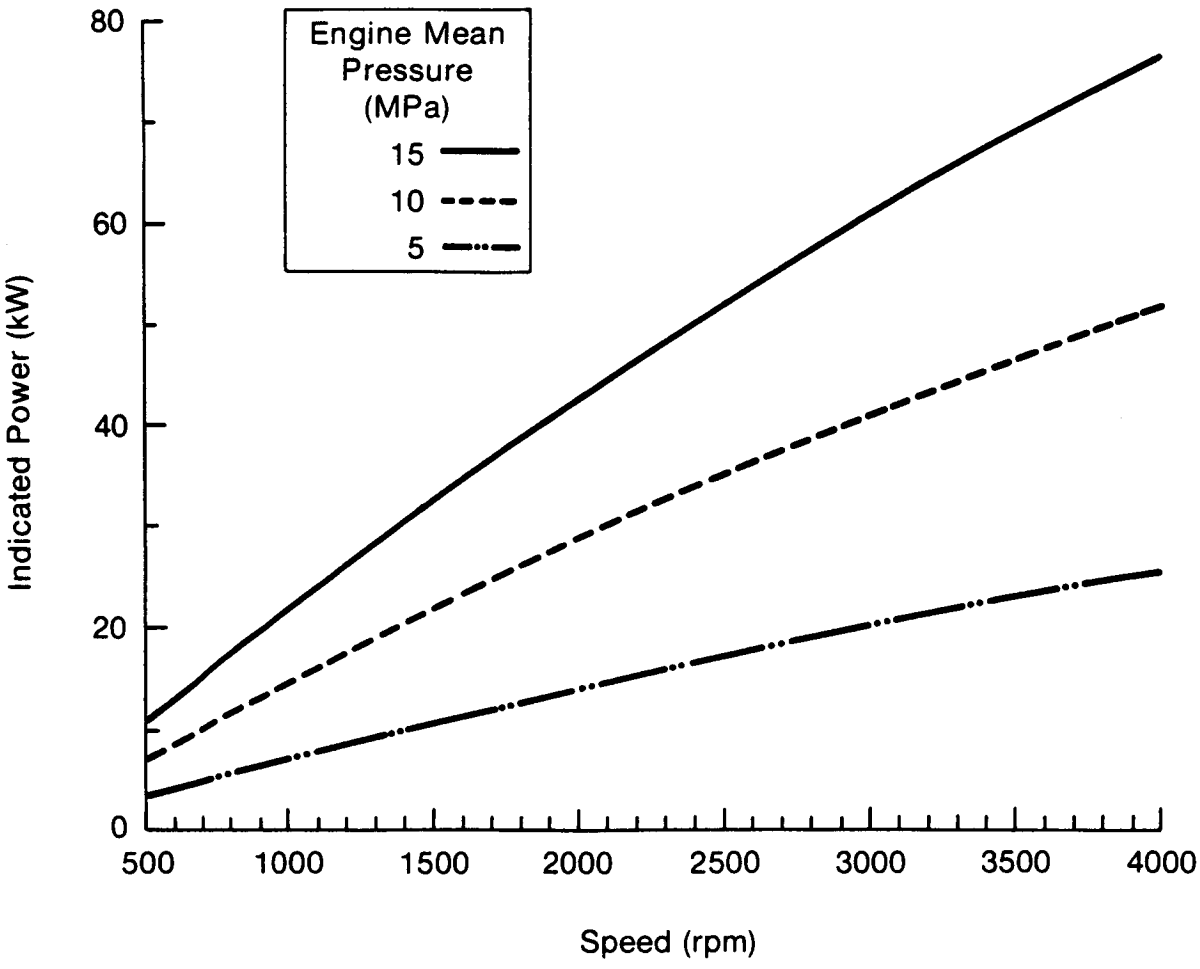


Figure 5-7 SAIL Indicated Power Curve

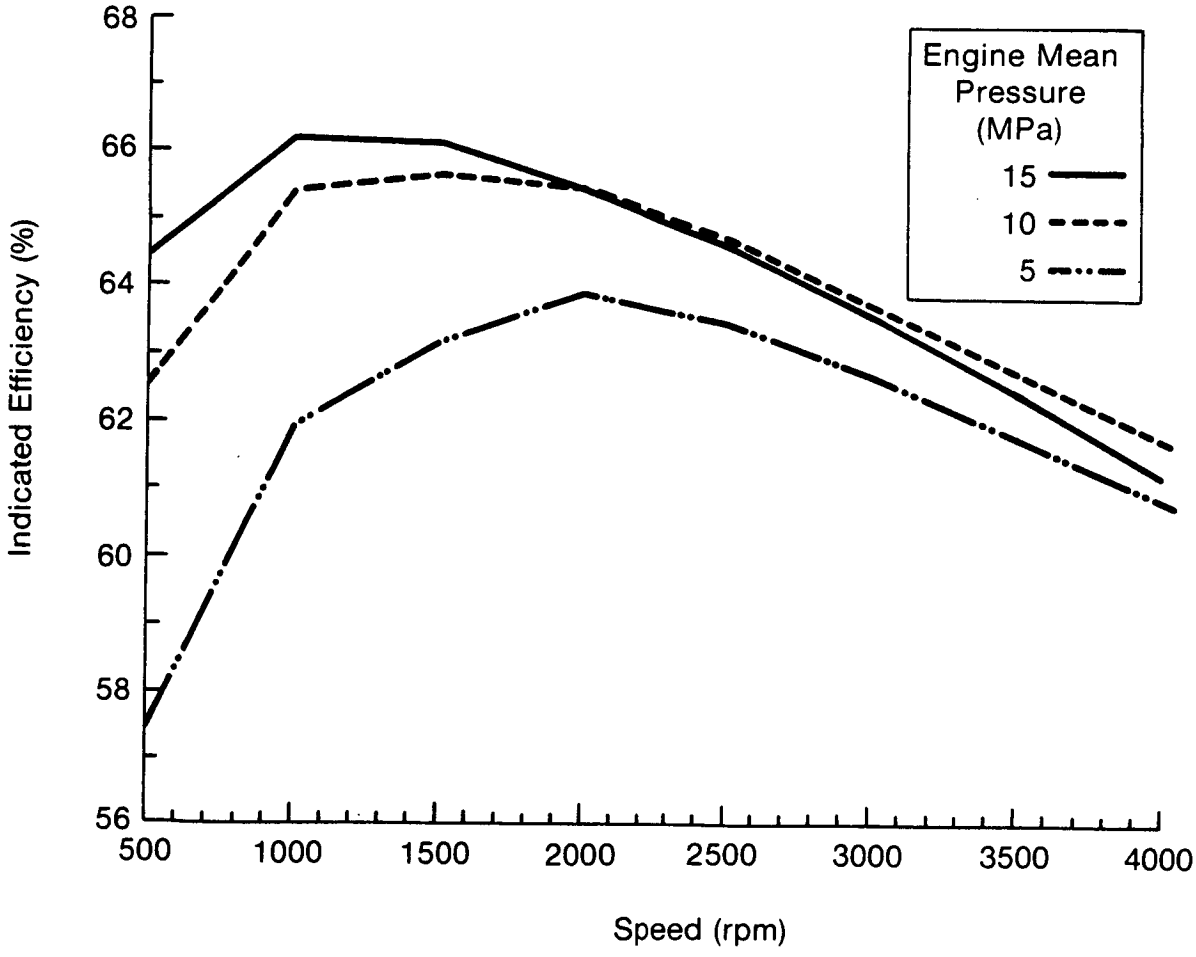


Figure 5-8 SAIL Indicated Efficiency Curve

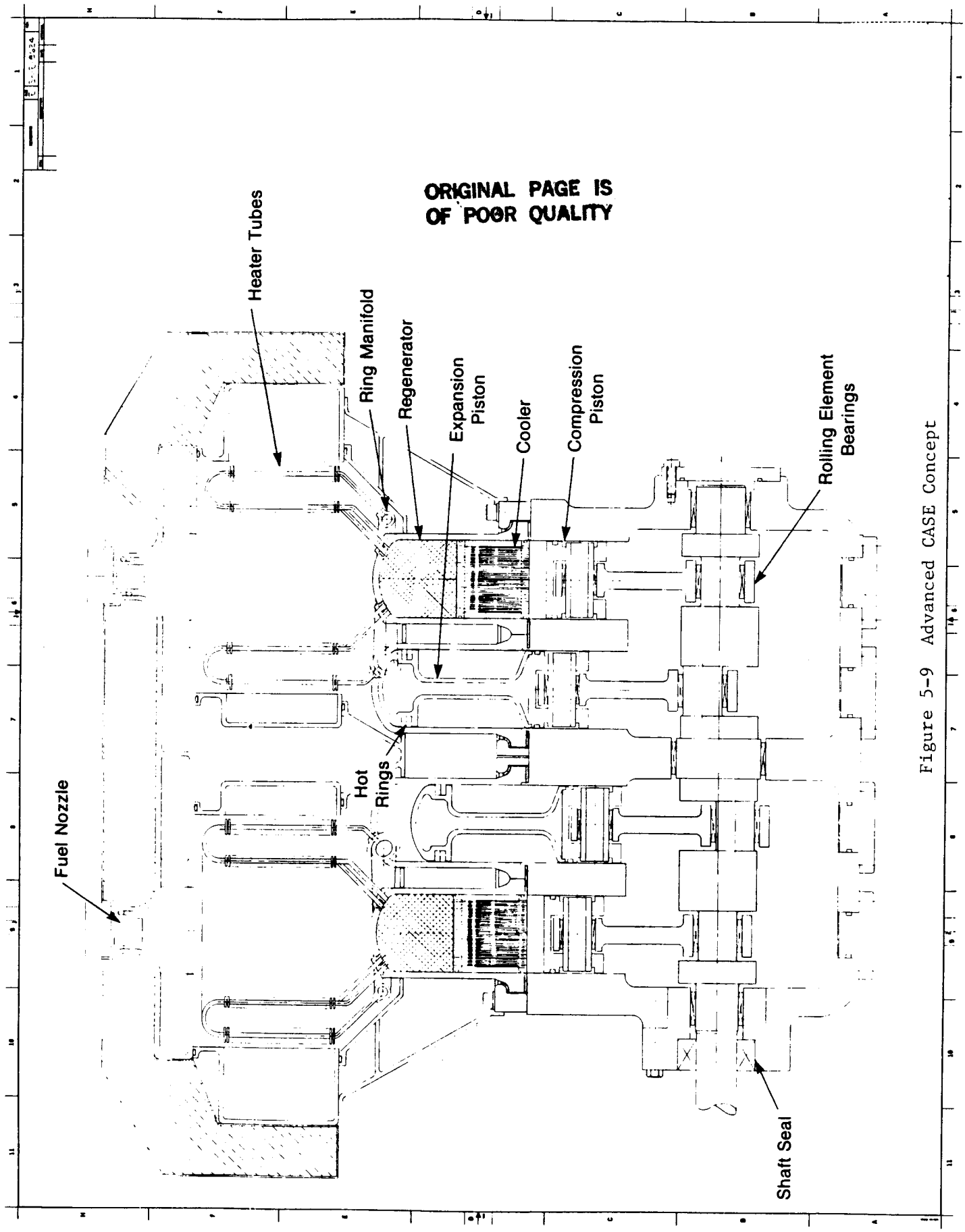


Figure 5-9 Advanced CASE Concept

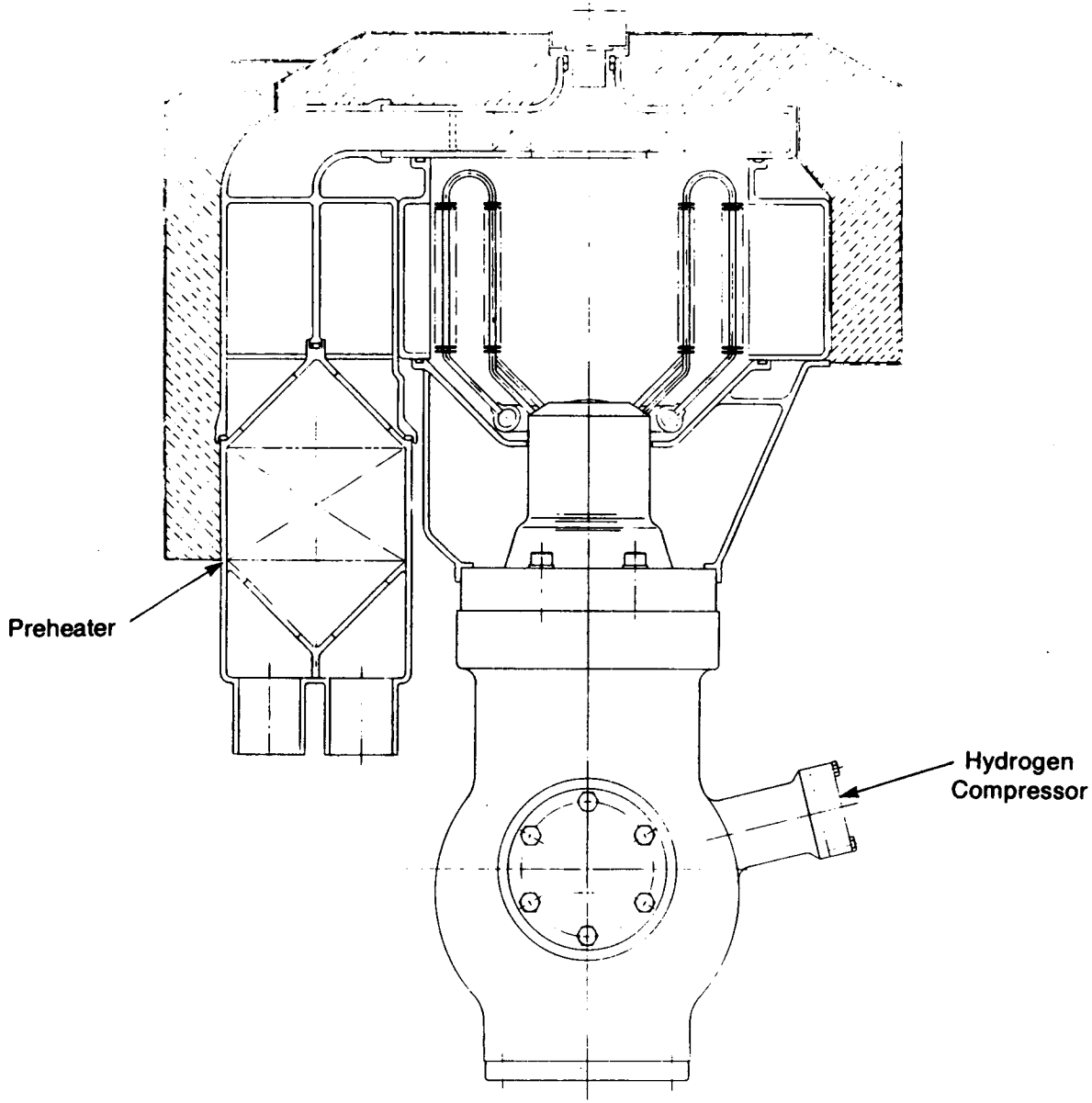


Figure 5-10 Advanced CASE Concept, End View

ORIGINAL PAGE IS
OF POOR QUALITY

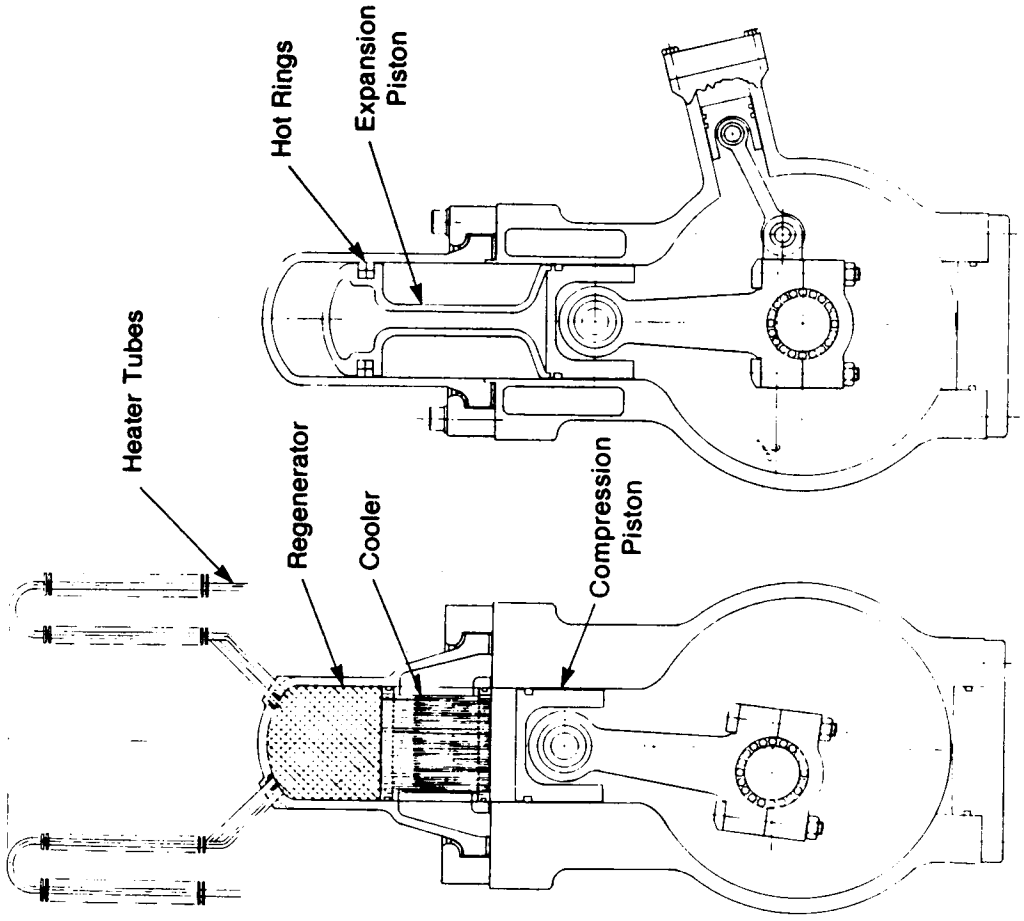


Figure 5-11 Advanced CASE, Concept, Engine Details

TABLE 5-3

TOTAL POWER LOSSES (kW)

Engine Speed (rpm)	Pressure (MPa) 5	10	15
500	.82	1.21	1.61
1000	1.23	1.94	2.67
1500	1.76	2.91	4.11
2000	2.22	3.85	5.46
2500	2.83	4.82	6.89
3000	3.45	5.88	8.41
3500	4.20	7.04	10.10
4000	5.04	8.36	11.93

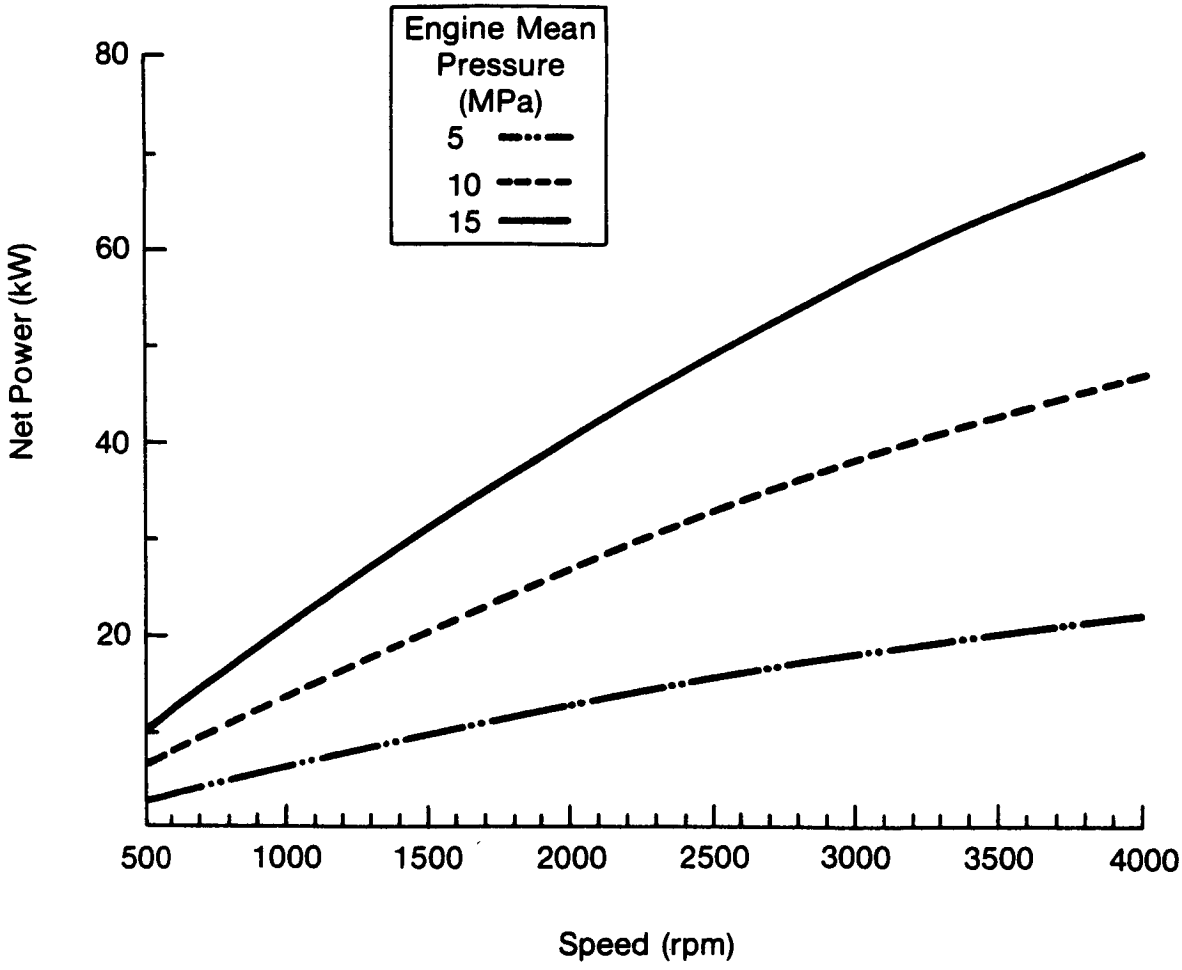


Figure 5-12 Final SAIL Concept Net Power

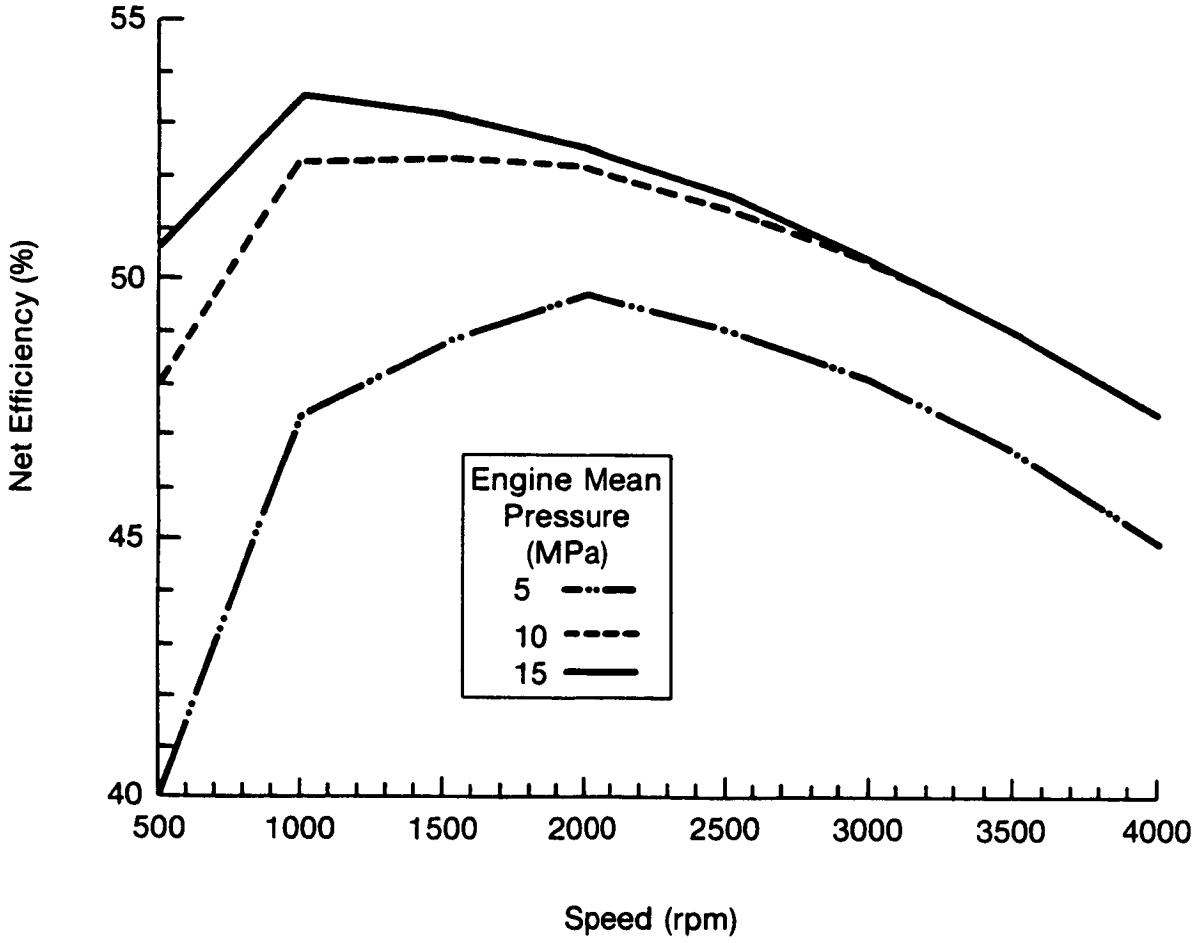


Figure 5-13 Final SAIL Concept Net Efficiency

engine losses, as a function of speed, is shown in Figure 5-14. These curves show the distribution of losses in the engine as a function of engine speed at 15 MPa mean pressure. The diagram shows the initial fuel input and then isolates the loss components associated with the combustion system, heat rejection to cooler, working fluid pumping losses. The magnitude of the losses are based on the first order thermodynamic code and the calculation of frictional/auxiliary losses. To estimate the combined mileage for the advanced CASE design, a determination of the stored energy in the heater head and EHS components was required. To calculate the stored energy, the mass and temperature of the components were calculated and the total stored energy of the hot components was determined. The total estimate of the stored energy is 17 MJ. A breakdown of the stored energy is shown in Table 5-4. This stored energy is significantly larger than the CASE design, (~8.5 MJ), however this is primarily due to the fact that the EHS has not been optimized to minimize the stored energy. If additional design efforts were applied to this actuation, it is estimated that the stored energy could be significantly reduced. The engine thermodynamic cycle is operating at ~87% of Carnot efficiency and most of the losses are associated with friction and auxiliaries.

The MTI vehicle simulation code was used in conjunction with the engine map and the stored energy to calculate the overall mileage. The initial mileage estimates were performed using a Chevrolet Celebrity as the vehicle. The calculations were performed using an inertia weight of 3125 lb, 2.84 rear axle ratio and an idle fuel flow of 0.1 g/s (ASE Mod II idle fuel flow will be 0.15 g/s). Under these conditions the engine will deliver a combined mileage of 53 mpg on gasoline and 61.0 mpg on diesel fuel. A summary of the mileage and performance for the advanced CASE design is shown in Table 5-5. A similar estimate was made for a Ford Topaz, a 2875 lb inertia weight vehicle. The combined mileage was 54.9 mpg on unleaded gasoline and 63.1 mpg on diesel. The performance results for the Topaz vehicle are shown in Table 5-6.

It should be noted that if the CSP were removed from the mileage calculation, the Topaz mileage would increase to 71.6 mpg on gasoline and 82.4 mpg on diesel fuel. This indicated the significance of the CSP on the overall mileage projection. As previously noted, the CSP becomes an increasingly larger factor in overall mileage as the base mileage increases with increasing heater head temperature. Thus the effect of higher heater head temperatures on overall mpg appears to become increasingly small.

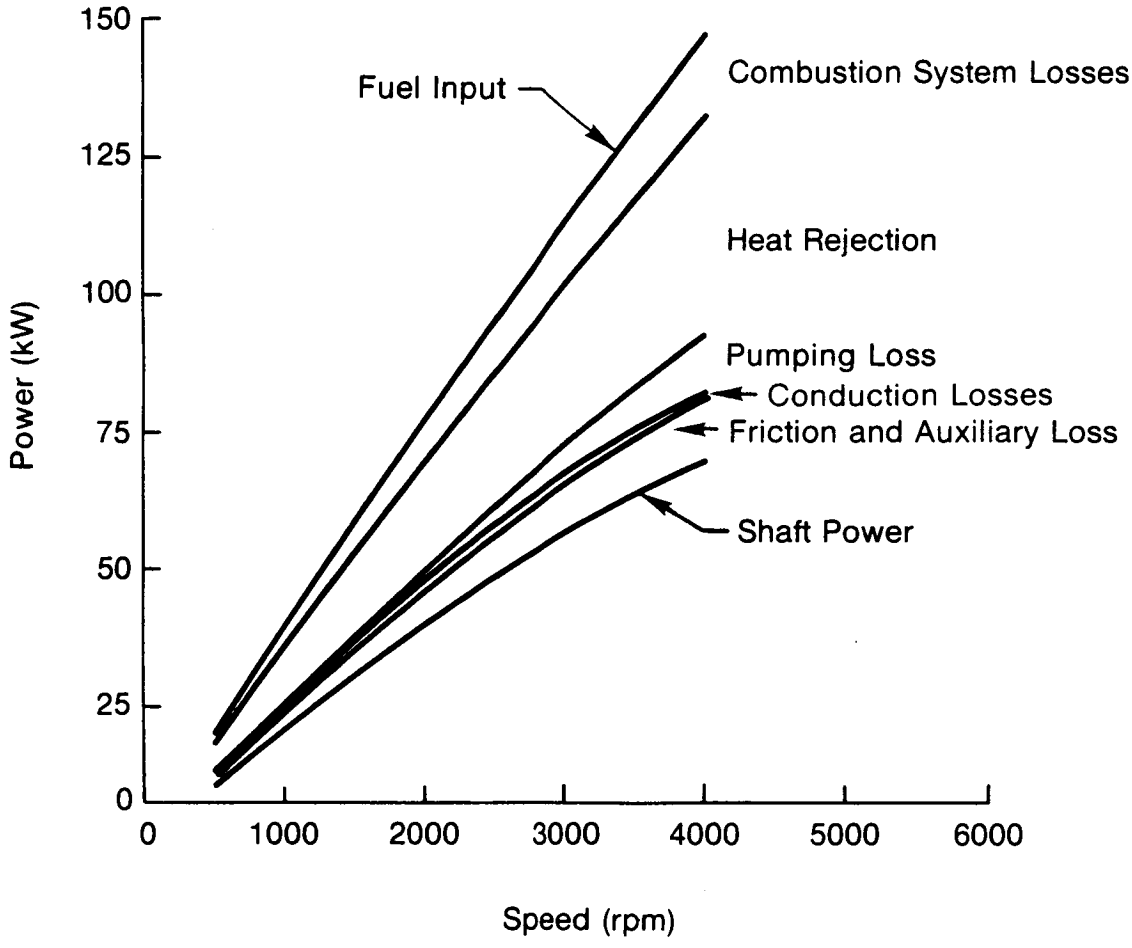


Figure 5-14 Final SAIL Concept Power Loss Breakdown

TABLE 5-4

SAIL CONCEPT STORED ENERGY

	Energy (MJ)
Heater Tubes	0.57
Heater Fins (Front and Rear)	3.90
Preheater	5.29
Regenerator Housing	0.67
Cylinder Housing with Dome	1.35
Regenerators	0.10
Combustor Liner and Cover	1.24
Scrolls	1.43
Preheater Baffles and Support Structure	1.26
Unaccounted for Components	1.20
Total	17.0

TABLE 5-5

FINAL SAIL CONCEPT MILEAGE PREDICTIONS

Vehicle 1986 Celebrity (3250 lb Inertia Weight)
Axle Ratio - 2.84 Manual - Four Speed

	Unleaded Gasoline (mpg)	Diesel (mpg)
Urban	40.6	
Without CSP	63.5	
Highway	84.5	
Combined	53.0	61.0
Performance		
0-60 mph	12.3 sec	
50-70 mph	8.1 sec	
0-100 ft	4.1 sec	

TABLE 5-6

FINAL SAIL CONCEPT MILEAGE PREDICTIONS

Vehicle 1986 Topaz (2875 # Inertia Weight)
Axle Ratio - 1.0 Manual - Four Speed

	Unleaded Gasoline (mpg)	Diesel (mpg)
Urban	40.9	
Without CSP	64.3	
Highway	94.8	
Combined	54.9	63.1
Performance		
0-60 mph	18.3 sec	
50-70 mph	7.8 sec	
0-100 ft	5.7 sec	

In conclusion, the advanced CASE SAIL engine concept appears to offer significant performance advantages over conventional metallic ASEs. However, the engine design incorporates many features which are clearly developmental in nature, such as ceramic bearings, hot rings, pressurized crankcase, and ceramic heater head. If these developmental problems can be solved without compromising the performance of the engine, the SAIL engine offers a significant potential for use in an automotive application.

The most important conclusion of the advanced study comes from comparing the SAIL to the RESD-based CASE. Rather unexpectedly, the major mileage gain availble from applications of ceramics in Stirlings comes not from increased temperature (as with turbine engines), but rather from increased design possibilities (e.g., nonoiled roller bearings, hot piston rings) which utilize ceramics' unique properties. This suggests that further development of ceramic materials for Stirling engines should concentrate on their frictional and wear properties at both high and low temperatures. It is worth noting that the SAIL engine, operating at 820°C (Mod II metallic head temperature), but preserving the design features made possible with ceramics would nonetheless retain most of its increased efficiency. Indicated efficiency would peak at 60% (versus 65% at 1100°C) compared to low 50s for the baseline (RESD). More importantly, the CSP fuel equivalent of the metal SAIL engine falls from 396 to 314 g based on stored heat ratio. Because of this, estimated urban mileage which, without CSP, falls from 63.5 to 58.6 is actually higher at 820° (41.5 versus 40.6) due to CSP reduction. The highway mileage estimate of 78.0 (versus 84.5) gives a combined mileage estimate of 52.6, just 0.4 mpg less than the hotter engine*. From this it can be seen that, for the automotive mission, where CSP is so strong an effect, that ceramics offer most of their promised advantage without elevated temperatures by allowing innovation in component design.

*See Table 3-1 SiC (Group 1) engine performance versus temperature.

6.0 CONCLUSIONS AND RECOMMENDATIONS

The overall conclusions and recommendations for the CASE study can be summarized as follows:

- The use of advanced ceramics in a Stirling engine heater head design based on the 1981 RESD does not result in significant mileage or efficiency improvements over conventional metallic engines.

- The use of an advanced ceramic heater head does represent a potential manufacturing cost savings compared to the 1981 RESD. However, the 1983 RESD heater head which incorporates lower cost materials (XF-818/CG-27) is only 17% more expensive than the CASE heater head. Thus the potential savings expected must be continuously monitored against the current state-of-the-art. Also it should be noted that the CASE heater head completely eliminates the need for chrome, nickel, and other rare metals, this may be an important consideration in the future.

- The use of advanced design features which are based on the use of ceramics, such as "hot rings" and nonlubricated ceramic bearings, can result in significant performance improvements if integrated into an overall engine design, perhaps even without significantly higher heater temperature.

6.1 Recommendations

Based on the results of the CASE and advanced CASE studies, it is evident that ceramics do offer potential benefits in Stirling engines, and that the following areas of development be considered for further investigation:

- Continued development of tough, strong low thermal conductivity matrix ceramics having repeatable material properties and capable of being fabricated in complex shapes.

- Joining of dissimilar ceramics/and ceramics to metals.

- Development of fabrication techniques suitable for mass production.

- Study of nonlubricated or solid lubricated ceramic or ceramic/metal wear couples at high and low temperatures.

- Implementation of selected features incorporating ceramics (partition walls, ceramic bearings, and hot rings) in existing engines.

7.0 REFERENCES

1. Mechanical Technology Incorporated; "Automotive Stirling Reference Engine Design Report"; MTI 81ASE164DR2 (NASA CR-165381); June 1981.

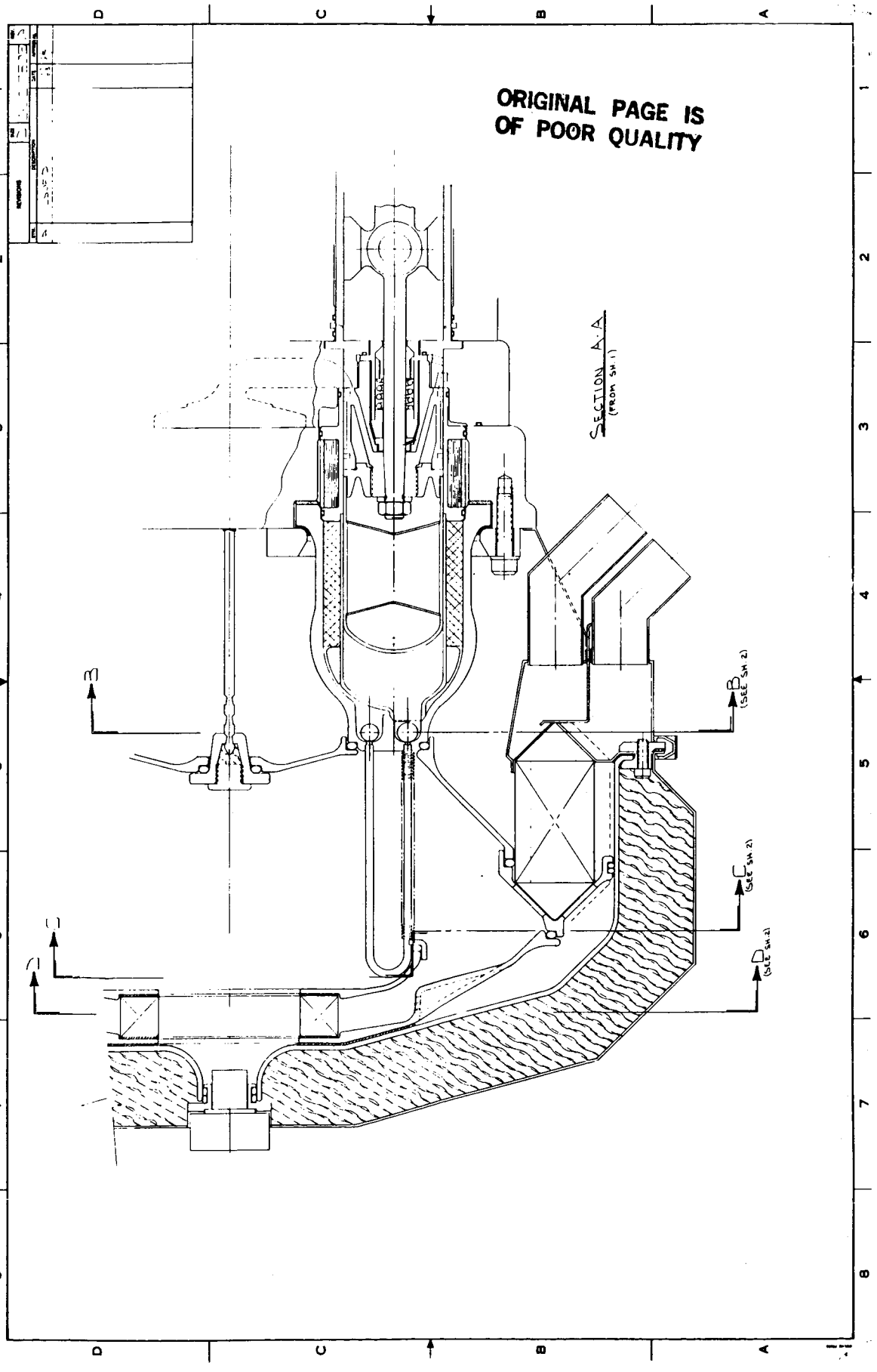
2. Faber, K.T.; "Toughening Mechanisms for Ceramics in Automotive Applications"; Ceramic Engineering and Science Proc.; Vol. 5, No. 5-6; 1984.

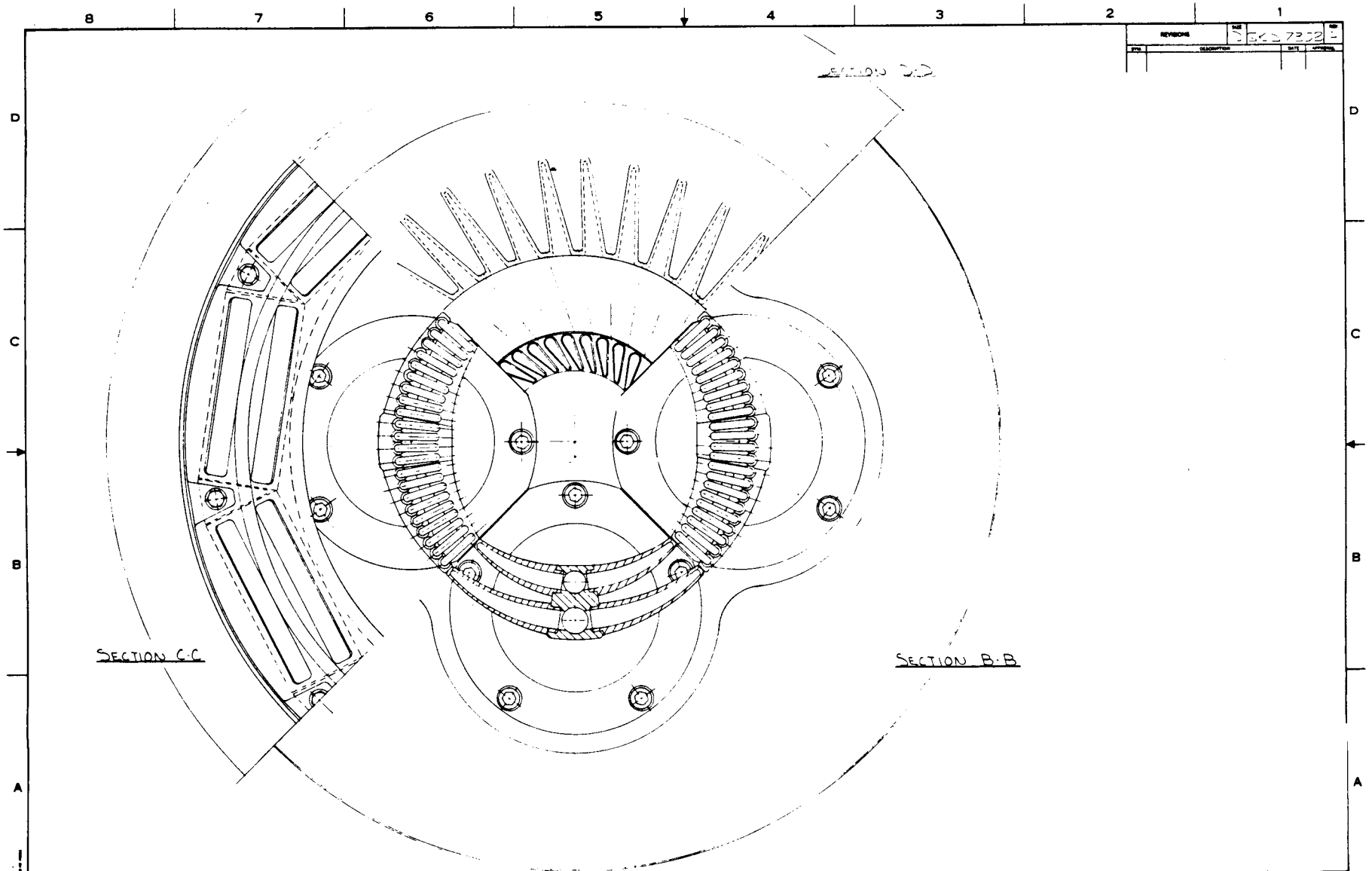
3. Verghesse, K., Zumwalt, L.R., Feng, C.P., and Elleman, T.S.; Journal of Nuclear Materials; 85 and 86 (1979); pp. 1161-1164.

4. Tso, S.T., and Pask, J.A.; "Reaction of Silicate Glasses and Mullite with Hydrogen Gas;" Journal of American Ceramic Society, 65 (8) p. 383-387; 1982.

5. Farrell, R., and Bolton, R.; "Comparison of Steady State and Transient CVS Cycle Emissions of an Automotive Stirling Engine;" SAE Paper 831700; November 1983.

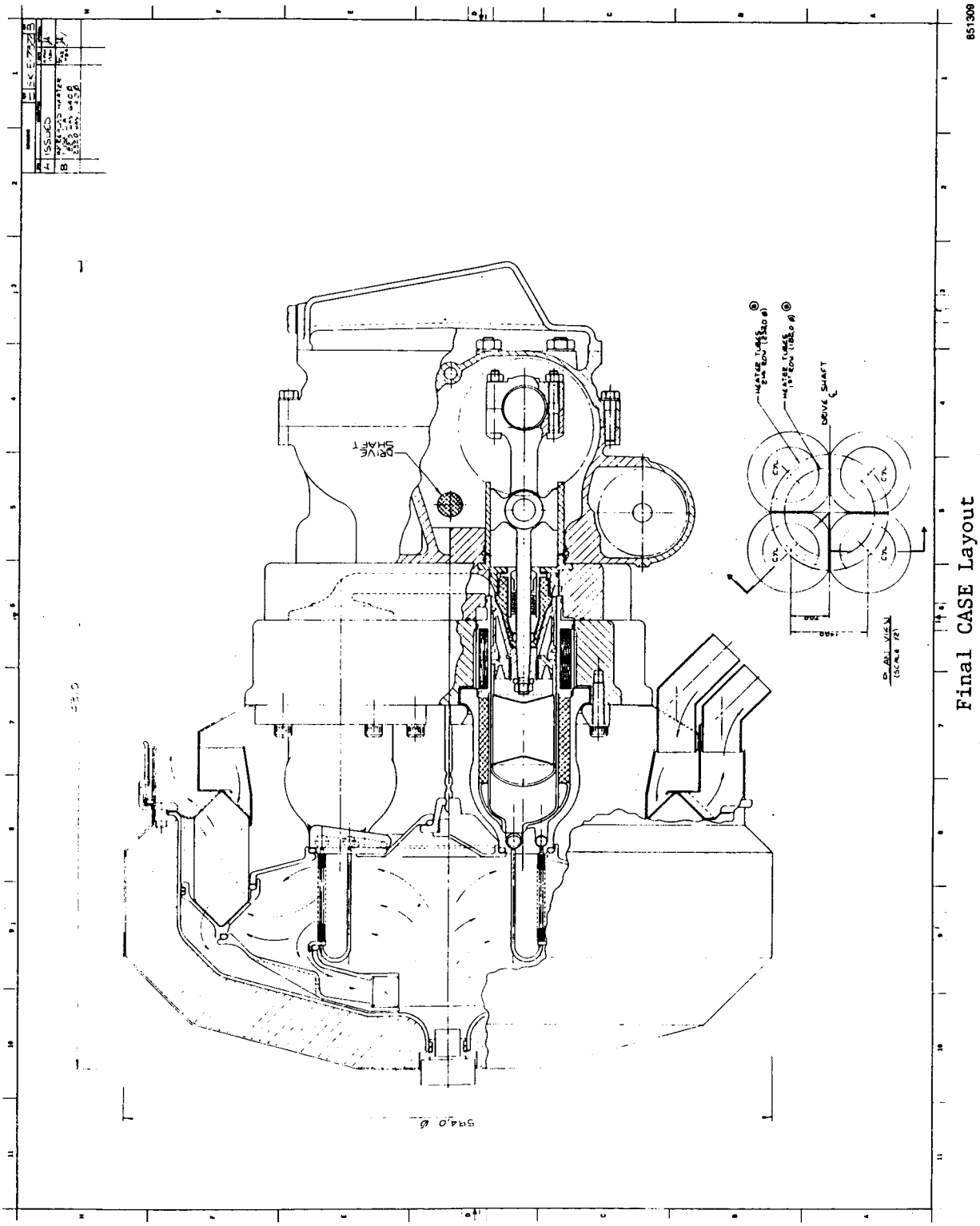
DRAWINGS


ORIGINAL PAGE IS
OF POOR QUALITY
SECTION A-A
(FROM SH 1)
B
(SEE SH 2)
C
(SEE SH 2)
D
(SEE SH 2)



851296

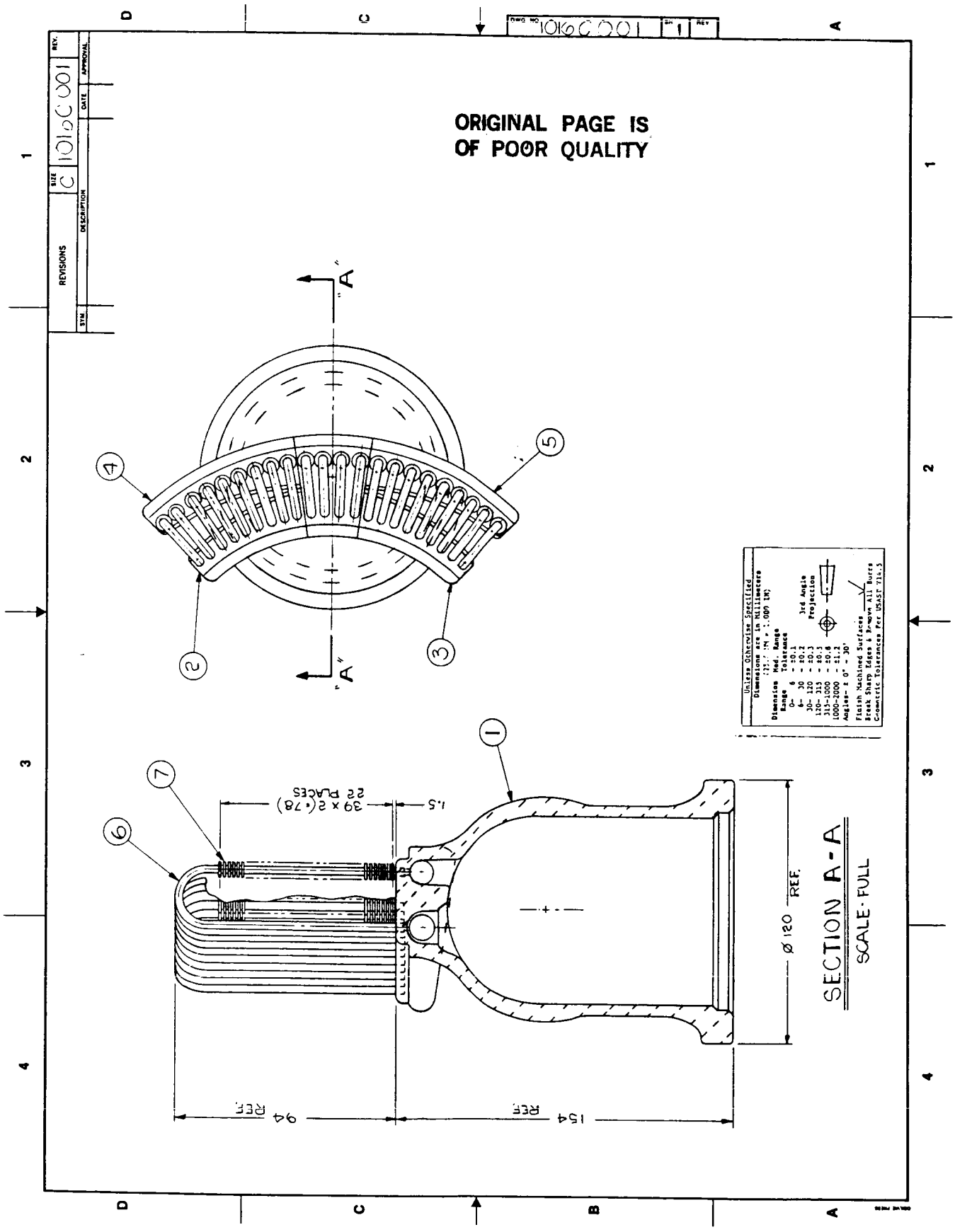
ORIGINAL PAGE IS
OF POOR QUALITY



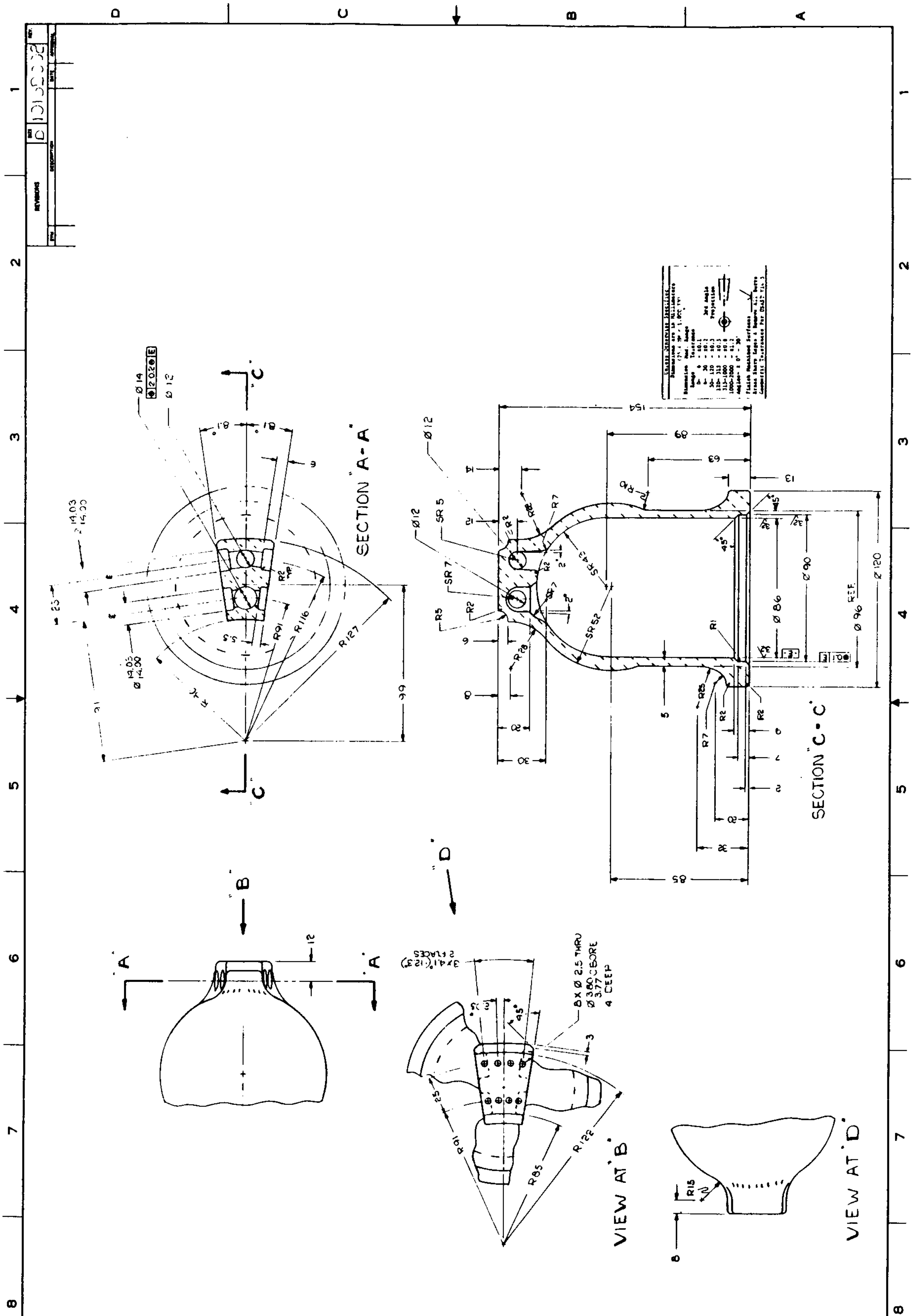
Final CASE Layout

Drawing Number Assignment for Job No. 1016 - "CASE"

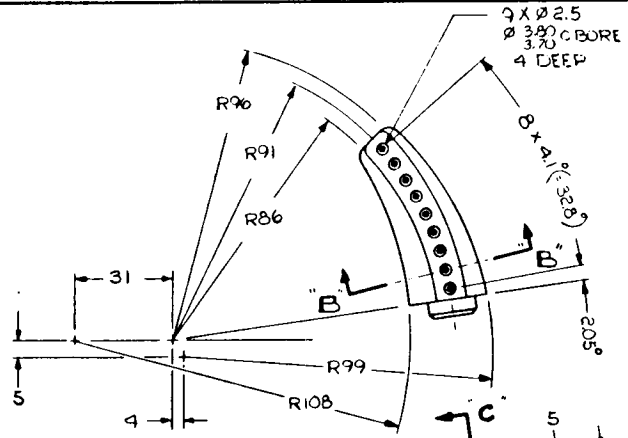
Drawing No. Job	Size	No.	Title
1016	D	001	Dome/Heater Assembly
1016	D	002	Dome
1016	C	003	Inner Manifold Left Hand
1016	C	004	Inner Manifold Right Hand
1016	C	005	Outer Manifold Left Hand
1016	C	006	Inner Manifold Right Hand
1016	B	007	Heater Tube
1016	B	008	Heater Fin
1016	C	009	Inner Combustor Assembly
1016	D	010	Inner Combustor Shell
1016	C	011	EGR Shell
1016	D	012	Preheater Support/Seal
1016	C	013	Flow Separator
1016	C	014	Flameshield
1016	C	015	Turbulator Support Plate
1016	C	018	Tip Fuel Nozzle
1016	B	019	Regenerator Cup Matrix
1016	D	023	Displacer Dome Assembly
1016	B	024	Stuffer
1016	B	025	Displacer Cylinder

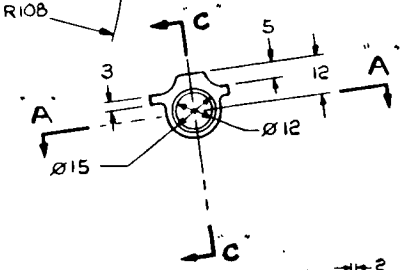

ORIGINAL PAGE IS
OF POOR QUALITY
REVISIONS
DESCRIPTION
DATE
APPROVAL
SIZE
C 1016C001
DWG NO 1016C001
SH 1
REV
"A"
"A"
SECTION A-A
SCALE · FULL
Ø 120 REF.
154 REF.
94 REF.
39 x 2 (.78)
22 PLACES
1.5
Unless Otherwise Specified
Dimensions are in Millimeters
Dimension Mod. Range Tolerance
0- 6 ± 0.1
6- 30 ± 0.2
30- 120 ± 0.3
120- 315 ± 0.5
315-1000 ± 0.8
1000-2000 ± 1.2
Angles- ± 0° - 30'
3rd Angle Projection
Finish Machined Surfaces
Break Sharp Edges & Remove All Burrs
Geometric Tolerances Per USASI Y14.5

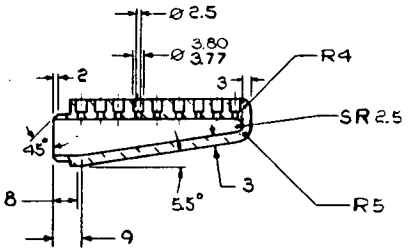
851292


SECTION "A-A"
SECTION "C-C"
VIEW AT "B"
VIEW AT "D"
8X Ø 2.5 THRU
Ø 3.80 CBORE
3.77
4 DEEP
3X4.1°(12.3°)
2 PLACES
Ø 14.03
14.00
R91
R116
R127
R122
R85
R15
SR 5
SR 7
SR 52
Ø 12
Ø 14
Ø 86
Ø 90
Ø 96 REF
Ø 120
154
89
63
85
3rd angle Projection

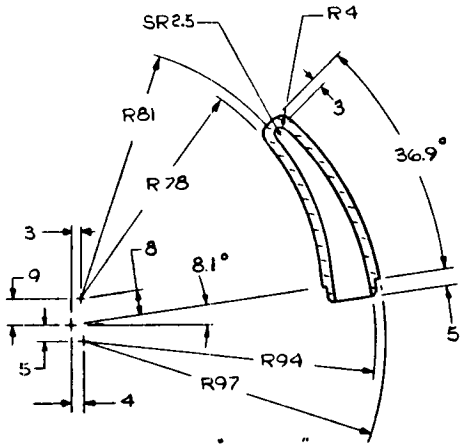
REVISIONS		SIZE C	10166003	REV.
SYM.	DESCRIPTION		DATE	APPROVAL



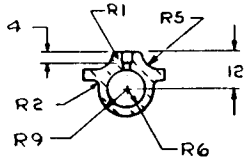




SECTION C-C



SECTION A-A



SECTION B-B

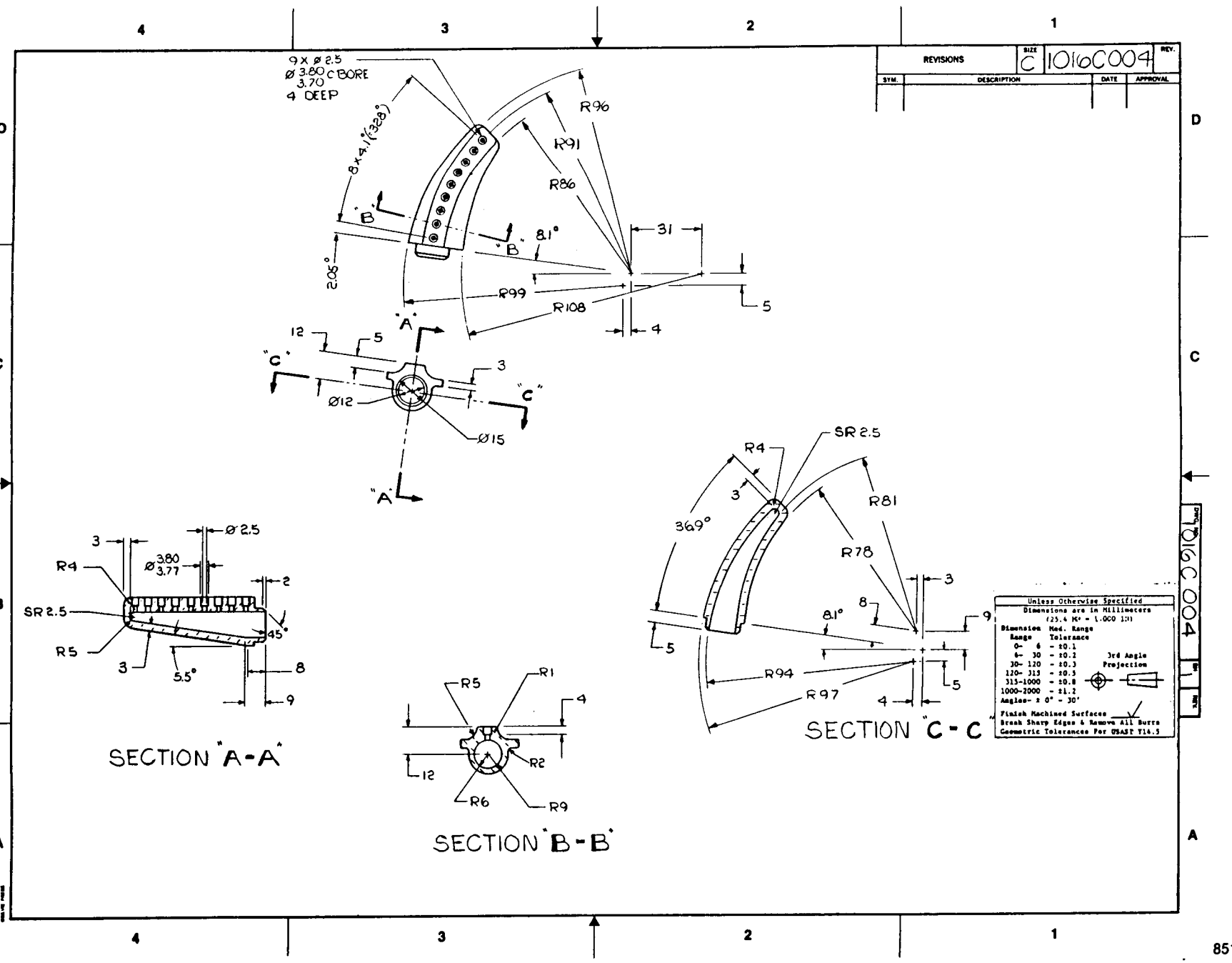
Unless Otherwise Specified		
Dimensions are in Millimeters (25.4 MM = 1.000 IN)		
Dimension Range	Mod. Range Tolerance	
0- 6	± 0.1	
6- 30	± 0.2	3rd Angle Projection
30- 120	± 0.3	
120- 315	± 0.5	
315-1000	± 0.8	
1000-2000	± 1.2	
Angles- ± 0° - 30'		
Finish Machined Surfaces ✓		
Break Sharp Edges & Remove All Burrs		
Geometric Tolerances Per USAST Y14.5		

ORIGINAL PAGE IS
OF POOR QUALITY

10166003

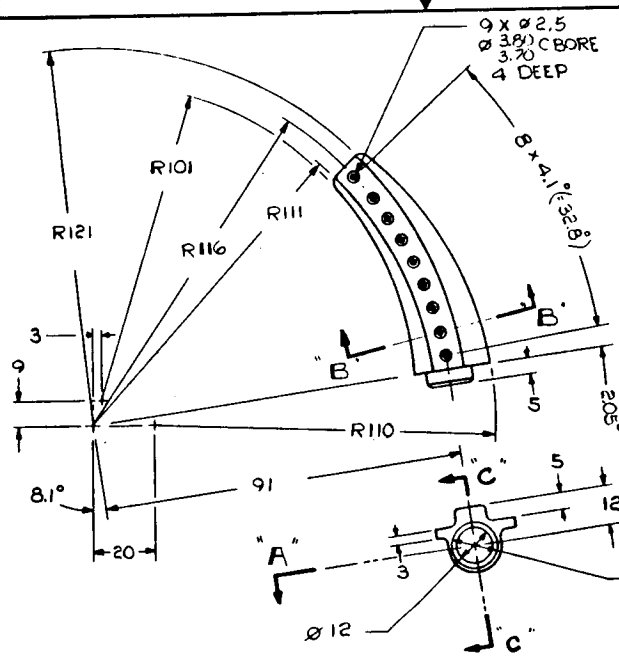
851307

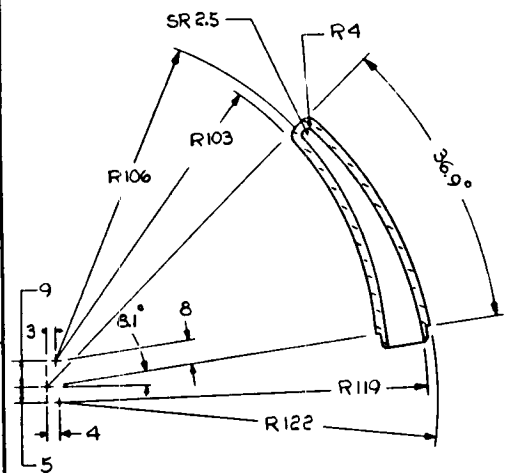
REVISIONS				SIZE	10160004	REV.
SYM.	DESCRIPTION	DATE	APPROVAL			



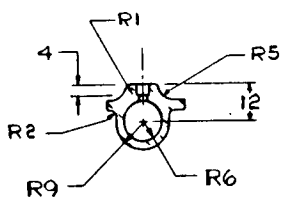
851303

REVISIONS		SIZE C	1016C005	REV.
SYM.	DESCRIPTION	DATE	APPROVAL	

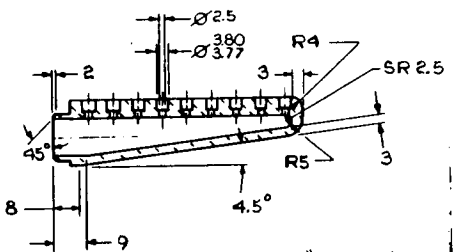




SECTION A-A



SECTION "B-B"



SECTION "C-C"

ORIGINAL PAGE IS OF POOR QUALITY

Unless Otherwise Specified	
Dimensions are in Millimeters	
Dimension Range	Med. Range Tolerance
0- 6	±0.1
6- 30	±0.2
30- 120	±0.3
120- 315	±0.5
315-1000	±0.8
1000-2000	±1.2
Angles- ± 0° - 30'	

3rd Angle Projection

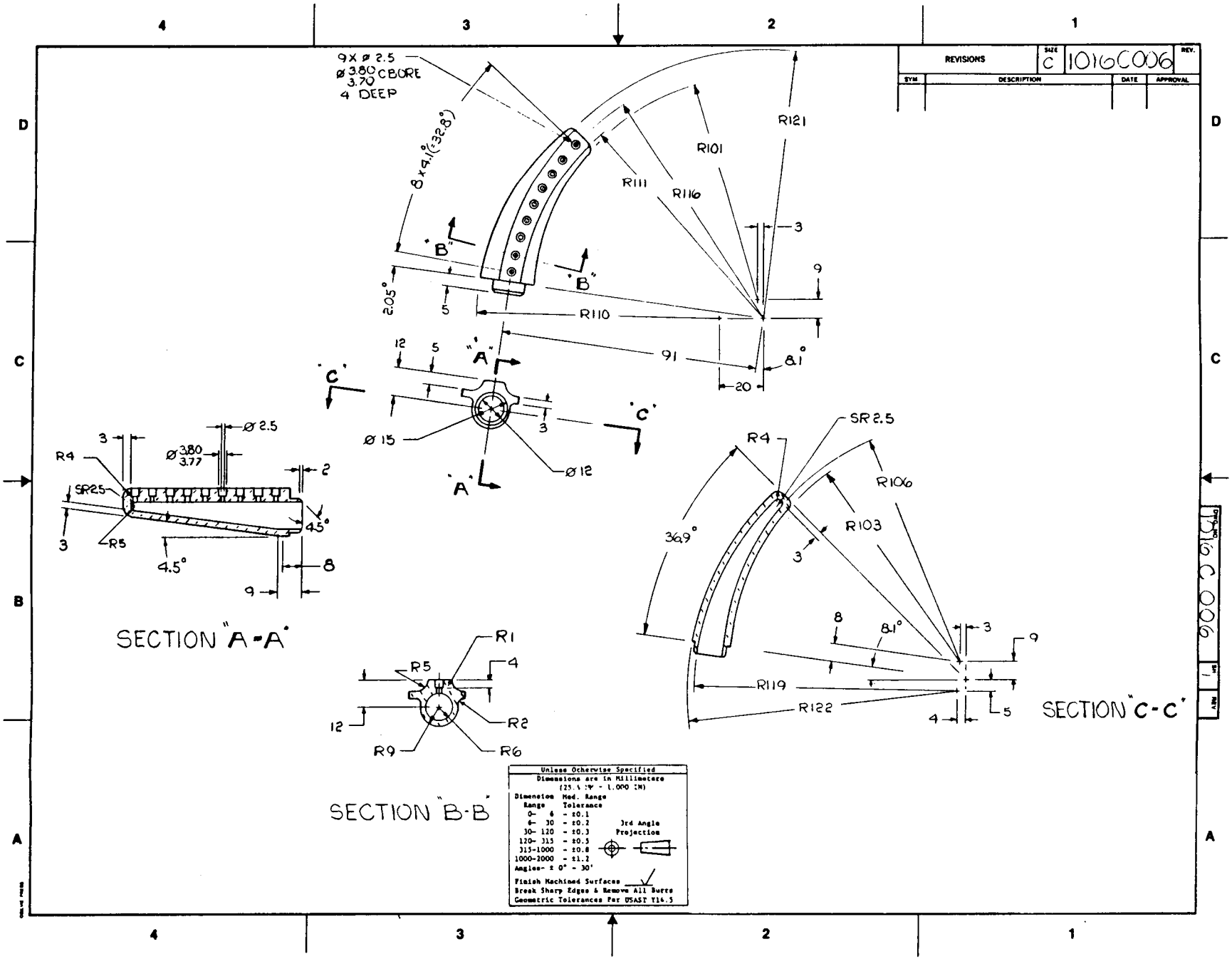
Finish Machined Surfaces

Break Sharp Edges & Remove All Burrs

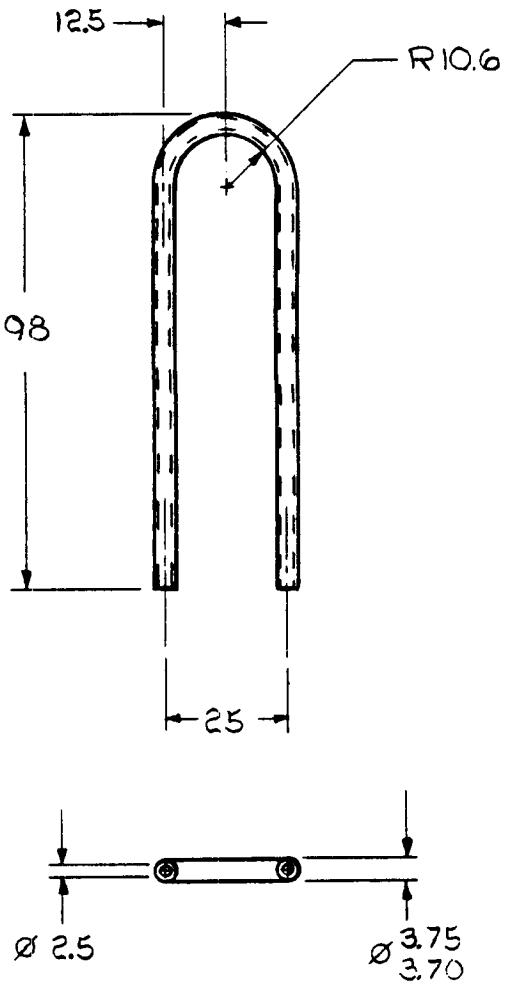
Geometric Tolerances Per ASME Y14.5

1016C005

851304


9X ø 2.5
ø 3.80 CBORE
3.70
4 DEEP
8 x 9.1° (=32.8°)
R121
R101
R111
R116
3
9
2.05°
5
R110
91
8.1°
20
12
5
"A"
"B"
"C"
ø 15
3
ø 12
ø 2.5
ø 3.80
3.77
2
R4
SR25
4.5°
3
R5
4.5°
8
9
SECTION "A-A"
R1
4
R5
12
R2
R9
R6
SECTION "B-B"
SR 2.5
R4
R106
R103
36.9°
3
8
8.1°
3
9
R119
R122
4
5
SECTION "C-C"
REVISIONS
SIZE C
1016C006
REV.
SYM
DESCRIPTION
DATE
APPROVAL
D
C
B
A
4
3
2
1
1016C006
Unless Otherwise Specified
Dimensions are in Millimetres
(25.4 "M" = 1.000 "IN")
Dimension Range
Med. Range Tolerance
0- 6 - ±0.1
6- 30 - ±0.2
30- 120 - ±0.3
120- 315 - ±0.5
315-1000 - ±0.8
1000-2000 - ±1.2
Angles- ± 0° - 30'
3rd Angle Projection
Finish Machined Surfaces
Break Sharp Edges & Remove All Burrs
Geometric Tolerances Per USAST Y14.5

REVISIONS	SIZE		REV.
SYM.	DESCRIPTION	DATE	APPROVAL



NOTE
DEV. LGTH. = 207

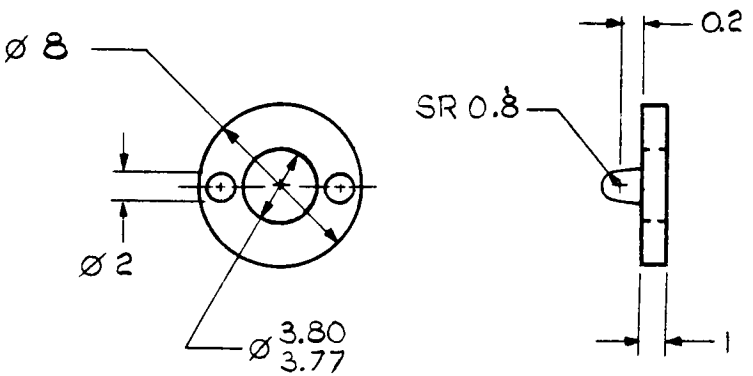
Unless Otherwise Specified	
Dimensions are in Millimeters	
(25.4 MM = 1.000 IN)	
Dimension Range	Med. Range Tolerance
0- 6	- ±0.1
6- 30	- ±0.2
30- 120	- ±0.3
120- 315	- ±0.5
315-1000	- ±0.8
1000-2000	- ±1.2
Angles- ± 0° - 30'	
Finish Machined Surfaces	
Break Sharp Edges & Remove All Burrs	
Geometric Tolerances Per USASI Y14.5	

3rd Angle Projection

ORIGINAL PAGE IS
OF POOR QUALITY

BRUNING 40-105 22145 6

REVISIONS		SIZE B	1016B008	REV.
SYM.	DESCRIPTION		DATE	APPROVAL



Unless Otherwise Specified	
Dimensions are in Millimeters	
(25.4 MM = 1.000 IN)	
Dimension Range	Med. Range Tolerance
0- 6	- ±0.1
6- 30	- ±0.2
30- 120	- ±0.3
120- 315	- ±0.5
315-1000	- ±0.8
1000-2000	- ±1.2
Angles- ± 0° - 30'	

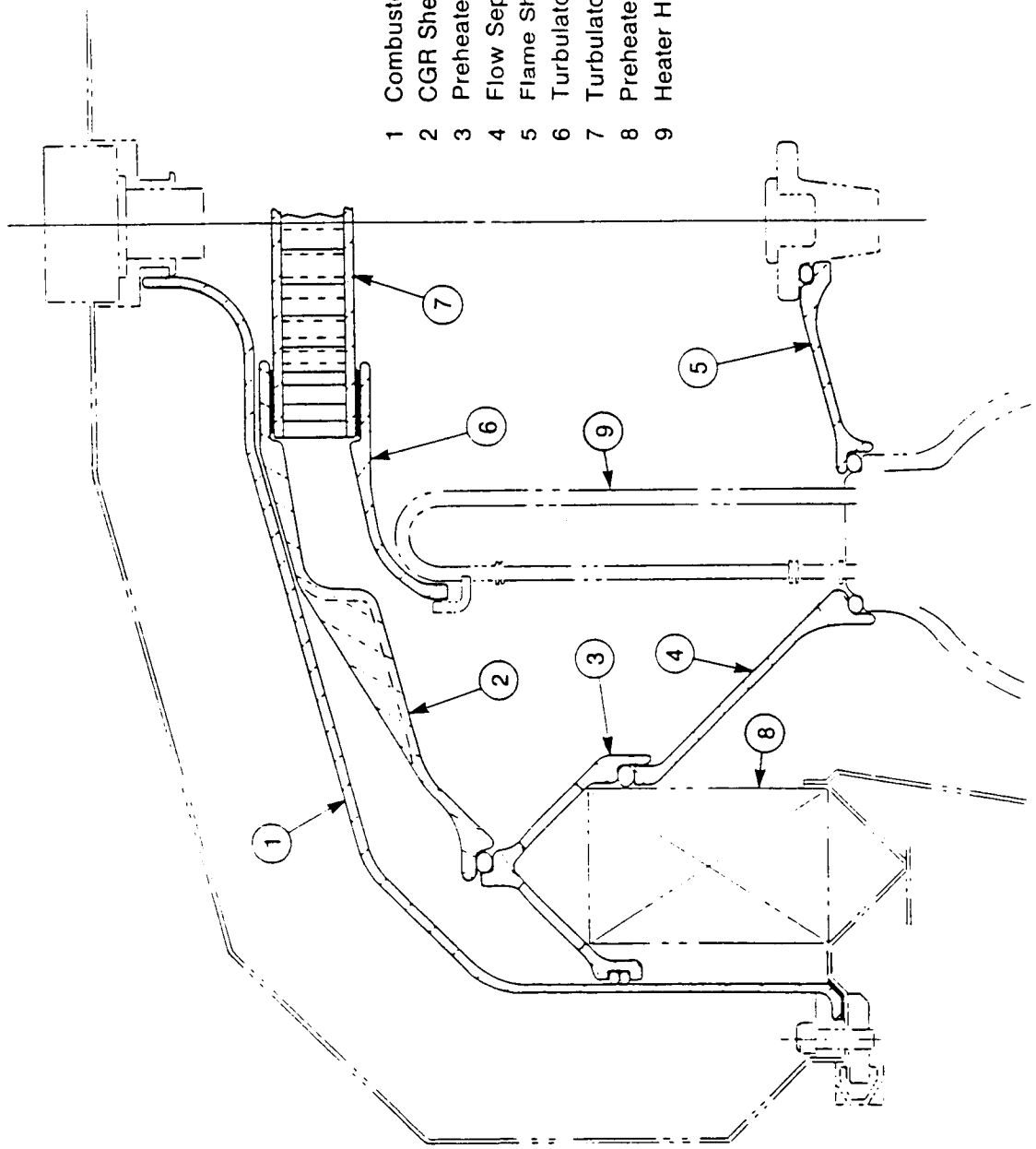
3rd Angle Projection

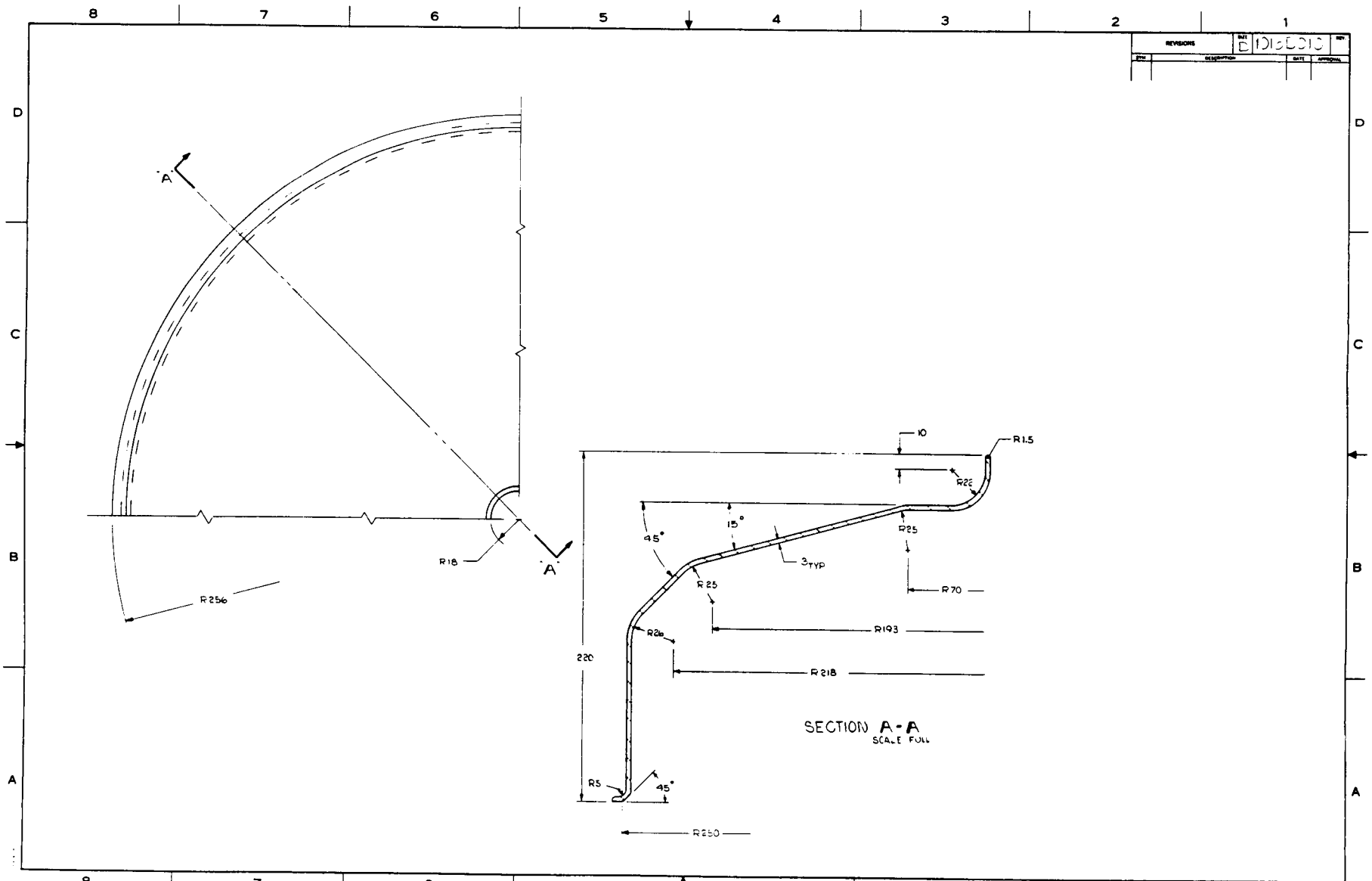
Finish Machined Surfaces
Break Sharp Edges & Remove All Burrs
Geometric Tolerances Per USAST Y14.5

8-12

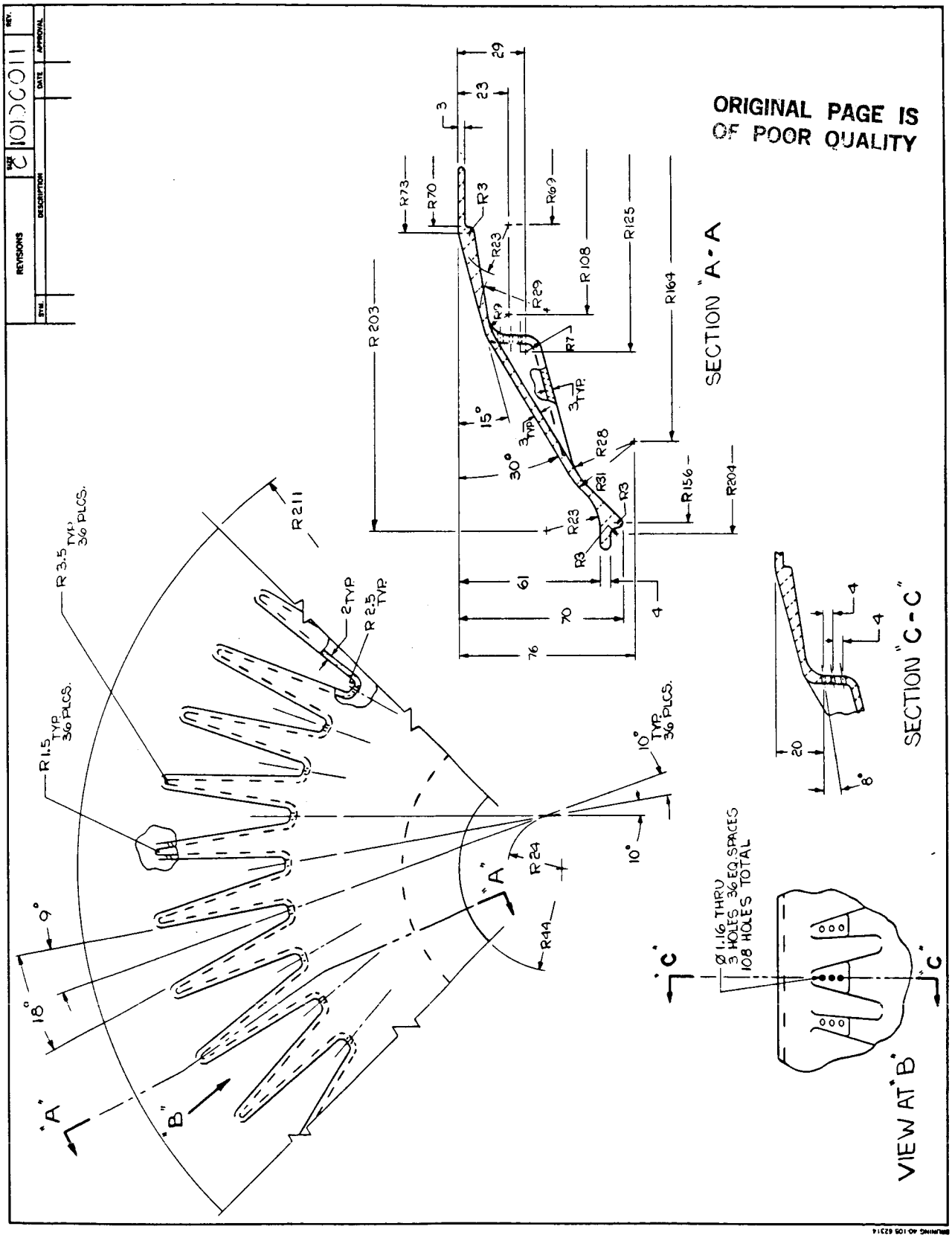
BRUNING 40-105 22145-6

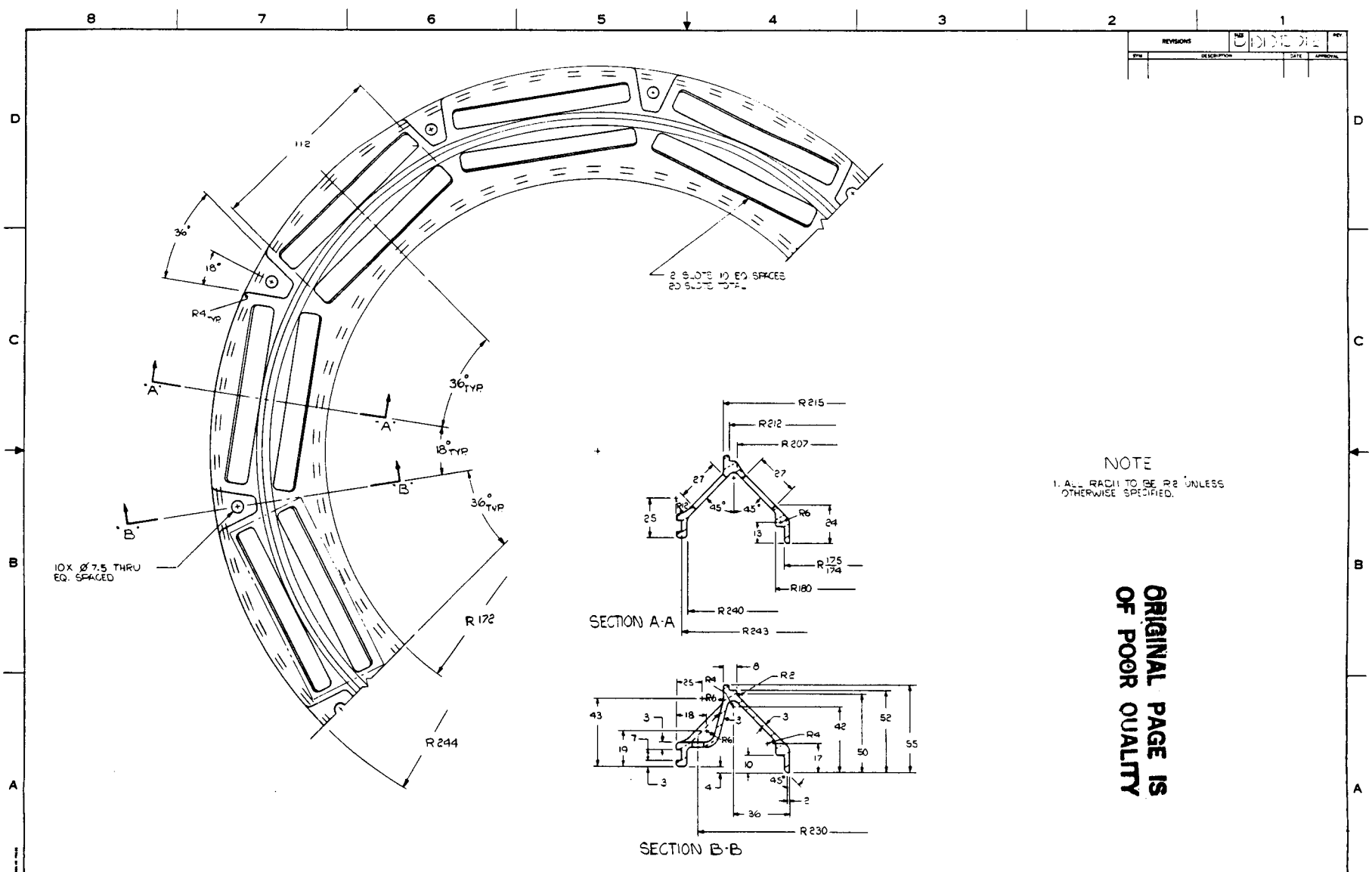
ORIGINAL PAGE IS
OF POOR QUALITY



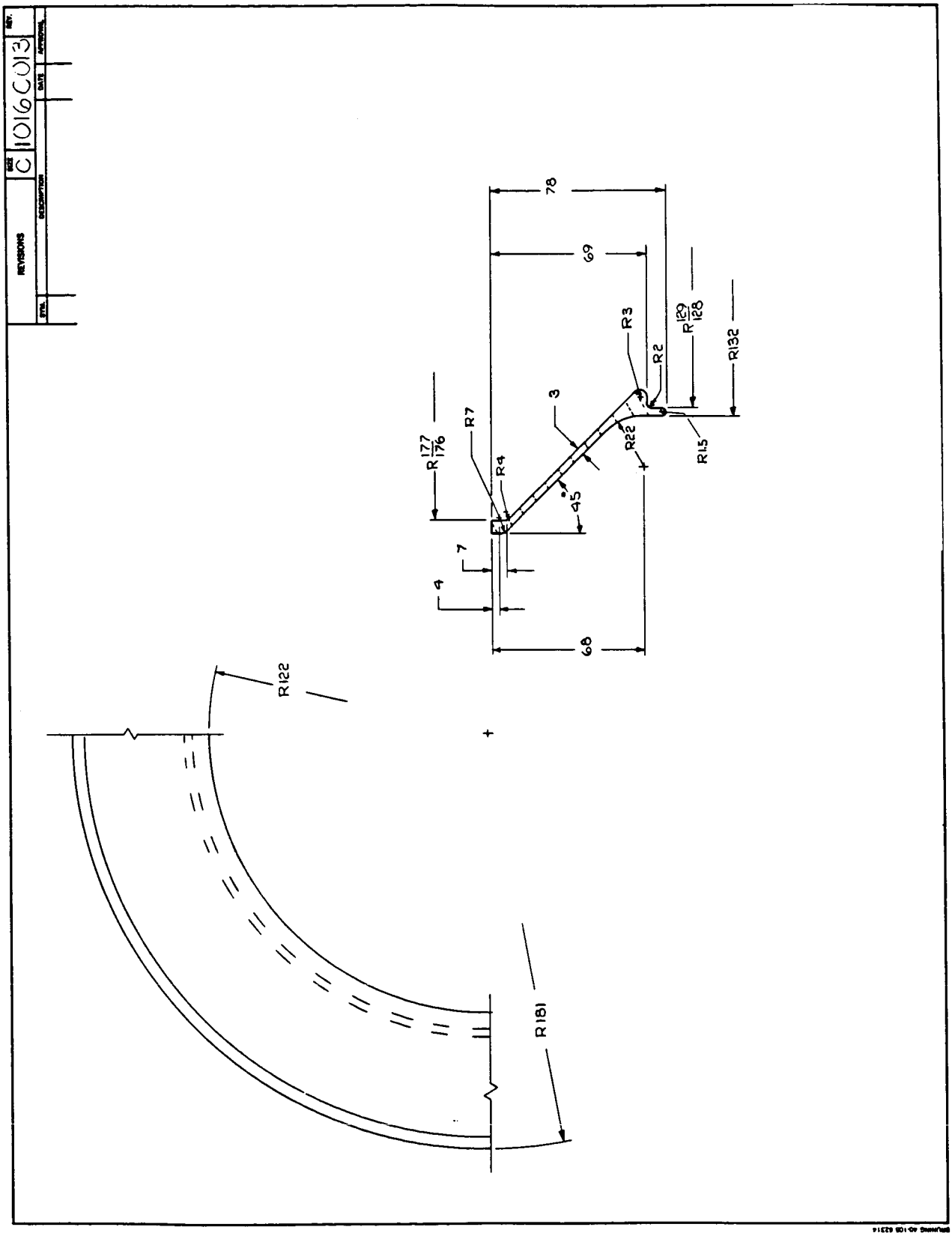

A
A
R18
R256
10
R1.5
R22
15°
45°
R25
3 TYP
R25
R70
R193
R26
R218
220
R5
45°
R250
SECTION A-A
SCALE FULL

851293

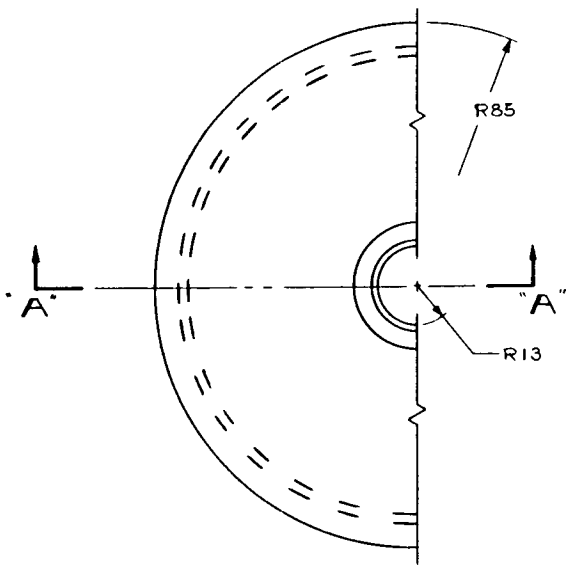

ORIGINAL PAGE IS
OF POOR QUALITY
REVISIONS
DESCRIPTION
DATE
APPROVAL
SECTION "A-A"
SECTION "C-C"
VIEW AT "B"
R211
R203
R164
R125
R108
R69
R73
R70
R3
R23
R29
R7
R28
R31
R156
R204
R24
R44
R3.5 TYP 36 PLCS.
R1.5 TYP 36 PLCS.
R2.5 TYP
2 TYP
10° TYP 36 PLCS.
Ø1.16 THRU 3 HOLES 36 EQ SPACES 108 HOLES TOTAL
9°
18°
10°
15°
30°
3 TYP
29
23
3
61
70
76
4
20
8°


112
36°
18°
R4 TYP
2 SLOTS 10 EQ SPACES
20 SLOTS TOTAL
A
A
36° TYP
18° TYP
B
B
36° TYP
10X Ø 7.5 THRU
EQ. SPACED
R 172
R 244
R215
R212
R207
27
27
25
R4
45°
45°
R6
24
13
R 175/174
R180
R 240
R 243
SECTION A-A
8
R2
25
R4
R6
43
3
18
3
3
42
52
55
7
19
R6
R4
50
10
17
3
4
45°
2
36
R 230
SECTION B-B
NOTE
1. ALL RADII TO BE R2 UNLESS OTHERWISE SPECIFIED.
ORIGINAL PAGE IS
OF POOR QUALITY
REVISIONS
DESCRIPTION
DATE
APPROVAL

851291

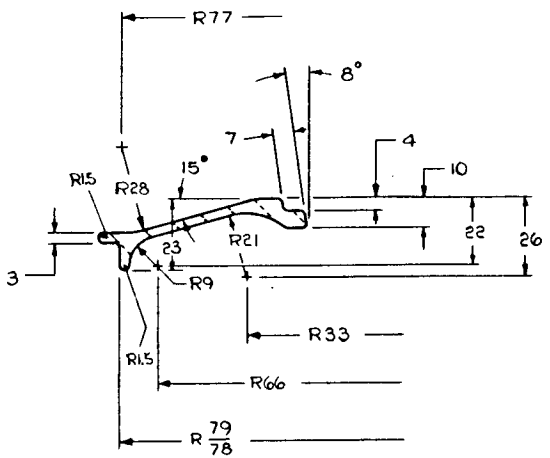

REVISIONS
DESCRIPTION
DATE
APPD.
C1016C013
78
69
R3
R2
R129
R128
R132
R177
R176
R7
R4
3
R22
R11.5
45°
7
4
68
R122
R181

REVISIONS		SIZE C	10160014	REV.
SYM.	DESCRIPTION		DATE	APPROVAL



NOTE

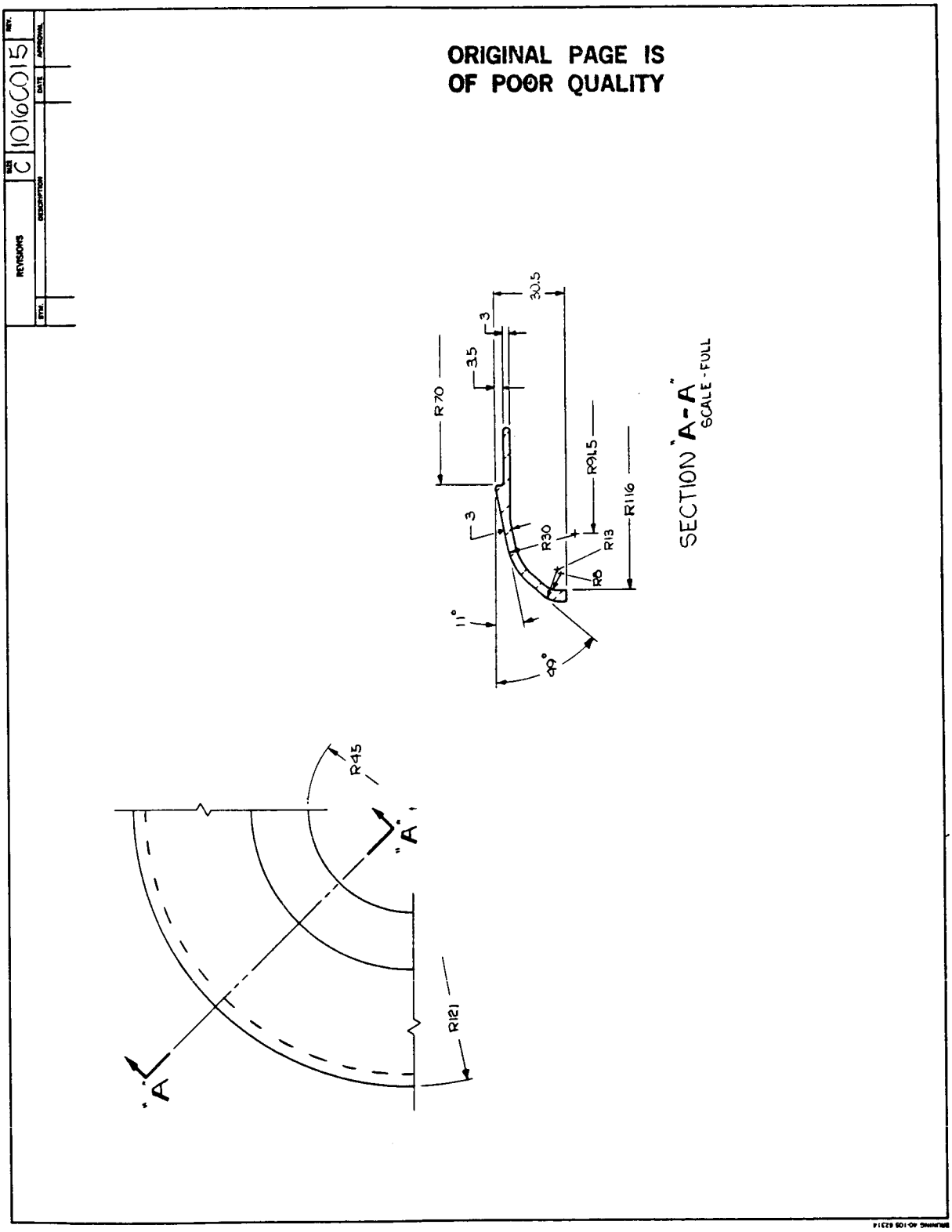
ALL RADII TO BE R2 UNLESS OTHERWISE SPECIFIED



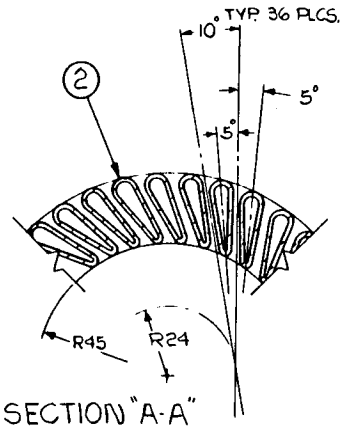
SECTION "A-A"
SCALE - FULL

BRUNING 40-105 82314

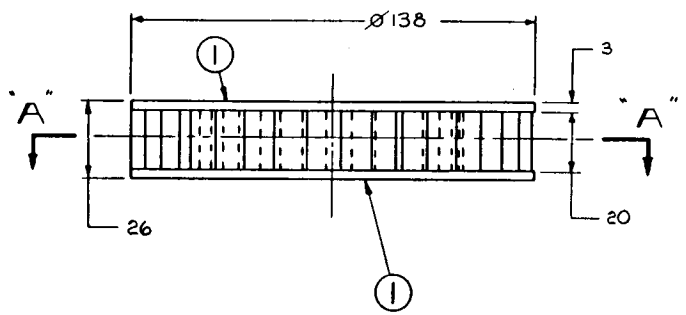
ORIGINAL PAGE IS
OF POOR QUALITY

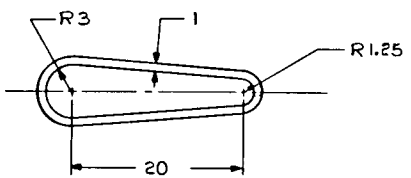


REVISIONS		SIZE C	10160016	REV.
SYM.	DESCRIPTION		DATE	APPROVAL

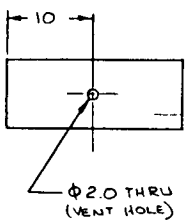


SECTION "A-A"

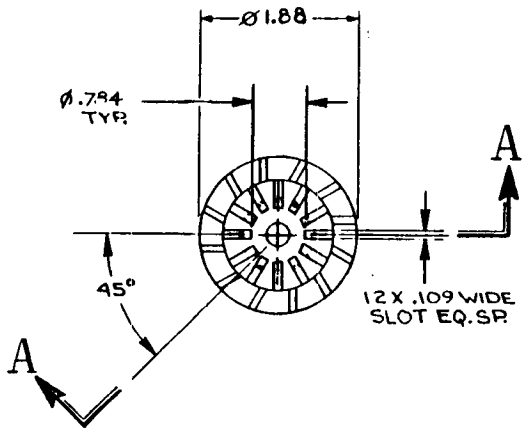


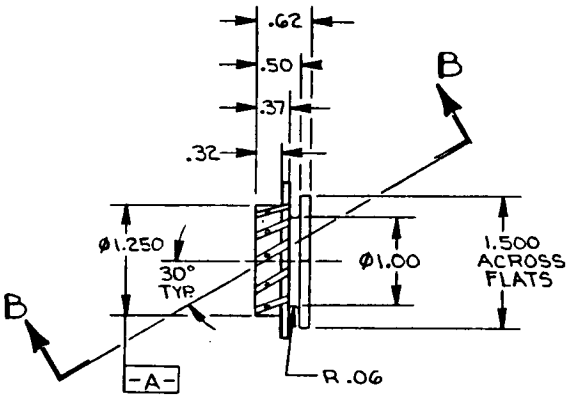


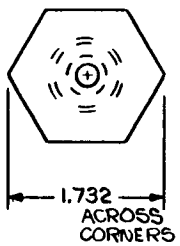
DETAIL (2)
SCALE 3 X

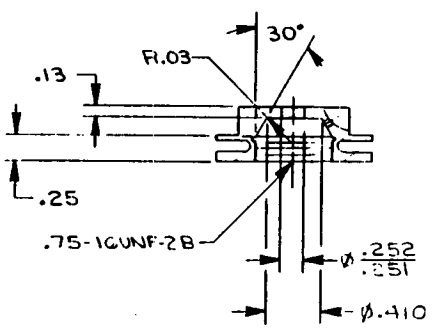


REVISIONS		SIZE C	1016C018	REV. A
SYM.	DESCRIPTION		DATE	APPROVAL
A	ISSUED			

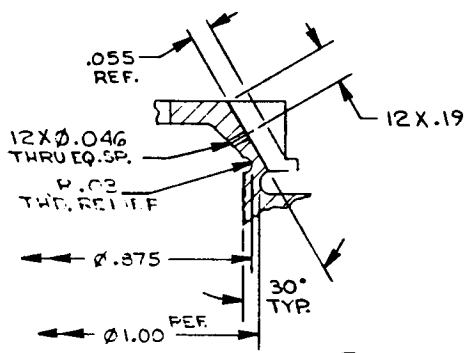








SECTION A-A



DETAIL - B B

NOTE:
DETAIL ROTATED INTO VIEW

NOTE:
ALL DIAMETERS ARE CONCENTRIC TO -A-

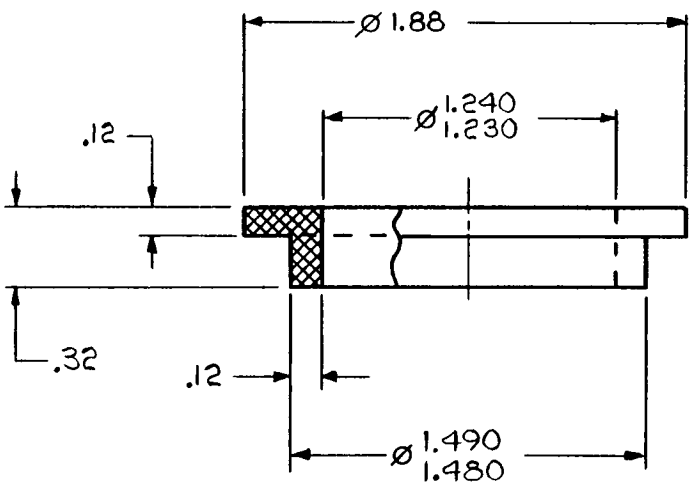
NOTE:
SEE DWG. 1008C505 FOR SIMILAR SWIRL NOZZLE

ORIGINAL PAGE IS OF POOR QUALITY

8-21

DWG. NO. 1016C018 MS REV.

REVISIONS		SIZE	1016B019	REV.
SYM.	DESCRIPTION		DATE	APPROVAL

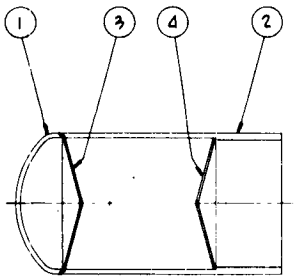


NOTES

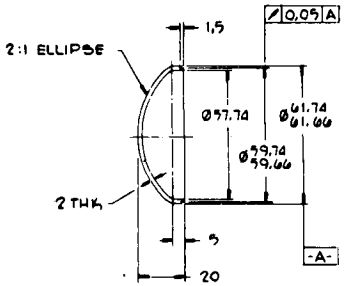
1. MATERIAL Ø.0035 KNITTED STN. STL. WIRE, TYPE 316
2. POROSITY TO BE 75%
3. APPROVED MFG.
   METEX CORP
   EDISON, NEW JERSEY 08817
4. POROSITY VARIATION AROUND CIRCUMFERENCE TO BE MINIMUM

BRUNING 40-105 22145-6

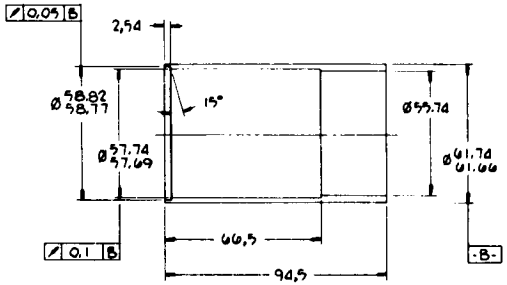
REVISIONS		SIZE D	10160023	REV A
ZONE	DESCRIPTION		DATE	APPROVED
A	ISSUED			



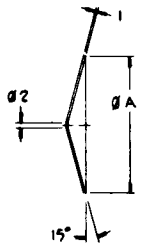
ASSEMBLY



① DETAIL



② DETAIL



DETAIL

PART NO	ØA
3	59.50 59.45
4	57.50 57.45

NOTES:

⚠ MATERIAL FOR PARTS 1 THRU 4, SEE ATTACHED MATERIAL SPEC

METRIC

Unless Otherwise Specified
Dimensions are in Millimeters
(25.4 MM = 1.000 IN)

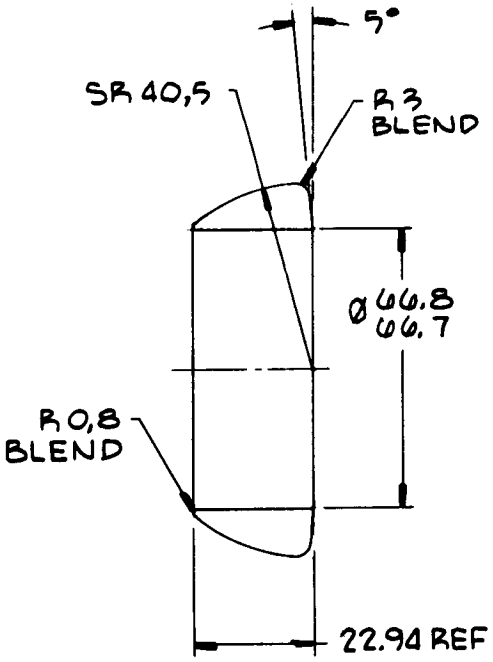
Dimension Range	Mod. Range Tolerance
0- 6	± 0.1
6- 30	± 0.2
30- 120	± 0.3
120- 315	± 0.5
315-1000	± 0.8
1000-2000	± 1.2
Angles- ± 0° - 30'	

3rd Angle Projection

Finish Machined Surfaces 32 µm RMS
Break Sharp Edges & Remove All Burrs
Geometric Tolerances Per ASME Y14.5

ORIGINAL PAGE IS
OF POOR QUALITY

REVISIONS		SIZE B	1016B024	REV. A
SYM.	DESCRIPTION		DATE	APPROVAL
A	ISSUED			



Unless Otherwise Specified	
Dimensions are in Millimeters	
(25.4 MM = 1.000 IN)	
Dimension Range	Med. Range Tolerance
0- 6	- ±0.1
6- 30	- ±0.2
30- 120	- ±0.3
120- 315	- ±0.5
315-1000	- ±0.8
1000-2000	- ±1.2
Angles- ± 0° - 30'	
Finish Machined Surfaces 32 µm	
Break Sharp Edges & Remove All Burrs	
Geometric Tolerances Per USASI Y14.5	

3rd Angle Projection

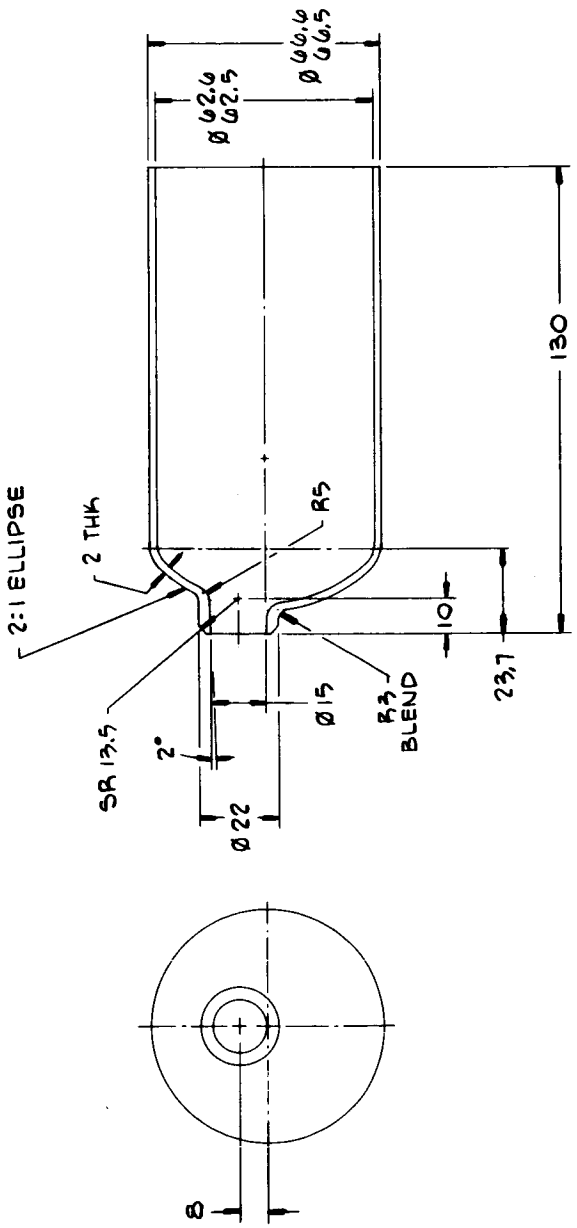
8-24

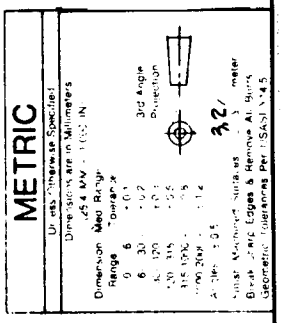
BRUNING 40-105 62314

REVISIONS					
SYM.	DESCRIPTION	SIZE		DATE	APPROVAL
A	ISSUED	C	1016C025		

REV. A

ORIGINAL PAGE IS OF POOR QUALITY





DRAWING 40-105 62314

1. Report No.	2. Government Accession No.	3. Recipient's Catalog No.
NASA CR-175042		

4. Title and Subtitle	5. Report Date
Ceramic Automotive Stirling Engine Program	August 1986
	6. Performing Organization Code

7. Author(s)	8. Performing Organization Report No.
	MTI 85SESD24
	10. Work Unit No.

9. Performing Organization Name and Address	11. Contract or Grant No.
Stirling Engine System Division Mechanical Technology Incorporated 968 Albany-Shaker Road Latham, New York 12110	DEN 3-311
	13. Type of Report and Period Covered
	Contractor Report

12. Sponsoring Agency Name and Address	14. Sponsoring Agency ~~Code~~ Report No.
U.S. Department of Energy Office of Vehicle Engine R&D Washington, D.C. 20545	DOE/NASA/0311-1

15. Supplementary Notes

Final Report. Prepared under Interagency Agreement DE-AI01-85CE50112. Contract Manger, William A. Tomazic, Power Technology Division, NASA Lewis Research Center, Cleveland, Ohio 44135.

16. Abstract

The Ceramic Automotive Stirling Engine Program evaluated the application of advanced ceramic materials to an automotive Stirling engine. The objective of the program was to evaluate the technical feasibility of utilizing advanced ceramics to increase peak engine operating temperature, and to evaluate the performance benefits of such an increase. Manufacturing cost estimates were also developed for various ceramic engine components and compared with conventional metallic engine component costs.

17. Key Words (Suggested by Author(s))	18. Distribution Statement
Ceramics, Stirling engine	Unclassified - unlimited STAR Category 44 DOE Category UC-96

19. Security Classif. (of this report)	20. Security Classif. (of this page)	21. No. of pages	22. Price*
Unclassified	Unclassified	182	A09

*For sale by the National Technical Information Service, Springfield, Virginia 22161

*U.S. GOVERNMENT PRINTING OFFICE: 1986-748-120-40409